HIGH RESOLUTION GAMMA-RAY SPECTROSCOPY OF ^{76}As, ^{207}Bi and ^{75}Se

Ruth Valerie Thomas

Thesis presented for the degree of

Doctor of Philosophy at the

University of London

Bedford College

London

1973

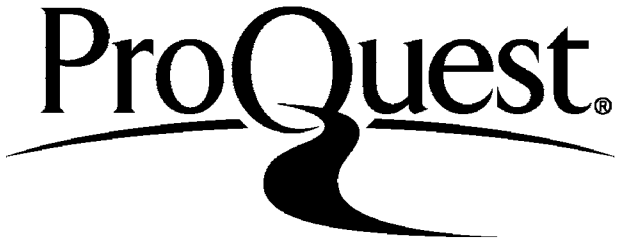

CONTENTS

	Page
Abstract	7
CHAPTER 1: General Introduction	
1.1 Summary of the studies undertaken	8
1.2 The emission of gamma radiation	9
CHAPTER 2: The use of Ge(Li) detectors in gamma-ray spectroscopy	
2.1 Introduction	14
2.2 Ge(Li) detector systems	14
2.3 Calibration of Ge(Li) detector systems for the measurement of energy	15
2.4 Measurement of the relative full-energy peak efficiency of Ge(Li) detectors	18
2.4.1 Relative efficiency for the 25 cm^3 detector	19
2.4.2 Relative efficiency for the X-ray detector	25
2.5 The general form of a gamma-ray spectrum and the validity of peaks in a singles spectrum	31
2.6 The determination of weak intensity gamma-ray transitions from a singles spectrum	33
2.7 The use of Ge(Li) detectors in a coincidence mode	36

Page

CHAPTER 3: Analysis of experimental data

3.1 General considerations 38

3.2 Initial approaches to analysis 39

3.3 The use of a computer programme in the analysis of gamma-ray spectra 40

3.4 The general features of Sampo 41

CHAPTER 4: Time analysis and coincidence mode systems

4.1 Introduction 49

4.2 General reasons and requirements for time measurements 49

4.3 Outline of timing systems and the assessment of their performance 50

4.4 Requirement of small resolving time in a system 52

4.5 Causes of non-ideal time spectra 54

4.6 Origins of jitter and walk for scintillation counters and for Ge(Li) detectors 57

4.7 Methods used for the extraction of a fast timing signal 59

4.8 Fast-slow coincidence systems 61

4.9 Corrections to coincidence spectra and possible sources of error 69

Page

CHAPTER 5: Instrumentation and Experimental Techniques

5.1 Introduction 73

5.2 Scintillation counter 73

5.3 Leading edge discriminator 74

5.4 Fast pulse shaper 88

5.5 Electronic systems for the measurement of singles spectra from Ge(Li) detectors 92

5.6 The electronic system and its adjustment for fast-slow coincidence measurements 94

5.7 The electronic system for sum-coincidence spectra 101

CHAPTER 6: The decay of ^{75}Se

6.1 Introduction 107

6.2 Previous work 108

6.3 Experimental details of singles spectra 110

6.4 Analysis of singles spectra 113

6.5 Discussion of the spectra below 100 keV 115

6.6 Discussion of the spectra above 100 keV 120

Page

6.7 Coincidence studies 122

6.8 Reduced transition probabilities 126

6.9 Conclusions 126

CHAPTER 7: The decay of ^{207}Bi

7.1 Introduction 129

7.2 Experimental details and analysis of the singles spectra 131

7.3 Results derived from the singles spectra 135

7.4 Sum-coincidence studies 140

7.5 Coincidence studies 143

7.6 Conclusions 143

CHAPTER 8: The gamma decay of ^{76}As

8.1 Introduction 147

8.2 Experimental procedure for singles spectra 147

8.3 Results of singles spectra 153

8.4 Experimental procedure for coincidence spectra 153

8.5 Analysis of coincidence spectra 159

8.5.1 Source stationary 160

page

8.5.2 Source moving 160

8.5.3 Calculation of the chance coincidence spectrum 163

8.5.4 Treatment of coincidence spectra 163

8.6 Results from the coincidence spectra 181

8.7 Conclusions 190

CHAPTER 9: General conclusions 194

Acknowledgements 195

References 196

Abstract

The decay schemes of ^{76}As, ^{207}Bi and ^{75}Se have been studied using Ge(Li) detectors and coincidence techniques with particular emphasis on the weaker modes of gamma decay. The feasibility of detecting weak modes of gamma decay is discussed and supporting electronic systems which have been developed to yield data suitable for reduction and analysis with computer programmes are described.

Low energy gamma transitions in the decay of ^{75}Se were studied using an X-ray Ge(Li) detector. Two previously unconfirmed transitions at 24.4 keV and 80.8 keV have been detected and their positions in the decay scheme of ^{75}As have been established.

In the decay of ^{207}Bi, an upper limit of 0.014 ± 0.008 relative to the 570 keV transition as 100 has been placed on the intensity of the 'l-forbidden' gamma transition at 328 keV.

The decay scheme of ^{76}As has been shown to include two previously unreported gamma-rays at 220 keV and 316 keV and coincidence experiments have indicated a new energy level at 2006 keV. Several gamma-rays and level energies suggested by previous authors were not confirmed by this work.

CHAPTER 1 GENERAL INTRODUCTION

1.1 Summary of the studies undertaken

The development of the Lithium - drifted Germanium, Ge(Li), detector with an energy resolution which is vastly superior to that of the high efficiency NaI gamma - ray detector would apparently offer the possibility of detection of many close lying and weak intensity gamma-ray transitions. This work was undertaken to set up and investigate the performance of suitable systems utilizing Ge(Li) detectors to advance the knowledge of the gamma transition decay schemes of three radioactive isotopes.

The course of the work led to consideration of the feasibility of searching with these detectors for previously unresolved gamma transitions and to the use of coincidence techniques employing these detectors. The use of a coincidence system required that good timing information could be extracted from the detectors and that the performance of a typical coincidence system should be carefully analysed.

Since the spectra obtained from such a high resolution system can be very complex it was an obvious requirement that a suitably refined analysis of the data should be made to extract the areas of the full energy peaks from the spectrum and the application of a computer programme written for this purpose was undertaken.

The isotopes studied were chosen because each presented different experimental requirements and it was apparent that all three had ill-defined features in the current knowledge of their decay schemes. The study of ^{207}Bi was aimed at establishing the transition intensity of the 'l-forbidden' gamma transition and thus of comparing its transition probability with the theoretical model predictions. ^{75}Se possesses several weak gamma transitions of very low energy which had proved difficult to detect and which might be more easily identified with a special purpose Ge(Li) X-ray detector. ^{76}As, while having a poorly defined and complex decay scheme, also presented the feature of a moderately short half-life thus requiring a modification of normal counting techniques.

For each isotope several transition intensities of previously poorly defined modes of gamma decay have been evaluated and for two of the isotopes some comparison has been made with the theoretical predictions.

1.2 The emission of gamma radiation by an excited nucleus

The study of the gamma decay of radioactive isotopes can be used to determine the energies and relative transition intensities of the gamma transitions involved.

The emission of electromagnetic radiation by a nucleus has been treated theoretically by a semi-classical

approach which describes the electromagnetic radiation source in terms of an oscillating distribution of electric or magnetic charges which constitute a multipole. This has then been incorporated into a quantum-mechanical formalism and used to describe and classify radiative transitions in nuclei. Nuclear models have been developed which aim to account for and to deduce values for various nuclear properties such as the energies, spins and parities of nuclear states. Within the context of a particular model it is then possible to calculate the expected gamma-ray transition probability between the various excited states.

Gamma-ray transitions are classified according to the total angular momentum, L, carried by the multipole. For a nuclear transition between states i and f having nuclear spins of J_i and J_f respectively it has been shown that a momentum selection rule applies which limits the permitted range of multipolarities. This is given by:

$$|J_i - J_f| \leqslant L \leqslant (J_i + J_f) \quad \ldots\ldots 1.1$$

In addition, a distinction is made between electric (EL) and magnetic (ML) multipoles according to the parity associated with the electromagnetic radiation. This depends on the parities of the two nuclear states involved. Electric multipole radiation of order L has parity $\pi_e = (-1)^L$ and magnetic multipole radiation of order L

has parity $\pi_m = (-1)^{L+1}$. Although equation 1.1 suggests a series of values for L for a given J_i and J_f, the radiation emitted is usually limited to the lowest one or two orders permitted as the probability of emission decreases rapidly with increasing L when the condition $R \ll \lambda$ is satisfied (R is the nuclear radius and λ the wavelength of the radiation). In addition, the relative probability of emission of magnetic multipole radiation is considerably smaller than that of electric multipole radiation of the same order. The transitions usually encountered have $L = |J_i - J_f|$ or $L = |J_i - J_f|$ with an admixture of $L = |J_i - J_f| + 1$.

The simplest model used to describe a nucleus is the independent particle model. This assumes very weak coupling between the individual nucleons so that in a gamma-ray transition only a single nucleon experiences a change in its quantum state. This nucleon moves in a central potential due to the other nucleons and makes a transition from a state of angular momentum L to a state of zero angular momentum.

The transition probabilities for the emission of gamma radiation during this change, W(EL) and W(ML), can be calculated on this basis and are usually expressed in terms of a reduced transition probability, B(EL) and B(ML), which is essentially the square of the multipole transition matrix element taken between the state i and the state f.

These transition probabilities are known as the Weisskopf or single particle estimates and are given by:

$$W(EL) = \frac{8\pi\,(L+1)}{L((2L+1)!!)^2}\,\frac{1}{\hbar}\left(\frac{E_\gamma}{\hbar c}\right)^{2L+1} B(EL) \quad \ldots\ldots\ldots \quad 1.2$$

$$W(ML) = \frac{8\pi\,(L+1)}{L((2L+1)!!)^2}\,\frac{1}{\hbar}\left(\frac{E_\gamma}{\hbar c}\right)^{2L+1} B(ML) \quad \ldots\ldots\ldots \quad 1.3$$

where E_γ is the energy of the gamma radiation and B(EL) and B(ML) are given by:

$$B(EL) = \frac{e^2}{4\pi}\left(\frac{3R^L}{L+3}\right)^2 \quad \ldots\ldots\ldots\ldots\ldots\ldots \quad 1.4$$

$$B(ML) = 10\left(\frac{\hbar}{M_p cR}\right)^2 B(EL) \quad \ldots\ldots\ldots\ldots\ldots \quad 1.5$$

The experimentally observed transition intensity or a theoretical estimate of a transition probability based on a more sophisticated nuclear model can then be compared with these values and the result expressed in single - particle units (spu) or Weisskopf units.

From the measurements made during the present work it is only possible to determine values of B(EL) or B(ML) relative to those for other transitions which de-excite the same energy level. These relative B(EL) or B(ML) values are obtained from the relative transition intensities using equations 1.2 and 1.3 with allowance made where

necessary for competing multipolarities. This occurs where the admixture of radiation having $L' = L+1$ (where $L=|J_i-J_f|$) is significant and the admixture is expressed by a mixing ratio, δ, which is related to the ratio of the transition intensities.

$$\delta^2 = \frac{W(L')}{W(L)} \qquad \ldots\ldots\ldots\ldots\ldots\ldots \quad 1.6$$

Usually such admixtures are present when the lowest order (L) is a magnetic multipole transition and the next permitted order is then an electric multipole transition.

CHAPTER 2 THE USE OF Ge(Li) DETECTORS IN GAMMA-RAY SPECTROSCOPY

2.1 Introduction

The use of Ge(Li) detectors in gamma-ray spectroscopy is outlined and the relevant experimental techniques are discussed. Details are given of the energy and relative efficiency calibrations of the detectors used in the present work. The nature of the gamma-ray spectrum obtainable from these detectors is examined with reference to the presence of 'spurious' peaks in the spectrum and consideration is given to the information obtainable from a singles spectrum.

2.2 Ge(Li) detector systems

The Ge(Li) detector has become a well-established device for the measurement of gamma-ray spectra. The excellent energy resolution and linearity obtainable with these detectors has meant that they have superseded the NaI scintillation counter in many applications which demand only these qualities from a counter system. One serious disadvantage in the field of coincidence work is their low photopeak efficiency which is typically only a few percent of that obtainable with a 3" x 3" NaI crystal. The difficulties encountered in extracting a good timing signal from a Ge(Li) detector, particularly at low energies less than about 200 keV,

also impose some limitations on their use in coincidence studies and in lifetime measurements.

The Ge(Li) detectors used in most of the present work were both manufactured by Nuclear Enterprises (Edinburgh) Limited. The main detector was a true coaxial diode with an active volume of 25 cm^3. Its resolution was about 3 keV at 1.33 MeV. The other detector was a special purpose X-ray detector with a very low noise pre-amplifier and which gave an energy resolution of 300 eV at 14 keV. The electronic system used with these detectors is described in section 5.5.

2.3 Calibration of Ge(Li) detector systems for the measurement of gamma-ray energies

The intrinsic response of a Ge(Li) detector has been found to give a good linearity of about $\pm$0.03% in the range 662 keV to 2614 keV[1] so that, provided that the supporting electronic system is of comparable linearity, it is possible to achieve an accuracy of about $\pm$0.5 keV at 1 MeV.

The energy calibration of the detector systems used in this work was carried out with a variety of sources producing well-defined reference lines. In general, these sources were adjusted in strength to give about the same counting rate as the source under investigation and when the digital stabilizer (see section 5.5) was in use they were counted in the presence of the source under investigation

(removed to a suitable distance). The centres of the photopeaks corresponding to the reference lines were found using the computer programme Sampo (see section 3.4) and the linearity of the response of the system could be found by fitting, in the least squares sense, a straight line to the data obtained. A typical system performance with the 25 cm^3 detector system is shown in figure 2.1 where the non-linearity is given for energies from 100 keV to 1600 keV. The deviation from linearity could also be illustrated (and allowed for) by fitting a higher order polynomial to the energy data. Sources used for these energy calibrations were ^{152}Eu, ^{182}Ta, ^{57}Co, ^{241}Am, ^{109}Cd, ^{60}Co, ^{137}Cs and ^{228}Th. The relevant data are contained in references 2,3,4,5,6, and 7.

For most experimental runs the energy standards were checked both before and after the runs. Where a long run was necessary for the evaluation of very weak peaks the stronger lines were used as internal standards, their energies being determined in suitable short runs.

Although the linearity of the detector and electronic system used proved to be only slightly worse than the best figures[8,9] quoted in the literature, it was noted that when a linear least squares fit was made to calibration data covering a fairly wide energy range from 0.1 to 3 MeV serious discrepancies (about 1 keV) could occur at the higher energies when other well established lines were measured with

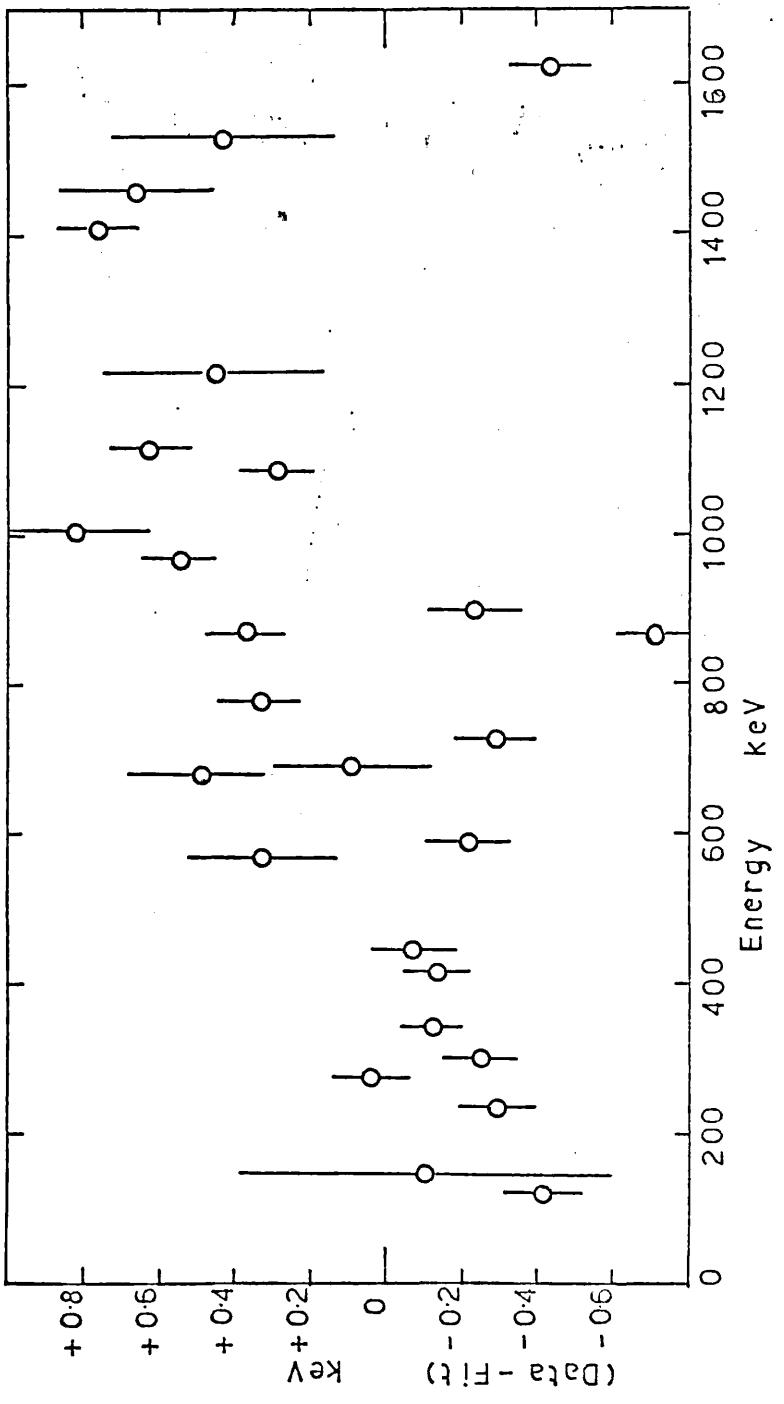

FIGURE 2.1 Non - linearity of 25cm^3 detector system

the system. If the energy is to be measured to an accuracy better than $\pm$1 keV at say 2 MeV it is obvious that an accuracy better than 0.05% is needed in the product of the gradient of the calibration line and the determination of the centroid of the photopeak to be measured. This is not easy to achieve with the system used and, in practice, it was found that the accuracy of energies measured with the system was improved by using a linear interpolation between neighbouring calibration points. In the energy region above about 1.7 MeV it was found to be more reliable to use the double escape peak when this was clearly defined. The single escape peak was not used as it has been shown[10] that its shape is broadened and its centroid slightly shifted relative to a full-energy peak of the same energy.

2.4 Measurement of the relative full-energy peak efficiency of Ge(Li) detectors

A gamma-ray spectrum can be used to determine the relative intensities of the transitions present provided that the response of the detector to gamma photons of different energies is known. Since the area of the full-energy peak is the convenient information to extract from an experimental spectrum, it is necessary to measure experimentally the relative full-energy peak efficiency of the Ge(Li) detectors used in this work. The absolute efficiency of a detector is a function

of the detector and of the solid angle it presents to the source. For a typical coaxial diode Ge(Li) detector and a non-point source the latter factor can be difficult to determine. Fortunately, this information is not required in these investigations but it was felt wise to check that the shape of the relative efficiency curve was not a rapidly changing function of the source - detector distance. This information (figure 2.3) determined that the actual geometry of the source relative to the detector was not of significant importance (within obvious limitations) in using the detectors to measure relative intensities. In practice this geometry was maintained as closely as possible to that used in the calibration runs.

2.4.1 Relative full-energy peak detection efficiency for the 25 cm^3 detector

The 25 cm^3 detector was used over an energy range from about 200 keV to 2 MeV so the relative efficiency calibration was designed to cover this range. The most convenient source to cover this range is ^{226}Ra where the main gamma transition intensities have been well established both by measurements made with other calibrated detectors[11] and with Ge(Li) detectors calibrated with other sources[12,13]. The coverage provided by the ^{226}Ra source was extended to slightly lower energies by measurements made with ^{152}Eu using

the data given in references 2 and 3.

The ^{226}Ra source available was mounted in a container with a wall thickness of 0.5 mm Platinum. The peak areas measured with the Ge(Li) detector were corrected for the attenuation by this mounting using figures obtained from reference 14. The ^{152}Eu source was mounted in an aluminium planchet with a paper label covering. No correction was applied to this as the attenuation by the paper was negligible at the energies of interest.

The relative efficiency curve resulting from these measurements with the sources on the axis of the detector and at a distance of 20 cm from the end window of the cold finger is shown in figure 2.2. The corresponding data is given in table 2.1. The areas used in the determination of the relative efficiency were extracted from the data using Sampo (see section 3.4) and the final points were fitted with the equation:

$$\eta = PR(1)\left[E_\gamma^{PR(2)} + PR(3)\exp(PR(4)E_\gamma)\right] \quad . \; . \; . \quad 2.1$$

where η = relative efficiency at energy E_γ

PR(1), PR(2), PR(3) and PR(4) are coefficients as suggested by Routti et al.[24].

This fitting could be performed by the computer programme.

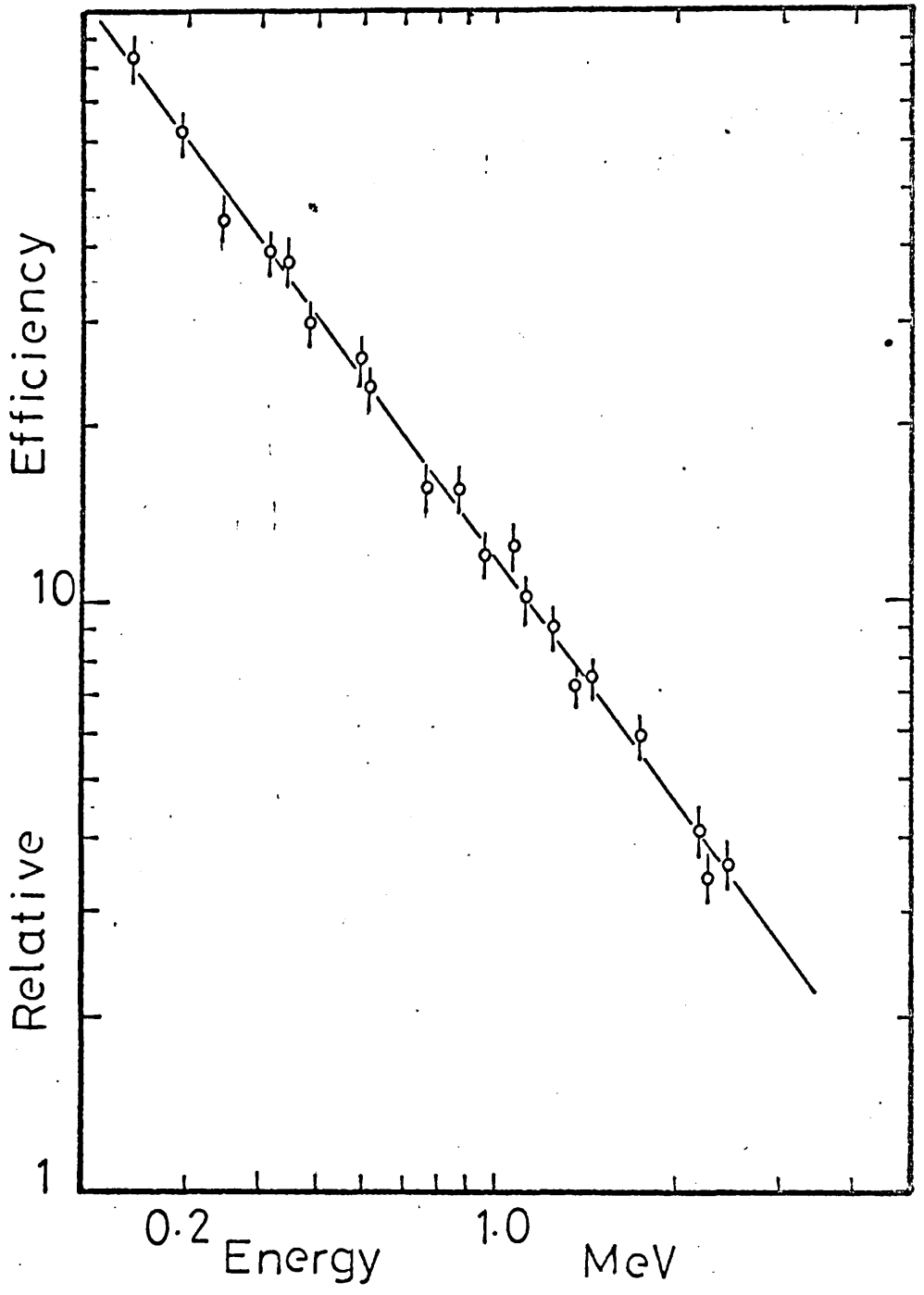

FIGURE 2.2 Relative full -energy peak detection efficiency of $25cm^3$ detector at 20cm

ENERGY keV	RELATIVE EFFICIENCY	ENERGY keV	RELATIVE EFFICIENCY
242	81 ± 8	1112	10 ± 1
245	87 ± 8	1120	10 ± 1
296	62 ± 6	1213	9.1 ± .9
344	44 ± 4	1274	9.1 ± .9
411	39 ± 4	1299	8.5 ± .9
445	38 ± 4	1377	7.2 ± .7
489	30 ± 3	1408	7.4 ± .7
586	26 ± 3	1509	7.4 ± .7
609	23 ± 2	1764	5.9 ± .6
779	16 ± 2	2119	4.1 ± .4
867	16 ± 2	2204	4.1 ± .4
964	12 ± 1	2295	3.4 ± .3
1086	13 ± 1	2450	3.6 ± .4

TABLE 2.1 Full-Energy Peak Efficiency for 25 cm^3 Detector at 20 cm

Further investigations were made with this detector and figure 2.3 shows the relative efficiency curves measured from the ^{226}Ra data at 20 cm, 10 cm and 5 cm from the end of the cold finger.

From equation 2.1 it can be seen that for any arbitrarily scaled set of relative efficiency values, η_i, as a function of energy, E_γ, that:-

$$\ln \eta_i = PR(2).\ln E_\gamma + C$$

where C is a constant provided that

$$PR(3)\ e^{PR(4)E_\gamma} \ll E_\gamma^{PR(2)}$$

so that η_i is not a strong function of geometry if PR(2) is not a function of the geometry.

The values of PR(2) at 20 cm, 10 cm and 5 cm were found to be constant to less than 1% which confirmed that the relative efficiency curve for this detector was not a strong function of the source - detector distance within this range; so relaxing possible stringent requirements on source positioning in subsequent measurements relying on these calibrations.

During the course of this work it was reported by one manufacturer[15] that Ge(Li) detectors could suffer a sizeable drop in efficiency with time and that this effect could amount to a change of 8% over the course of a year.

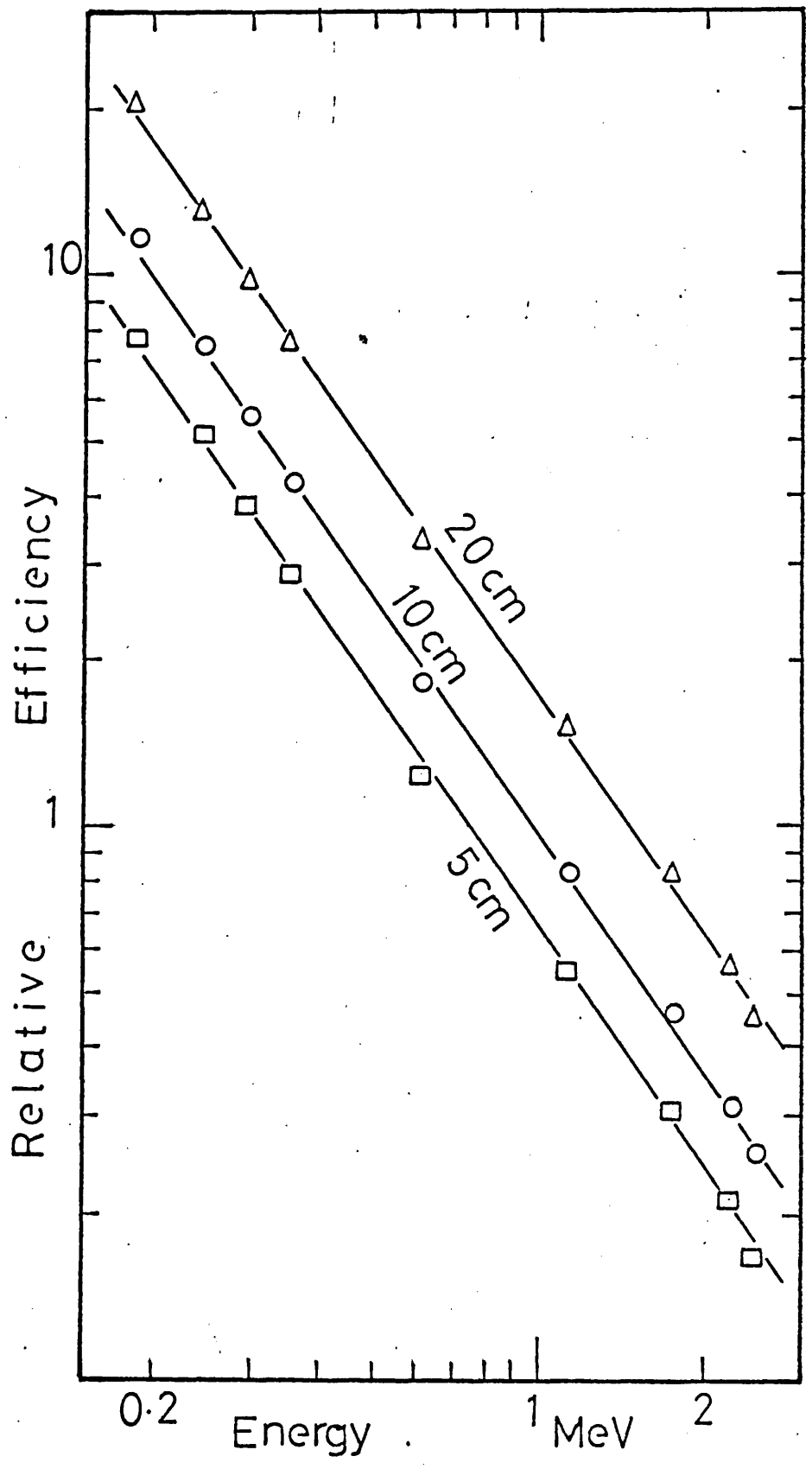

FIGURE 2.3 Relative efficiency at 20cm, 10cm & 5cm for 25cm^3 detector

The efficiency of the detector used could be determined from the ^{226}Ra data as the source used was calibrated by the Radiochemical Centre (Amersham) to 4%. This efficiency was remeasured after 18 months using the same source and, after correction for the source decay, the new values were shown to be unchanged relative to the original measurements to within 1%. The accuracy of this measurement was, unfortunately, limited by the possible error in source positioning since the need for this measurement only arose after the first measurement had been made and the definition of the source position was only about 0.5%. These results are shown in figure 2.4.

Finally, the information obtained could be used to determine the efficiency of the detector relative to a 3" x 3" NaI crystal used at the same distance from the source. This figure is frequently used as a convenient measure of the performance of a Ge(Li) crystal as it gives more information than the measurement of the sensitive volume. This figure is a function of energy and the values obtained are given in table 2.2.

2.4.2 Relative full-energy peak detection efficiency of the X-ray detector

The relative full-energy peak detection efficiency curve for the Ge(Li) X-ray detector was established using

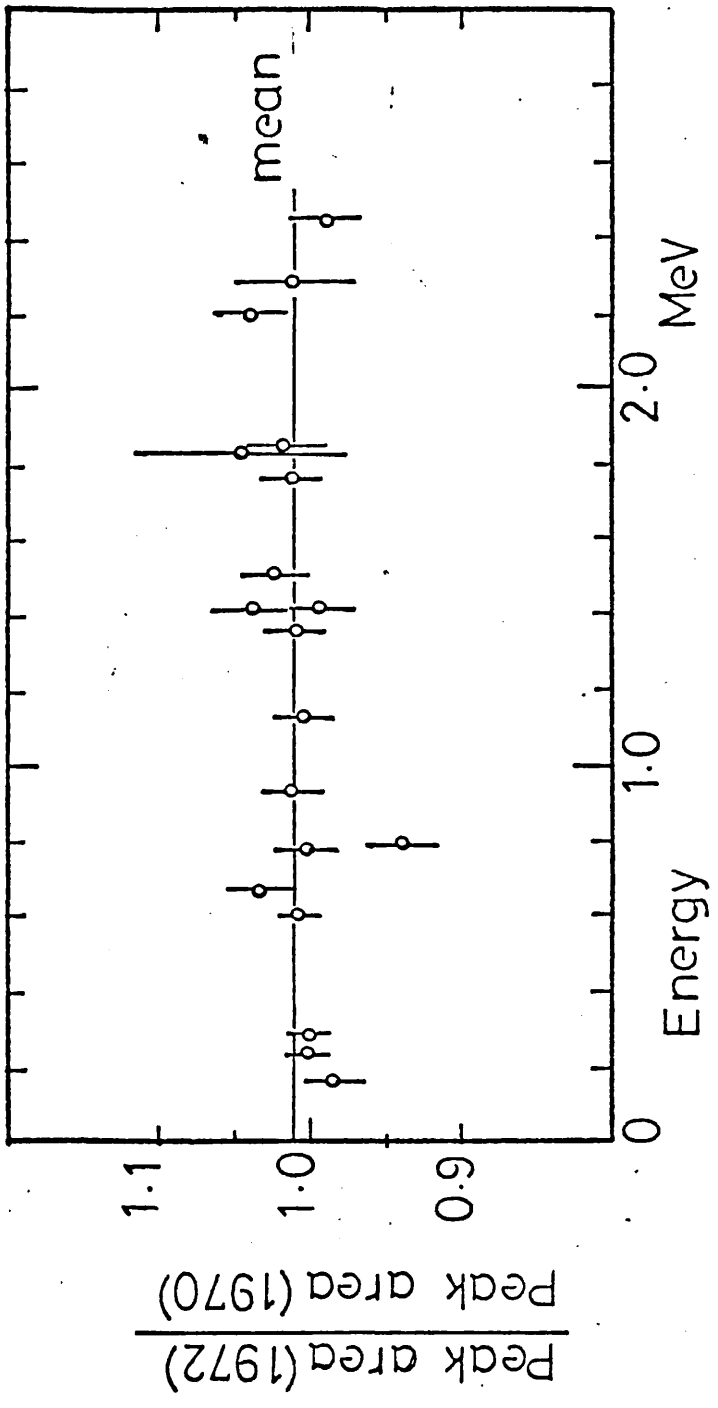

FIGURE 2.4 Variation of relative efficiency with time

ENERGY keV	EFFICIENCY % compared with 3"x3" NaI crystal at 20 cm
242	22 ± 2
295	19 ± 2
352	16 ± 2
609	$7.7 \pm .8$
935	$4.9 \pm .5$
1120	$4.0 \pm .4$
1764	$2.6 \pm .3$
2205	$2.0 \pm .3$
2450	$1.7 \pm .3$

TABLE 2.2 Full-Energy Peak Detection Efficiency of 25 cm^3 Ge(Li) Detector at 20 cm

sources of ^{226}Ra (data in references 11,12 and13), ^{152}Eu (references 2 and 3), ^{182}Ta (reference 4), ^{57}Co (reference 6), ^{109}Cd and ^{137}Cs (reference 5) and ^{75}Se (reference 16). The technique used was to mount the sources (except for ^{226}Ra as given in section 2.4.1) in aluminium planchets covered with a paper label and positioned at 7 cm from the Beryllium end-window of the cold finger containing the detector. The curve thus measured was the relative efficiency of the detector with the absorption by the source mount cover and the end-window included. In future runs sources were made and mounted in the same manner so that the curve could be used without correction for these effects.

The resulting calibration curve up to 200 keV is shown in figure 2.5 and table 2.3 gives the data measured up to 1 MeV. This curve was deduced from the data measured with the individual sources by fitting a curve of the form given in equation 2.1 to the values in the high energy region well away from the maximum of the curve and normalizing the curves obtained to each other. Points in the region below the maximum efficiency were obtained by an extension of the pair - point method[5].

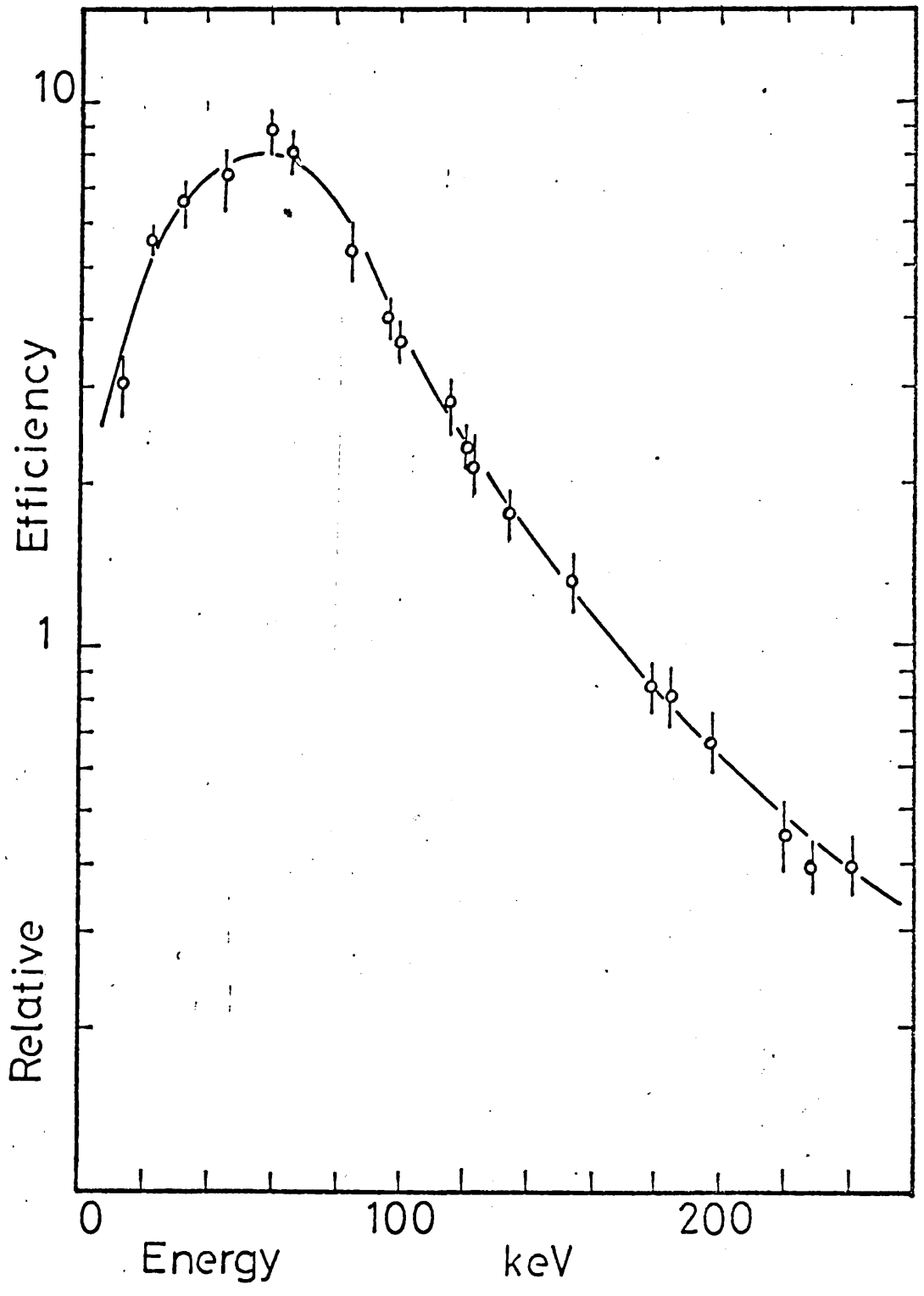

FIGURE 2.5 Relative full - energy peak detection efficiency for X-ray detector at 7cm

ENERGY keV	RELATIVE EFFICIENCY	ENERGY keV	RELATIVE EFFICIENCY
14.4	30 ± 4	179.4	8.4 ± .8
22.7	55 ± .8	185.7	8.1 ± .9
45.2	73 ± 10	198.4	6.6 ± .7
60.0	90 ± 9	222.1	4.5 ± .5
66.2	81 ± 6	229.3	3.9 ± .4
84.7	53 ± 5	241.9	3.9 ± .4
96.7	40 ± 2	244.8	3.9 ± .4
100.1	37 ± 4	264.1	3.3 ± .3
113.7	29 ± 3	295.2	2.3 ± .2
116.4	28 ± 3	295.8	2.3 ± .3
121.1	24 ± 2	344.4	1.7 ± .2
121.9	23 ± 2	352.0	1.5 ± .2
122.0	22 ± 2	368.0	1.5 ± .2
136.0	18 ± 1	411.3	1.0 ± .1
136.4	17 ± 2	444.2	.84 ± .09
152.5	14 ± 1	609.4	.36 ± .04
156.4	12 ± 1	1120.0	.11 ± .01

TABLE 2.3 Relative Full-Energy Peak Detection Efficiency for X-Ray Ge(Li) Detector at 7 cm

2.5 The general form of a gamma-ray spectrum obtained with a Ge(Li) detector and the validity of peaks found in a singles spectrum

As with many detector systems the Ge(Li) detector presents a gamma-ray spectrum which contains some peaks not attributable directly to gamma-ray transitions in the isotope of interest. The well known general features of a gamma-ray spectrum taken with a NaI counter are present in a Ge(Li) detector spectrum and include the double and single escape peaks resulting from pair production and the corresponding annihilation peak and also peaks due to summing in the detector of the full-energy corresponding to two gamma-ray transitions. In addition to these, the low energy spectrum taken with a Ge(Li) detector exhibits spurious peaks due to two other causes. In a small detector there is a fairly high probability that the Germanium K X-rays following a photoelectric interaction will escape from the detector thus resulting in a 'Germanium escape peak' which lies below its corresponding full-energy peak and separated from it by the Germanium K X-ray energies (9 and 11 keV). The other common feature of small detectors is that they are frequently mounted near to or are constructed with comparable volumes of other materials which then give rise to fluorescent X-rays in the presence of even a fairly weak radioactive source.

The typical elements giving these effects are Indium (used in making electrical contact to the detector) and Gold (used in some detector windows). In addition our X-ray detector was found to 'contain' lead and bismuth, although these elements are not commonly reported in other X-ray detectors! The fluorescent X-rays produced by a source are then detected and can be a serious nuisance in a spectrum particularly as it is possible to obtain them even when the detector is used in a coincidence mode.

These effects of summing, escape and fluorescent peaks together with the possibility of peaks due to contaminants and background radiations must all be eliminated in searching for weak gamma-ray transitions in a particular isotope.

In general it is a simple matter to predict the energies of the significant peaks due to escape and summing effects as these will result from the most intense gamma-ray energies giving the major peaks in the spectrum. The fluorescent X-rays obtained with the X-ray detector are at well established energies and thus pose no problem in identification. Contaminant isotopes can often be identified by half-life considerations. The effects of random summing and of background radiations can both be identified by using sources of different strengths, when the spurious peaks thus generated will appear to change their intensity

relative to the true peaks due to the source under investigation. This method was used for the background radiations in preference to a simple energy elimination technique as the background radiations to be seen with the detector can not be easily established experimentally as the counting rate obtained is necessarily very low. One recent report by Bertolini et al.[17] gives a comprehensive list of possible background radiations.

2.6 The determination of weak intensity gamma-ray transitions from a singles spectrum

Most work in gamma-ray spectroscopy with isotopes having half-lives greater than a few hours is concerned with the establishment of the intensities of very weak gamma-ray transitions. For a full-energy peak to be present in the singles spectrum it is necessary for the area of the peak to be 'statistically significant' above the continuum upon which it sits - this continuum being due to Compton detected events from higher energy gamma-ray transitions either from the source itself or from the background radiations. The literature is frequently found to contain maximum intensities quoted for gamma-ray transitions for which no 'visible' evidence was found in the spectra but the criterion used to establish this maximum intensity is not frequently found. In this work the criterion used is that a peak is deemed to

exist when its statistical significance expressed as a number of standard deviations of the continuum plus peak is greater than four standard deviations.

i.e.
$$\frac{N_p}{\sqrt{N_p + N_B}} \geqslant 4 \quad \ldots\ldots\ldots 2.2$$

where N_p = no. of events in peak

N_B = no. of events under peak

The search for weak intensity peaks can be divided according to the major source of continuum under the prospective peak. When this continuum is due to high energy transitions from the source of interest the figure of merit for the detector system is largely its ability to produce full-energy events rather than lower energy Compton events (i.e. its peak to Compton ratio) as well as the general requirement that the absolute full-energy peak efficiency and resolution are as high as possible. Fortunately these requirements are compatible with each other (but not with cost) and, in general, the sensitive volume of the detector may be increased without decrease in resolution and with a consequent increase in peak to Compton ratio - a typical detector having a sensitive volume of about 60 cm^3, a resolution of 2.5 keV for ^{60}Co, a peak to Compton ratio of 30:1 and a photopeak efficiency of 10% relative to a 3"x3" NaI crystal for ^{60}Co.

When the weak peak is at an energy above that of the major transitions in the source then the continuum is due largely to Compton events generated by background radiations. Although the general requirements of high efficiency, resolution and peak to Compton ratios apply here, the ability of the complete detector system to count rapidly is of equal importance. If for example a given system can count (without significant deterioration in resolution) at a rate such that the intensity of a peak, N_p, resulting from the source and which can just be detected above the background continuum, N_B, in time t is produced. Then to detect a peak of intensity aN_p (a less than1) the counting time required is kt where:

$$\frac{a\,N_p\,k}{\sqrt{N_B\,k}} \geqslant 4 \qquad \text{where } N_p \ll N_B$$

or since $$\frac{N_p}{\sqrt{N_B}} = 4$$

$$k^2 \geqslant 1/a \quad \ldots\ldots\ldots\ldots\ldots \quad 2.3$$

Thus if the required detection level is say 0.5 that obtained in time t, the time to reach this level is 4t.

The highest possible performance is required from both the detector and its supporting electronic system to

investigate the intensities of weak gamma-ray transitions in those isotopes where this information is still unestablished.

2.7 The use of Ge(Li) detectors in a coincidence mode

Weak intensity gamma-ray transitions can often be more easily identified by effectively removing the Compton continuum events beneath the peak. The use of an anti-Compton shield for the detector is well known but unless a large (expensive) NaI annulus can be employed the reduction in Compton events, although significant, is often not sufficient to reveal the peak of interest. The more useful technique which employs two gamma-ray detectors operated in a coincidence mode, not only often achieves the required reduction in Compton events, but can supply additional useful information about the structure of the decay scheme and the lifetimes of its energy levels.

The use of a coincidence mode system does, however, suffer from several disadvantages and the use of a singles spectrum technique or a coincidence mode must be carefully evaluated for a particular situation.

A typical Ge(Li) detector does have a very poor efficiency compared with a NaI crystal (at best 10% - the 25 cm^3 detector used in this work was about 4% for ^{60}Co). This means that two such detectors used in coincidence would have a coincidence efficiency of only 1% that of a system

using two 3"x3" NaI crystals. This severe reduction in coincidence efficiency, coupled with a timing performance which is no better than the NaI system, enhances the poor true to chance ratio typically obtained with a moderately sized source; thus resulting in the general requirement that a weak source be used with the resulting long times necessary to collect a statistically significant result. The obvious advantage of Ge(Li) detectors is their resolution which enables the energy gate to be more selective; this feature finding particular application in the study of isotopes with close lying gamma-ray transition energies.

A significant improvement can be made when several possible cascades are under investigation by using a form of dual-parameter processing. This can be accomplished by using two ADCs so that when any two events are coincident each ADC analyses the signal from its respective detector and a pair of coincident addresses are written into some form of storage. A search (computer aided) through the data can then select any required addresses fromone detector and thus determine all pulses in the other detector which are in coincidence. Thus all possible coincidence spectra from a given isotope can be collected simultaneously.

CHAPTER 3 ANALYSIS OF EXPERIMENTAL DATA

3.1 General considerations

The main features of a gamma-ray spectrum taken with a Ge(Li) detector are well known. When an isotope contains several competing modes of decay, the resulting spectra must be processed to reveal the areas and positions of the full-energy peaks produced by each gamma energy so that the transition intensities and energies may be obtained. The full-energy peak areas must be separated from each other and from the Compton continuum of the same energy produced from higher energy gamma-rays. The extraction of these peak areas and positions requires that an estimate of this continuum under the peak can be made from consideration of the surrounding continuum and that the general form of the peak shape produced by the detector system is known so that overlapping peaks may be separated for analysis.

Once the peak areas and positions are established it is then necessary to refer to the efficiency and energy calibrations to establish the intensities and energies respectively. It is thus desirable that the relevant calibration curves should be fitted by a mathematical function to effect an interpolation between the data points. This can be achieved in some circumstances by fitting the entire

set of calibration points with a suitable function or by using a more limited approach of interpolating between two encompassing calibration points.

Finally a checking system is required to eliminate peaks formed in the spectrum by 'spurious' effects (see section 2.5).

3.2 Initial approaches to analysis

Visual examination of a gamma-ray spectrum will reveal the main full-energy peaks and some estimate can be made of their positions. Their areas can be measured if the background beneath them can be measured. The problem of the technique to be used for this 'background' subtraction has recently been discussed by Pratt[18] but many approaches are in current use. Some authors adopt the approach[19] involving the drawing of two straight lines through the surrounding high and low energy continuum points and using as the zero line for full-energy events a straight line drawn between two points, one on the low energy side and the other on the high energy side of the peak where the actual spectrum deviates from the relevant straight line. A second technique is to fit a smooth curve (usually a second or third order polynomial) to the data points on either side of the full-energy peak which are considered to represent pure Compton events. This latter approach was tried initially and computer routines were written by the author

to achieve it but it was felt generally desirable to adopt an approach which did not place such emphasis on subjective assessment of the 'ends' of the full-energy peak. The technique finally adopted involved the fitting, in the least squares sense, of a mathematical function which describes both the background continuum and the full-energy peak shape to the data points.

The use of the experimental calibration data (energy and relative efficiency) was initially achieved by using a linear least squares fitting procedure to the energy data and by reading the relevant efficiency data from a smooth curve drawn through the calibration points.

A simple computer programme was also written by the author to generate the positions and the rough intensities of the spurious peaks to be expected in a typical spectrum; given the major modes of gamma decay.

3.3 The use of a computer programme in the analysis of gamma-ray spectra

The vast quantity of data, necessarily generated when a gamma-ray spectrum is recorded from a Ge(Li) detector system, is obviously more easily reduced if use can be made of a computer programme to search for full-energy peaks and to determine their areas and positions.

Ideally, the programme should then incorporate routines to effect the energy and efficiency assignments and thus provide a full analysis in terms of energies and intensities of the gamma-ray transitions present.

Many techniques for such programmes are reported in the literature[20,21,22]. The coding of two programmes was obtained. The first tried[23] was not entirely suitable as it was designed to analyse neutron time-of-flight spectra and identified its peaks by locating regions where successive data points increased or decreased in magnitude with respect to an assumed linear or parabolic background. This had the serious disadvantage that Compton edges appeared (to the programme) as peaks but failed to be fitted by a standard peak shape - thus causing the programme to fail! The second programme was a copy of Sampo[24] and this excellent, purpose built programme, was used throughout the analyses reported in later chapters.

3.4 The general features of Sampo

The detailed mathematical techniques used in this programme are fully described by Routti et al.[24]. The application of the programme to a typical Ge(Li) gamma-ray spectrum is illustrated below.

Taking a typical spectrum of ^{226}Ra obtained with

the 25 cm^3 detector, the computer programme was used to locate the exact channel locations and the areas of the full-energy peaks and thus to determine the energies of the corresponding gamma-rays. Since the intensities of the main gamma-rays in the decay of ^{226}Ra are well established, the areas of the full-energy peaks were then used to determine a relative efficiency curve for the detector.

The first stage in the analysis of the spectrum involved the selection of a few strong, well-isolated lines in the spectrum to be used as peak shape standards. Since the peak shapes are found to vary with gamma energy it was necessary for the analysis of some spectra to run extra spectra of calibration isotopes to obtain isolated lines well distributed over the range of interest. The peak shape is approximated by a Gaussian function with exponential tails at both high and low energies. The peak shape parameters; - the width of the Gaussian and the distances from its centroid to the junction points of the 'tails' are found to vary smoothly with energy so that their values for any other line in the spectrum can be found by interpolation. The fitting of this function and a straight line approximation for the continuum is performed by a least squares technique and the programme provides a printed result of the numerical information of the fit, the final peak shape parameters

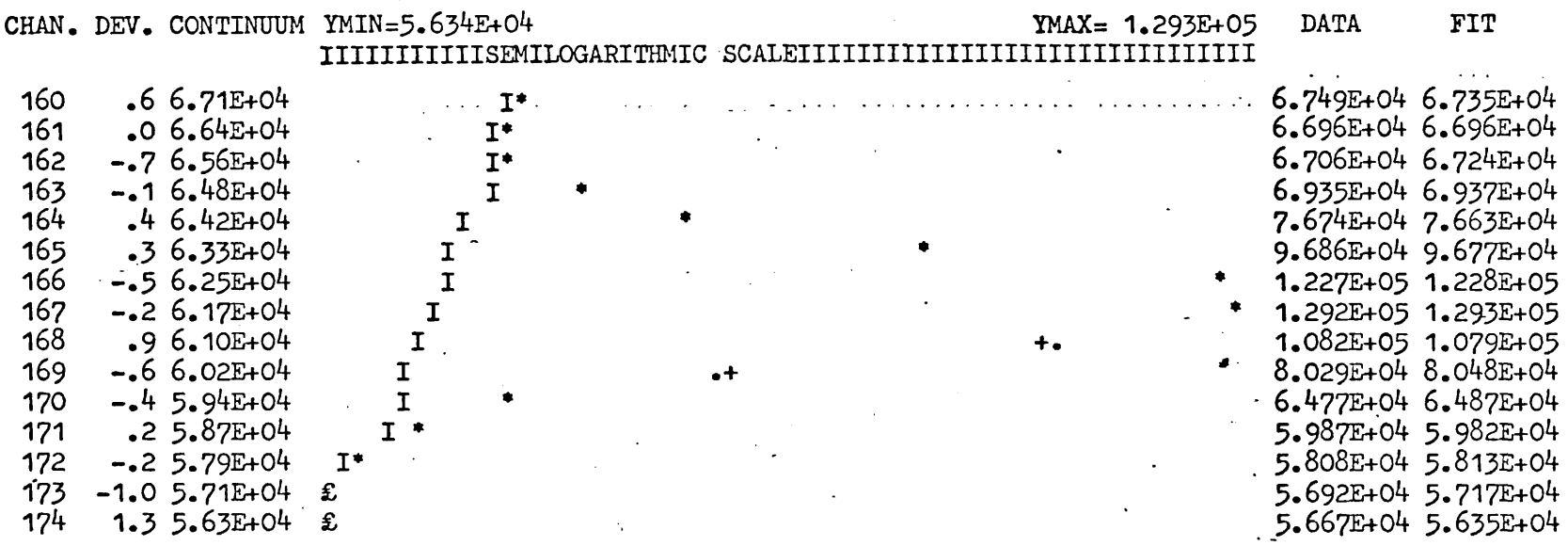

FIGURE 3.1 An example of the routine to find peak shape parameters

and a line-printer plot of the data and fit so that a visual assessment can be made. In addition, the numerical information of the residuals (in standard deviation units) of the fit and the chi-square value for the fit are given. An example of this operation is shown in figure 3.1.

Once a good table of shape parameters has been obtained, an automatic peak searching routine can be called which lists all potential peaks in a spectrum together with the results of a statistical significance test and a line shape test. The spectrum can then be broken up into fitting regions (initially an automatic routine is used for this) and then the accurate channel locations and peak areas are determined by fitting the data points with the predetermined line shapes and a polynomial approximation for the continuum. Again the numerical information of the fit is printed so that a visual assessment may be made and unresolved peaks may be seen from the residuals of the fit. The best goodness of fit and the fitting of small lines close to intense lines is often not achieved by the automatic selection of fitting intervals and it is then performed with a routine FITS by specifying the region of the spectrum and the approximate channel locations of the peaks. An example of a region of a ^{226}Ra spectrum which has been fitted in this way is shown in figure 3.2.

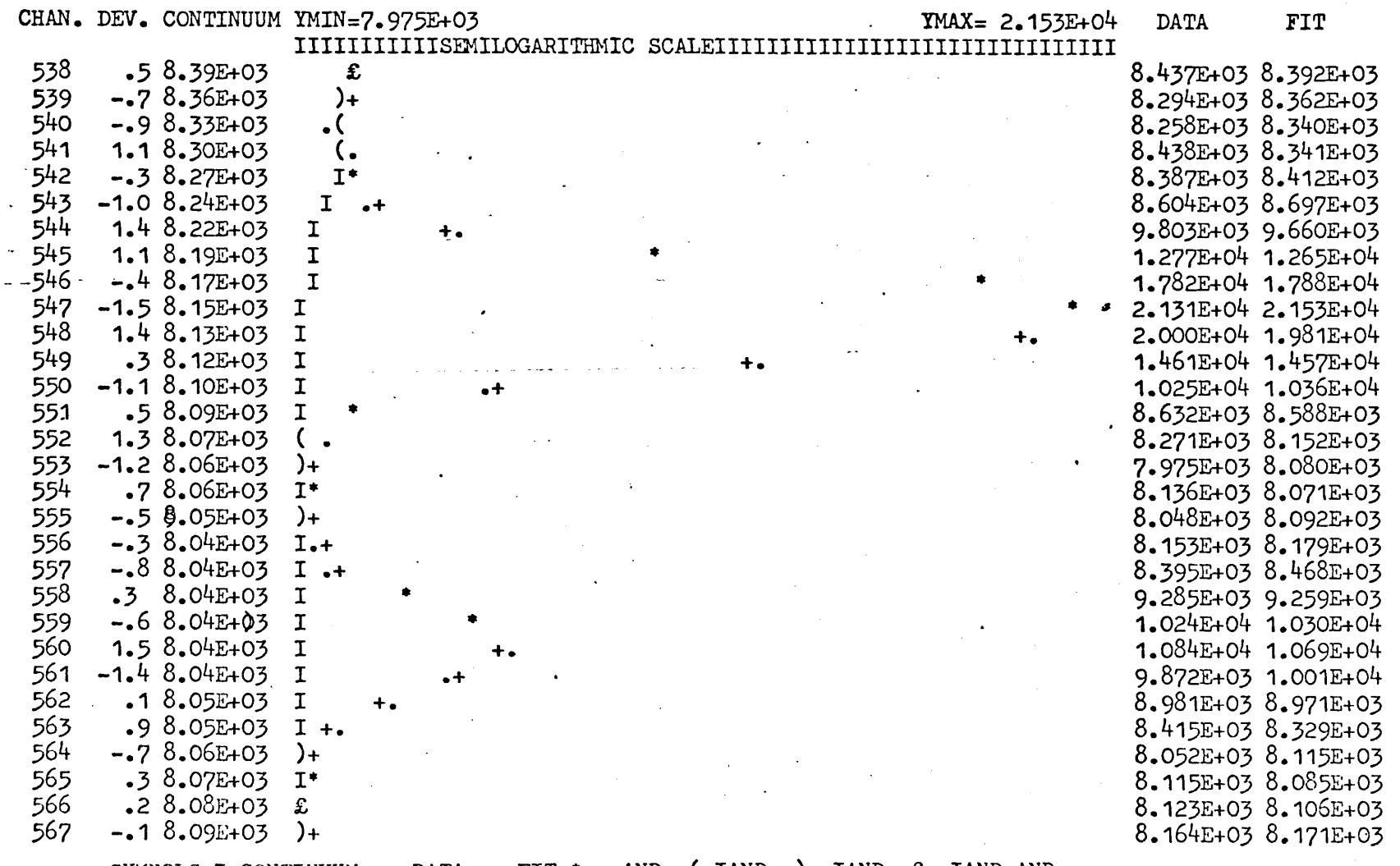

FIGURE 3.2 An example of the routine FITS

FIGURE 3.2 (continued)

SUMDATA= 6.07484E+04 SUMCALC= 6.07250E+04

RESULTS FROM THE ABOVE FIT, BE CRITICAL WITH THE ERROR ESTIMATES
REJECT IF CHISQUARE = 2.3387E+01 OR SIGMA= 1.055 IS UNACCEPTABLE,CHECK PLOT FOR MISSING PEAKS

CHANNEL	FIT-ERR-CH	ENERGY-KEV	CAL-ERR-KEV	EN-ERR-KEV	AREA-COUNTS	FIT-ERR-PC	INTENS-COUNT
EFFICIENCY DATA NOT READ IN							
547.2021	.0051	768.6481	.5000	.5000	5.0623E+04	.2981	5.0623E+04
EFFICIENCY DATA NOT READ IN							
559.8475	.0225	786.1247	.5000	.5010	9.9783E+03	1.4138	9.9783E+03
EFFICIENCY DATA NOT READ IN							
572.7931	6.0983	804.0153	.5000	8.4423	5.4570E+04	1.5613	5.4570E+04

TIME IN SECONDS= .033 3.384 .214 10.594 DATE= 10/05/72

RUN NUMBER AND INDICATIVE DATA

24.4.72 RA 226 AT 20 CM FROM 25CC DETECTOR

COMMENTS=

The energy calibration of the spectrum can be made by one of two methods. One method uses a number of energy calibration points and interpolates linearly between them. The other method fits a polynomial to the points and then uses the resulting curve (defined by parameters which are printed out by the programme for future use) for the energy assignments. The errors associated with the energy determinations are estimated by combining in the root mean square sense the errors in the peak centroid and the errors in the calibration points.

In the usual application of the programme, the intensities of lines in a spectrum can then be determined if a set of relative efficiency calibration points is available. These can be obtained from a spectrum such as ^{226}Ra if the intensities of the main gamma lines are known. The programme then calculates, from the fitted peak area, the relative efficiency at a given energy and thus assembles a table of relative efficiency calibration points. These can be used by the programme in two ways. The first method is to use a logarithmic interpolation procedure between the points. The second method fits a mathematical representation of the efficiency curve to the data. The equation is given in section 2.4.1 (equation 2.1).

The parameters found by the least squares fitting routine are printed out so that they may be used in other runs. The errors associated with an intensity calculation are obtained by adding in the root-mean-square sense the calibration error and the statistical error associated with the peak area.

Finally, the programme can be requested to print out all calibration details and a table of results giving channel locations, energy assignments, peak areas and intensities together with their respective areas.

In practice, this programme was found to be very effective and efficient. It was found that the peak shape calibrations had to be very carefully scrutinized until the best fit was obtained and even when this was done it was found that some regions of spectra were particularly difficult to fit. The use of the peak fitting routines was found to give slight difficulties when a peak or group of peaks was situated on a rapidly varying continuum but variations in the fitting region could usually achieve a good fit. In spite of these small difficulties it was felt that the programme provided a reliable and consistent means of extracting information from a gamma spectrum and it was used to process all the data reported in this work.

CHAPTER 4 TIME ANALYSIS AND COINCIDENCE MODE SYSTEMS

4.1 Introduction

The purpose of timing systems in nuclear spectroscopy is discussed together with the general requirements of such systems. The main sources of timing uncertainty and their origins are outlined for scintillation counter and Ge(Li) detector systems. A complete fast-slow coincidence system suitable for gamma-gamma spectroscopy is analysed and consideration is given to its adjustment for optimum performance. Sources of error in the resulting spectra are then considered.

4.2 General reasons and requirements for time measurements

The evaluation and interpretation of complex nuclear decay schemes is often greatly simplified by isolating those transitions which satisfy a specified time relationship with each other. Commonly this means identifying two transitions which follow each other within a resolving time, 2τ, (usually of the order of a few nanoseconds) and are thus designated as prompt transitions. A natural extension of this is to determine two transitions which are separated by a time $t \pm \tau$ and which are thus correlated in the same sense as are 'prompt' transitions. These observations often serve to place unambiguously a second transition in a decay scheme when a first transition is well established. The method relies on

the lifetime of the intermediate level being considerably smaller than the resolving time of the measuring system for 'prompt' transitions and typically of the order of nano or microseconds for delayed coincidences. The electronic system used to provide this information is a coincidence system and the signals derived from the detectors which are processed by the system are known as timing signals. With modern electronic systems the actual 'intrinsic' instrumental resolving time, $2\tau_0$, of the coincidence unit employed is frequently one or two orders of magnitude better than the resolving time imposed on the system by the requirement that a reasonable fraction of all events which are in reality prompt are registered as such by the system. The electronic processing of the detector signal prior to its presentation to the time analyser contributes to a large degradation of the intrinsic performance of a typical fast coincidence unit.

4.3 Outline of timing systems and the assessment of their performance

A typical electronic system used to process the signals from two detectors for time analysis makes use of a time pick-off circuit to derive a standard pulse from the detector signal and which then conveys the time information to the time analyser (time to pulse height converter, TPHC,

or a fast coincidence unit). A TPHC gives an output pulse whose amplitude is proportional to the time difference between the arrival of the timing pulse from detector 1 and the arrival of the timing pulse from detector 2. The absolute magnitude of these time differences is unimportant in the assessment of the performance of the system; the criterion necessary to judge the system is the spread of the time differences with respect to time. Ideally two genuinely prompt nuclear transitions in the source should produce a time distribution as measured with a TPHC which is simply due to the statistical spread of emission times of the photons corresponding to the transitions. Due to the non-ideal performance of the detection and analysis of these events this spread of times is completely masked and the TPHC output, recorded on a multichannel analyser (MCA), reveals a time spectrum whose origin is due to the analysis of the electrical signal created in the detector. The time spectrum can thus be used to assess the performance of the time pick-off circuits and to deduce a sensible value of resolving time to be set by a fast coincidence unit which can replace the TPHC for use in a typical nuclear spectroscopy application. Such a coincidence unit can be considered to select those events which fall within a given window on the time spectrum; the resolving time, 2τ, of the coincidence

unit giving the width of such a window.

For a Gaussian time distribution the coincidence efficiency of a system employing a coincidence unit with 2τ set equal to the full width at half maximum (FWHM) of the time spectrum is about 76% and rises to 98% when 2τ is set equal to the full width at tenth maximum (FWTM) of the time spectrum.

The performance of time pick-off circuits can also be assessed from the shape of the 'delay curve' obtained from the output rate of a fast coincidence unit when one or both of its input signals are moved (delayed) in time with respect to each other. This method is much more tedious and the information contained in such a curve needs careful 'unfolding'.

4.4 Requirement of small resolving time in a system

Since initially simultaneous events can not be registered as such by a coincidence system, an additional 'nuisance' becomes apparent in any system. The arrival at the coincidence unit of two non-related signals within the set resolving time will generate an output signal which is indistinguishable from a true coincidence event. The number of such chance coincidences per unit time, N_c, and their relationship to the true coincidence rate, N_t, is of critical importance in most spectroscopy applications. These relationships can be seen as follows.

Consider a source emitting N photons per second and detected by two detectors having absolute efficiencies e_1 and e_2 respectively. The singles counting rates observed at the two detectors are N_1 and N_2 respectively where:-

$$N_1 = e_1 N \quad \text{and} \quad N_2 = e_2 N$$

The true coincidence counting rate is given by N_t where

$$N_t = e_1 e_2 I N \quad \ldots\ldots\ldots\ldots\ldots 4.1$$

where I is the coincidence intensity[25].

The chance counting rate observed with a resolving time 2τ is given by: -

$$N_c = 2\tau N_1 N_2$$

or, substituting for N_1 and N_2

$$N_c = 2\tau e_1 e_2 N^2 \quad \ldots\ldots\ldots\ldots 4.2$$

and the true to chance ratio, G, is given as:-

$$G = I / 2\tau N \quad \ldots\ldots\ldots\ldots\ldots 4.3$$

From equation 4.1 it can be seen that N_t is proportional to e_1, e_2 and N. (I is outside our control and only features in overall considerations of investigation feasibility). Thus it is desirable to maximize the efficiencies of the detectors used.

From equation 4.2 it is apparent that the chance rate is directly proportional to the resolving time utilised and hence the general requirement that this should be as small as possible. From equation 4.2 it is also clear that the chance rate increases as the square of the source strength and thus, although equation 4.1 might suggest that the source strength should be high to increase the true coincidence counting rate, it is clear that a compromise must be made as measured by the true to chance ratio, G, which is inversely proportional to the resolving time and the source strength, N.

The overall picture is then to maximize the counter efficiencies and to minimize the resolving time required in order to yield a given statistical accuracy on the true coincident counts.

4.5 Causes of non-ideal time spectra

The observed spread in the time spectrum can be attributed broadly speaking to two main causes. These are known as walk and jitter.

Jitter is a source of timing error which is statistical in nature. It is the intrinsic time jitter of the detector signal as seen by the time pick-off device. Jitter can be generated in the detector itself or in the

electronic instruments required to amplify the signal prior to the time discriminator and also in the actual time discriminator. The effect of jitter on the time response of a discriminator output gives rise to a variation in the time at which the signal crosses a fixed discriminator.

Walk can be introduced into a timing signal obtained from a time discriminator as a result of variations in input pulse amplitude or rise time from the detector. The main features of walk are illustrated in figure 4.1. Figure 4.1 (a) illustrates the case found in both scintillation counters and semiconductor detectors where two signals caused by events occurring at the same time have the same rise time but different amplitudes. There is thus a shift in time of crossing the discriminator threshold which becomes increasingly serious as the threshold approaches the pulse height and as the rise time of the pulse increases. Also any real discriminator is usually charge driven and will delay firing until it has collected a certain charge. The time to do this, t_1, t_2, will increase as the threshold increases towards the amplitude of the pulse and thus any discriminator must be designed to minimize the charge necessary to trigger it. Figure 4.1 (b) illustrates the case of pulses originating at the same moment in time with equal amplitudes but having different rise times. This case is particularly apparent for

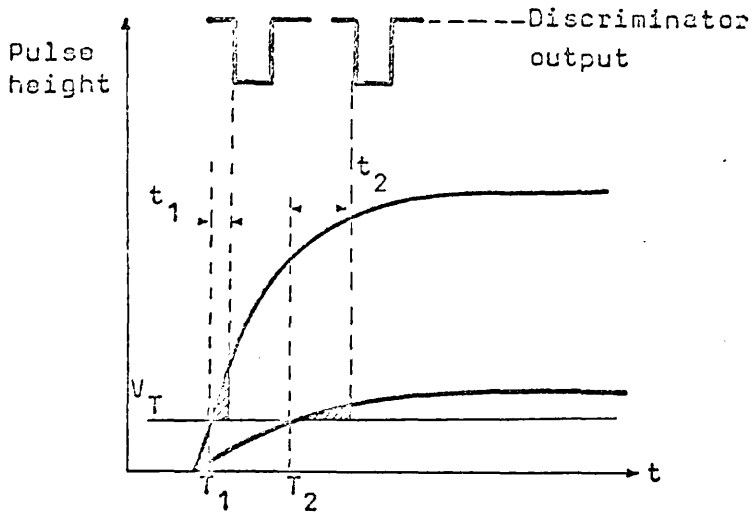

(a) Pulses of different amplitudes but equal rise time

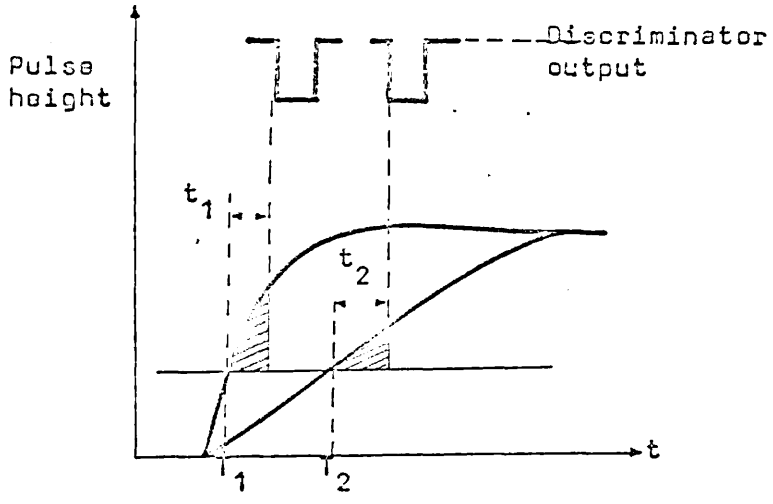

(b) Pulses having same amplitude but varying rise times

FIGURE 4.1 Origins of timing walk obtained with a fixed threshold discriminator

coaxial Ge(Li) detectors where the rise times of pulses can vary considerably.

4.6 Origins of jitter and walk for scintillation counters and for Ge(Li) detectors

In a scintillation counter system jitter is generated both by the statistical nature of the light emission in the scintillator and also by the photomultiplier used to convert the light into an electrical signal when statistical processes in the emission of photoelectrons and in their transit time through the tube produce a jitter in the output signal with respect to time. The time behaviour of a scintillation counter can be assessed by considering the current pulse available at the anode which at t=0 is given[26] by:

$$I(0) = \frac{R}{\tau - \tau_1} \quad \ldots\ldots\ldots\ldots 4.4$$

where τ_1 is the rise time constant of the photomultiplier and τ the decay time constant of the scintillator and assuming an ideal photomultiplier with no transit time fluctuations. R is the total number of photoelectrons per scintillation.

For a NaI scintillator and a fast photomultiplier tube $\tau_1 \ll \tau$ (and $\tau \sim 250$nS) so the time resolution of such a system is determined by R/τ. Thus it is desirable to use a

high gain tube.

Walk is generated in any timing discriminator following a scintillation counter due to the finite rise time of the output pulse generated at the anode. For a NaI scintillator this rise time can be dramatically improved by processing the pulse in a current mode.

If the anode load used with the photomultiplier tube is of the order of 50 or 100 ohm (typical values used with 'fast' photomultipliers) then the anode time constant, τ_a, is very much smaller than τ and the output pulse is designated a current pulse with rise time determined mainly by the rise time of the photomultiplier tube. This can be of the order of 2 nS with a 'fast' photomultiplier even for NaI scintillators so that walk can be considerably reduced by this method. The use of an anode time constant considerably greater than τ gives an integrated output pulse with rise time comparable with the decay time of the scintillator. This voltage mode of operation represents the classical use of a NaI scintillator and photomultiplier where the output has a rise time of about 250 nS. This is, however, the mode necessary to obtain the best energy resolution which is degraded by the use of an anode time constant significantly less than τ[27].

For a semiconductor detector the actual time accuracy of an event depends on the signal obtainable at the output of the subsequent amplifier and the noise of this amplifier plays a dominant part in the final time accuracy due to jitter. For a Ge(Li) detector the most serious timing spread comes from walk. This has two origins; that of pulses having the same rise time but differing amplitudes and that of varying pulse rise times.

4.7 Methods used for the extraction of a fast timing signal

Fast timing describes the application of techniques to a system which minimise the effects of jitter and walk. The choice of the appropriate method depends on the detector, the required time resolution (measured as the FWHM of a TPHC spectrum) and the range of input pulse heights to be processed (measured as the dynamic range accepted and given by $(E + \Delta E)/E$ where E and $E + \Delta E$ represent the lower and upper energies admitted respectively). In general three main methods are available and have found application for both scintillation counters and semiconductor detectors. These are leading edge, cross-over and constant fraction timing. An extension of the constant fraction method known as amplitude and rise time compensation (ARC) offers advantages for Ge(Li) detectors.

The simplest type of time pick-off system is the leading edge discriminator which was used in the present work. Here a fixed threshold discriminator is used with its threshold set as low as possible (consistent with the noise level) to minimise the effects of walk. This system gives good results only for a narrow dynamic range but its simplicity means that it finds frequent application especially where cost is of importance.

For a NaI counter the optimum performance is obtained when the discriminator threshold is set at about 0.01 of the pulse height. The typical good performance figures quoted for a NaI - fast photomultiplier response are a FWHM of the order of 1 nS[28] for a very narrow dynamic range. Of more significance is the FWTM which increases very rapidly with the dynamic range used. Performance figures for a leading edge device built by the author for a NaI counter are given in section 5.3. Typical figures for a leading edge device used with a Ge(Li) detector range from 6 nS to 12 nS[29] FWHM dependent on the detector configuration used. The figures quoted are obtained by measurements against a plastic scintillator counter system when reported for a NaI system and against a NaI system for the Ge(Li) detector measurements. They therefore represent the 'true' performance for the detector concerned as the reference system response is negligible.

4.8 Fast - slow coincidence systems

A schematic outline of a fast - slow coincidence system is given in figure 5.9. The actual form used in this work and the methods used to adjust it for optimum performance are discussed in section 5.6.

During these studies it became necessary to analyse the performance of such a system in order to arrive at expressions for the final true to chance ratio obtained at the multichannel analyser (MCA) and a 'recipe' for the source strength and position to be used in a given experiment. The following analysis was made by the author.

For a correctly adjusted system, the pulse from detector A which triggers any output from the fast and then the slow coincidence units arrives at the MCA at a fixed time with respect to the linear signal from detector A which is analysed by the ADC when its internal gate is opened by a coincident gating signal. In the case of the MCA employed in most of this work (Northern Scientific NS630) the arrival of the 'A' pulse at the MCA was adjusted to be 0.5 μS later than the pulse from the slow coincidence unit which opened the coincidence gate of the ADC. This time delay allowed for the internal delay of the linear signal in the ADC.

At the fast coincidence unit the output is due to either true coincidences from the source where one photon entering counter A or B is followed within the resolving time

of the fast coincidence unit by a second related photon entering the other counter or to the random arrival of two photons at the counters within the resolving time of the fast coincidence unit.

At the slow coincidence unit these outputs from the fast coincidence unit are gated by pulses from detector B which fall within a selected energy interval. The slow coincidence unit thus gives an output pulse for one of two reasons. The true output pulses due to the selection of those true coincidences from the fast coincidence unit which also satisfy the energy requirement imposed on detector B, giving an output C_{TT} and a chance output giving a chance rate of C_{ABB} at the slow coincidence unit. It is important to note that C_{ABB} can arise from two sources. Either the pulse from B which was responsible for a chance output at the fast coincidence unit also satisfies the energy gate requirement or any pulse passing the energy gate together with an unrelated pulse from the fast coincidence unit which arrive within the resolving time of the slow coincidence unit can give rise to a chance output. At the MCA the true counting rate C_{TTT} is due to the true coincidence output from the fast coincidence unit satisfying the energy requirement on detector B and to the correct time arrival at the MCA of the 'A' linear pulse and the ADC gate opening pulse from the slow

coincidence unit. The chance spectrum at the MCA is due to the arrival of an 'A' pulse which also passes the chance selection requirements at the fast and slow coincidence units and to the random arrival of 'A' pulses with the output of the slow coincidence unit within the resolving time of the ADC gating arrangements.

The magnitudes of these terms can be related as follows:-

Let the counting rates be:

Singles from detector A above ADC discriminator = A

" " " " which triggers TPO = A'

" " " B " " " = B

True coincidences at fast coincidence unit = C_T

Chance coincidences at fast coincidence unit = C_{AB}

B pulses which satisfy energy gate = B_G

True coincidence output at slow unit = C_{TT}

Chance coincidence output at slow unit = C_{ABB}

True coincidences at MCA = C_{TTT}

Chance coincidences at MCA = C_{ABBA}

Resolving time of fast coincidence unit = $2\tau_F$

" " " slow " " = $2\tau_S$

Effective resolving time of ADC gate = $2\tau_G$

Also let B_G/B = x

The following relationships apply:

$$C_{AB} = 2\tau_F . A' . B \quad \ldots\ldots\ldots 4.5$$

$$C_{ABB} = 2\tau_S B_G (C_T + C_{AB}) + xC_{AB} \quad \ldots\ldots 4.6$$

$$C_{ABBA} = 2\tau_G A (C_{ABB} + C_{TT}) + C_{ABB} \quad \ldots 4.7$$

At the fast coincidence unit the true to chance ratio, G, is given as:

$$G = C_T / C_{AB} = I / 2\tau_F N \quad \text{from equation 4.3}$$

where I is the coincidence intensity

N is the source strength

At the slow coincidence unit:

$$C_{ABB} = xC_{AB} + 2\tau_S xB(G.C_{AB} + C_{AB}) \quad \text{from equation 4.7}$$

and thus

$$C_{ABB} = xC_{AB}(1 + 2\tau_S B(G + 1)) \quad \ldots\ldots\ldots 4.8$$

For $2\tau_S B(G + 1) \ll 1$ $\quad \ldots\ldots\ldots 4.9$

the result of the fast coincidence unit is simply modified by the energy gate fraction;

i.e. $C_{ABB} = x\, C_{AB}$

The slow coincidence resolving time can thus be said to degrade the chance output from the slow coincidence unit by s% where:-

$$2\tau_S B(G + 1) = s.10^{-2} \quad \ldots\ldots\ldots 4.10$$

The true to chance ratio at the slow coincidence unit is:-

$$G_S = C_{TT}/C_{ABB} = \frac{x' C_T}{xC_{AB}(1 + 2\tau_S B(G + 1))}$$

or
$$G_S = \frac{x'C_T/C_{AB}}{x(1 + 2\tau_S B(G + 1))} \quad \ldots\ldots\ldots 4.11$$

where x' is the fraction of all coincidences recorded which meet the energy requirement

x'/x is largely outside our control since it is mainly a function of the particular isotope and transitions under investigation.

so,
$$G_S = \frac{kG}{(1 + 2\tau_S B(G + 1))} \quad \ldots\ldots\ldots 4.12$$

where $k = x'/x$

Thus the maximum G_S is obtained when $2\tau_S B(G + 1) \ll 1$ which is as predicted by equation 4.9

and
$$G_S(max) = k.G \quad \ldots\ldots\ldots\ldots 4.13$$

When equation 4.9 is satisfied the resolving time of the slow coincidence unit does not contribute significantly to the final chance rate.

At the MCA:-

$$C_{ABBA} = 2\tau_G A(C_{TT} + C_{ABB}) + C_{ABB}$$

or
$$C_{ABBA} = (2\tau_G A(G_S + 1) + 1)C_{ABB} \quad \ldots\ldots\ldots 4.14$$

so provided that

$$2\tau_G A(G_S + 1) \ll 1 \qquad \text{then } C_{ABBA} = C_{ABB} \quad \ldots 4.15$$

and then the resolving time of the ADC gate does not contribute significantly to the final chance rate.

If also equation 4.9 is satisfied then,

$$C_{ABBA} = x\, C_{AB} \quad \ldots\ldots\ldots\ldots\ldots 4.16$$

The final chance rate is simply that of the fast coincidence unit modified by the energy selection.

This gives the final true to chance ratio at the MCA as:-

$$G_F = C_{TTT}/C_{ABBA}$$

$$= C_{TT}/C_{ABBA} \text{ if we assume that all true}$$

coincidences at the slow unit are registered at the MCA.

since $C_{TT} = G_S C_{ABB}$

then $G_F = G_S\, C_{ABB}/C_{ABBA}$

$$= \frac{G_S}{(2\tau_G A(kG + 1) + 1)} \quad \ldots\ldots\ldots 4.17$$

assuming that equation 4.9 is satisfied.

The maximum true to chance ratio obtainable at the MCA is then:-

$$G_F(\max) = k.G$$

$$\text{when } 2\tau_G A(G_S + 1) \ll 1 \quad \ldots\ldots\ldots 4.18$$

As for the slow coincidence unit the MCA gate can be considered to degrade the best chance rate obtainable by g% where:

$$2\tau_G A(kG + 1) = g.10^{-2} \quad \ldots\ldots\ldots\ldots 4.19$$

These considerations thus show that the final true to chance ratio obtained at the MCA is that of the fast coincidence unit modified by a factor k, provided that the conditions given by equations 4.9 and 4.15 are met.
k is the ratio x'/x which is a function of the particular isotope and transitions under consideration. The maximum true to chance ratio obtainable can, for small percentage deviations, be considered to be degraded by the resolving time of the slow coincidence unit as given by equation 4.10 and by the MCA gate as given by equation 4.18.

A fast - slow coincidence system to study a particular isotope may be optimised by the following procedure:-

Taking the minimum acceptable true to chance ratio at the MCA gate as $G_S(min)$ and with a knowledge of the ratio x'/x for the transitions of interest the minimum true to chance ratio at the fast coincidence unit may be found from equation 4.13 as:-

$$G(min) = \frac{G_S(min)}{k} \quad \ldots\ldots\ldots\ldots 4.20$$

With the coincidence intensity, I, evaluated the maximum usuable source strength, N(max), can be found from equation 4.3 as:

$$N(max) = \frac{I}{2\tau_F G(min)} \quad \text{photons/sec} \quad . \; . \; . \; 4.21$$

A knowledge of the main features of the decay scheme can then give a source strength in μCi.

The maximum singles counting rates B_{max} and A_{max} for a given degradation in the chance rate can be found from equations 4.10 and 4.18 as:

$$A_{max} = \frac{g.10^{-2}}{2\tau_G(kG + 1)} \quad . \; . \; . \; . \; . \; . \; . \; . \; . \; . \; 4.22$$

$$B_{max} = \frac{s.10^{-2}}{2\tau_S(G + 1)} \quad . \; . \; . \; . \; . \; . \; . \; . \; . \; . \; 4.23$$

and, provided that these are consistent with the total counting rate capabilities of the system, the source position can be adjusted to give these rates bearing in mind the possibility of inter-counter scattering. A knowledge of the counter efficiencies would then allow an estimate of the time to collect a given number of true coincidences to be made from equation 4.1.

This analysis of a fast - slow coincidence system

was used to calculate the optimum source strength for use in the coincidence studies reported in chapters 6, 7 and 8. In addition, it was used to assess the feasibility of several proposed coincidence investigations.

4.9 Corrections to coincidence spectra and possible sources of error

The coincidence spectrum obtained with a fast - slow system has frequently to be corrected for contributions due to (a) chance coincidences and (b) coincidences arising from photons corresponding to transitions with energies higher than the energy gate region but which are detected by their Compton interaction which falls at an energy passing the gate requirements set by the single channel analyser. These 'Compton' coincidences can thus give rise to full-energy peaks in the coincidence spectrum which are not in coincidence with the full-energy peak used for the energy gate. Corrections can be applied to the coincidence spectrum for these two cases.

Chance coincidences can be assessed by delaying the pulse from detector A by say 1 μs so that only chance coincidences are produced at the fast coincidence unit. The delay to the MCA of the linear energy pulse from detector A must also be increased by the same amount to preserve the correct timing conditions at the MCA. Assuming that the

contributions to chance from the slow coincidence unit resolving time and the ADC gate 'effective' resolving time do not make an excessive contribution (see section 4.3) then a spectrum recorded in this way is a reliable (but time consuming) assessment of the chance contribution.

An alternative method which allows for chance coincidences can be obtained provided that the contributions due to the resolving time of the slow coincidence unit and the ADC gate are negligible. Equation 4.16 shows that the final chance spectrum counting rate under these conditions can be obtained as follows:-

$$C_{ABBA} = x\, C_{AB} \quad \text{where } C_{ABBA} = \text{chance counts } S^{-1}$$

$$= 2\tau_F . A . B . x$$

$$= 2\tau_F . A . B_G \quad \ldots\ldots\ldots\ldots \quad 4.24$$

where A = singles detector A above ADC discriminator

B_G = gate counting rate

The resolving time of the fast coincidence unit can be measured by using two separate sources and with the two detectors completely isolated from each other so that the coincidence output from the fast coincidence unit, N_C, is recorded when the singles rates N_1 and N_2 are present at the two input channels.

Then provided that N_C is significantly less than N_1, N_2:

$$2\tau_F = N_C / N_1 N_2$$

With $2\tau_F$ determined the chance spectrum present during a given coincidence run can be calculated if the total gate counts are recorded and also a straight spectrum is recorded from detector A. (It is wise to gate this spectrum with its own timing discriminator output to achieve reliable results near the threshold of the discriminator).
The chance spectrum is then found for each channel as:-

Chance counts in channel n for a coincidence recording time t = $2\tau_F B_G t$ X channel n counts per unit time in singles spectrum from A.

This method avoids the long counting time associated with the earlier experimental method.

Coincidences due to Compton detected events in detector B can be assessed by moving the energy gate clear of the full-energy peak (high energy side) and, assuming a smooth Compton region, this method works reasonably well. The actual width of the gate can be adjusted slightly if necessary so that the area of Compton contribution remains constant. This can be measured as described in section 5.6 with the aid of the MCA.

A further possible source of error which occurs in close geometry systems is that of intercounter scattering. This means that a photon can enter detector A, undergo a Compton interaction and then scatter into detector B and there deposit part or all of its remaining energy which can satisfy the energy gate selection requirements[30]. When the energy gate is relatively narrow this can give a fairly sharp peak in the coincidence spectrum which could be mistaken for a coincident full-energy peak since it does not disappear when the usual corrections described above are made. The only solution (apart from elaborate counter shielding) is to calculate the possible range of such scattered coincidences from the geometry of the system and to adjust this geometry if necessary to check on the validity of any peak that may be due to this cause. Fortunately in the present work the energy gates were usually at least 10 or 15 keV wide so that any scattered peaks were too broad to be mistaken for a true full-energy peak.

CHAPTER 5 INSTRUMENTATION AND EXPERIMENTAL TECHNIQUES

5.1 Introduction

The design and testing of a scintillation counter and of electronic circuits constructed for use in gamma-gamma coincidence studies is described. A brief outline is given of the electronic systems used in this work together with details of their adjustment for optimum performance.

5.2 Scintillation counter

A scintillation counter, suitable for use with nano-second resolving times, was constructed by the author using an EMI photomultiplier tube 9594B and a $1\frac{1}{2}$"x$1\frac{1}{2}$" NaI scintillator. This photomultiplier tube is a focussed tube with a high gain and fast rise time of 2 nS with a FWHM of 3nS and a transit time of 50 nS. The base chain constructed for the tube was a standard non-linear chain as suggested by the manufacturers and included Zener diode stabilisation for the cathode-D1 voltage. A low output load (100 ohm) was used at the anode in order to satisfy the requirement (section 4.6) that the output was essentially a current pulse. The linear energy signal was taken from dynode 9 using a high output impedance. The focussing voltage adjustment was made at an overall voltage to the base chain of 2kV to give the maximum pulse amplitude. The anode pulse had then a rise time better than 5 nS.

The overall base chain voltage was maintained at 2kV as this gave the best timing performance. The energy pulse, extracted from the dynode, was processed with a charge sensitive preamplifier (Ortec 113) which produced an output with a decay constant of 50 μS suitable for the pole-zero cancelling network in the main amplifier. The energy resolution with an overall base chain voltage of 2kV was not spectacular (10% at 662 keV) but could only be improved by working at a lower tube voltage (1.6kV) with a consequent worsening in the time performance. However, the counting rate handling ability of the counter and amplifiers was good, - the resolution being maintained to about 20 kc/s..

5.3 Leading edge discriminator

A leading edge discriminator which is to be used with a NaI scintillation counter needs to be capable of triggering on a very small fraction of the input pulse height (0.01). Since the output of this discriminator is used to signal the time of arrival of the event to succeeding circuitry it should have a fast rise time and produce a standard amplitude signal. A simple device capable of satisfying these requirements is a tunnel diode used as a monostable circuit.

A typical tunnel diode characteristic is shown in figure 5.1a. A schematic biassing network and its equivalent

circuit (assuming an ideal tunnel diode without L and R) is shown in figure 5.1b. This biassing gives a load line of slope $1/R_B$ on the tunnel diode characteristic with intercepts of V_B and V_B/R_B on the 'V' and 'I' axes respectively. For monostable operation the value of R_B is selected so that the load line, as indicated, intersects the tunnel diode characteristic at one stable point below the peak current, I_p. When a trigger is applied to the tunnel diode such that an input current I_{in} is delivered to it where $I_1 + I_{in}$ exceeds I_p, the tunnel diode switches to its high voltage state. The actual transfer proceeds from point (1) to (1)' to (2) on the characteristic with a switching speed which depends on the charging of the diode capacitance, C_D.

$$\text{Since} \quad \frac{dV}{dt} = I_C / C_D \quad \text{where} \quad I_C = I_1 + I_{in} - I_p$$

then the speed is low when the input current only just carries the diode over its peak current. In practice this gives rise to a delay, t_d, in the output pulse which rapidly decreases with rising overdrive. When the input current pulse is cut-off the tunnel diode moves to point (3) as the voltage, V_I, across the inductance falls and the working point falls to (4). The tunnel diode then recovers to (1) as the current

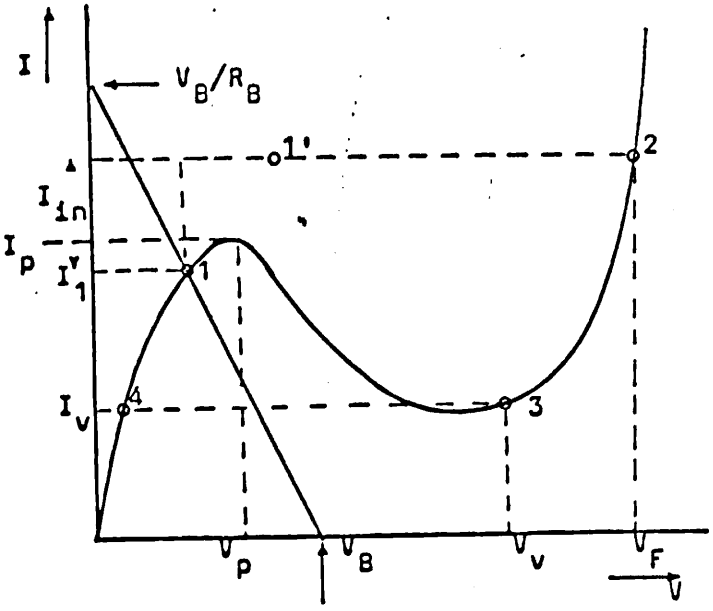

(a)

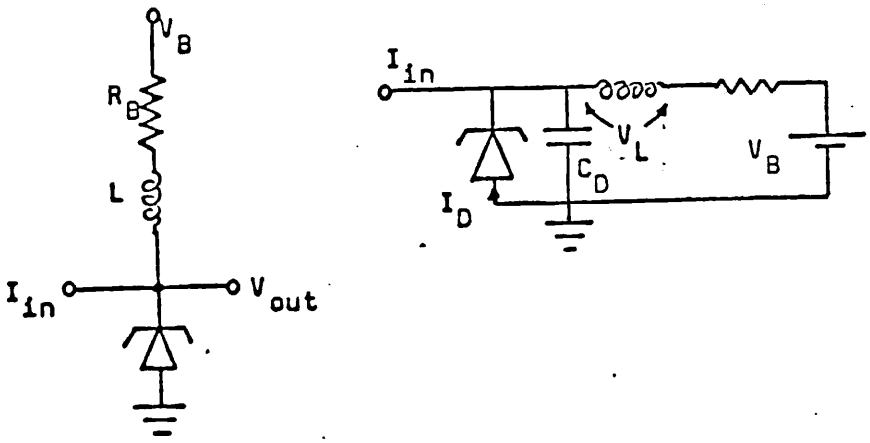

(b)

FIGURE 5.1 Tunnel diode monostable behaviour

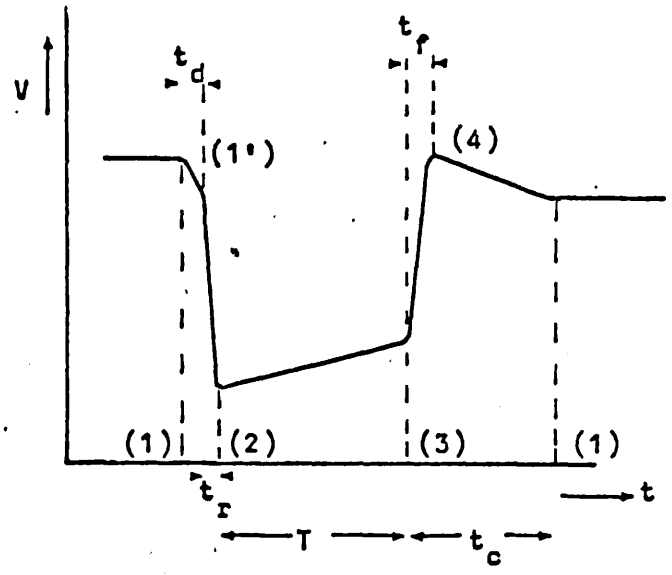

(c)

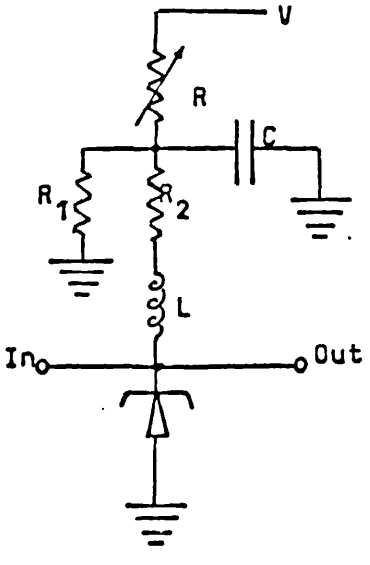

(d)

FIGURE 5.1 (continued)

through L rises. The corresponding output pulse is shown in figure 5.1c and is about 500 mV in amplitude.

In practice the bias for the tunnel diode is provided with a network of the form shown in figure 5.1d. The effective bias is given by

$$V_3 = R_1 / (R_1 + R_2 + R)$$

and the effective bias resistor by

$$R_3 = R_1(R_2 + R)/(R_1 + R_2 + R)$$

R provides a variable threshold whilst C decouples to earth providing a constant AC load line independent of the DC threshold set.

The tunnel diode selected was J.60A with a peak current of 5 mA This was used as it was necessary to provide a stable bias as near as possible (in terms of the dc current through the tunnel diode) to the peak current so that good overdrive was obtainable even for small input currents. Since this quiescent dc point was essentially voltage controlled by the biassing network, the low peak current tunnel diode allowed a smaller I_{in} to be used without significant output delay.

The output of this leading edge trigger needed to drive either a Harwell 2035C fast coincidence unit requiring an input pulse of 2V (or more) or an Elron fast coincidence

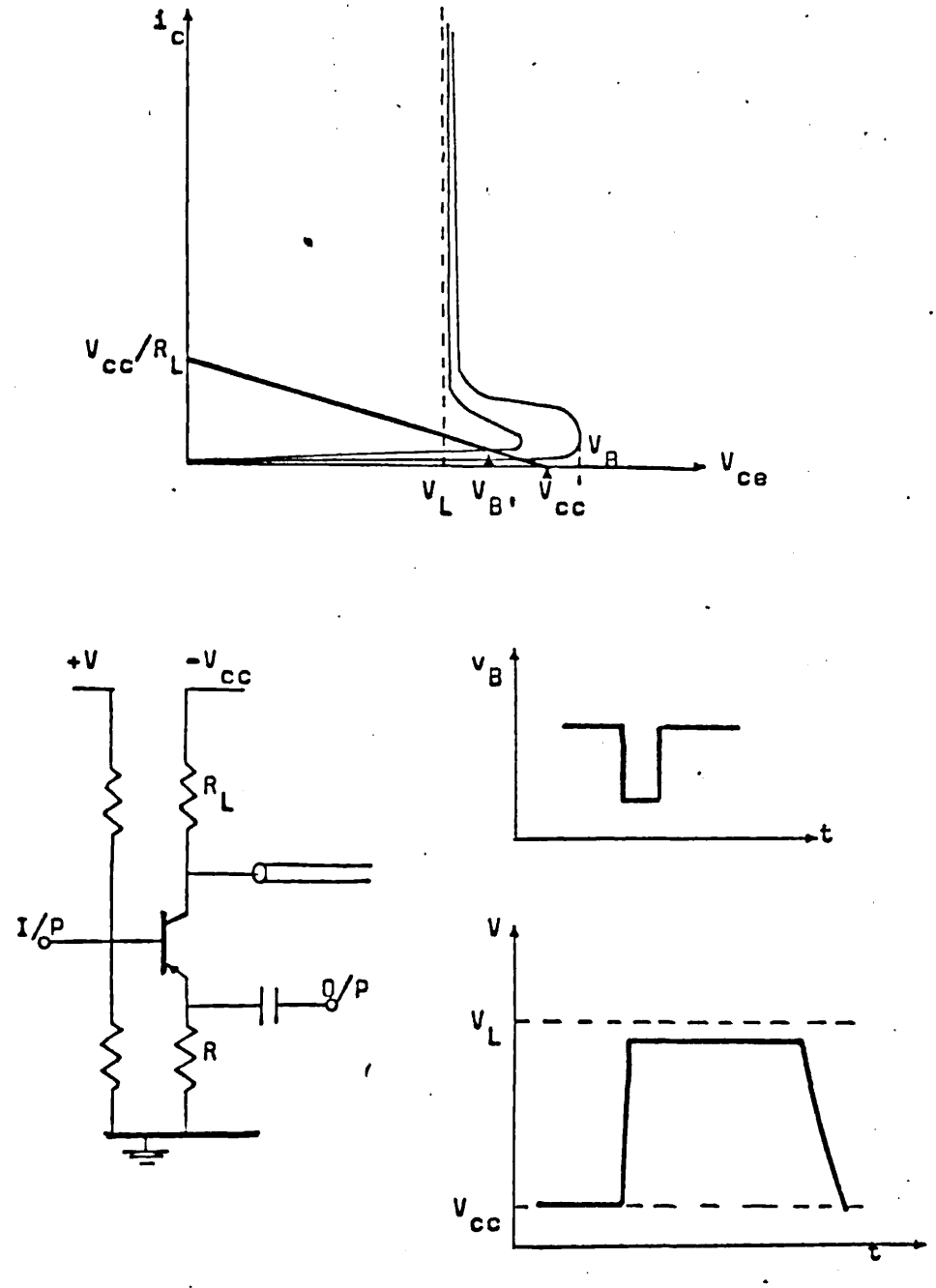

FIGURE 5.2 Avalenche mode of switching a transistor

unit requiring an input pulse height greater than 250 mV. The Harwell unit required an input pulse width longer than the required resolving time and the Elron required a width less than the required resolving time. The output stage of the discriminator made use of the avalanche mode of switching a transistor to obtain a very fast rise time output pulse with the desired amplitude and with easily controllable width.

The avalanche switching mode of operation is illustrated in figure 5.2 where the breakdown characteristics of a pnp transistor are shown. The transistor base is reversed biassed and the supply voltage, V_{cc}, and the load resistor, R_L, are selected to give a load line which intersects the transistor characteristics in a single point as shown. V_{cc} is then between the latching voltage, V_L, and the breakdown voltage, V_B, for the particular base bias. A small negative input to the base of the transistor lowers the breakdown voltage, V_B. The collector, which is initially at V_{cc}, with the coaxial line capacitance charged through R_L, falls towards the latching voltage and the line discharges through the transistor. Thus a positive voltage step travels down the coaxial line and is reflected at the open end, returning to the collector in a time $2t_d$ where t_d is the time down the line. The voltage step, on returning to the collector (which is at a fixed potential V_L), reduces the current through the transistor

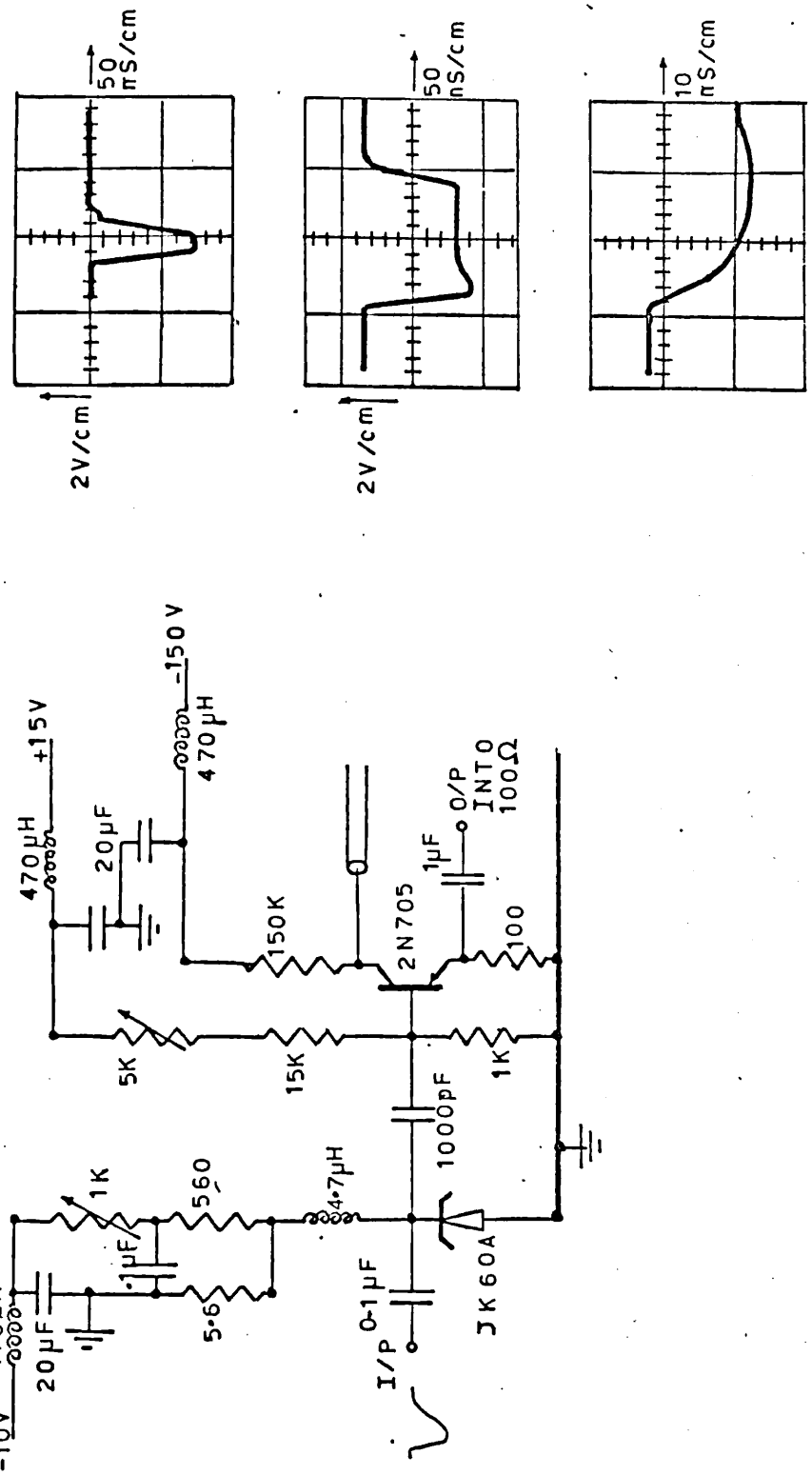

FIGURE 5.3 Leading edge discriminator and examples of the output pulse

to a value which can no longer sustain the collector voltage V_L and regeneration occurs as the coaxial line recharges through R_L. Thus a corresponding negative pulse appears at the emitter across the resistor R.

The transistor used was a germanium mesa pnp type 2N705. The base was suitably reverse biassed with a variable control to allow testing of this stage by increasing the base current and allowing the transistor to act as an astable device. Similarly the threshold on the tunnel diode stage was adjusted so that it was possible to test it by increasing the bias until the load line intersected the tunnel diode characteristic in the negative resistance region and the circuit then acted as an astable multivibrator. The output pulse from the avalanche stage was taken from the emitter across a resistor of either 100 ohm or 50 ohm, dependent on the impedance of the coaxial cable used to the following instrument. The output pulse width could be adjusted by changing the length of coaxial cable on the collector from about 20 nS to 200 nS. The final circuit which was designed and constructed by the author is shown in figure 5.3.

The discriminator was tested to check that it did not multiple trigger on the input pulses from the anode of the scintillation counter. Its minimum threshold was measured and its timing response was investigated.

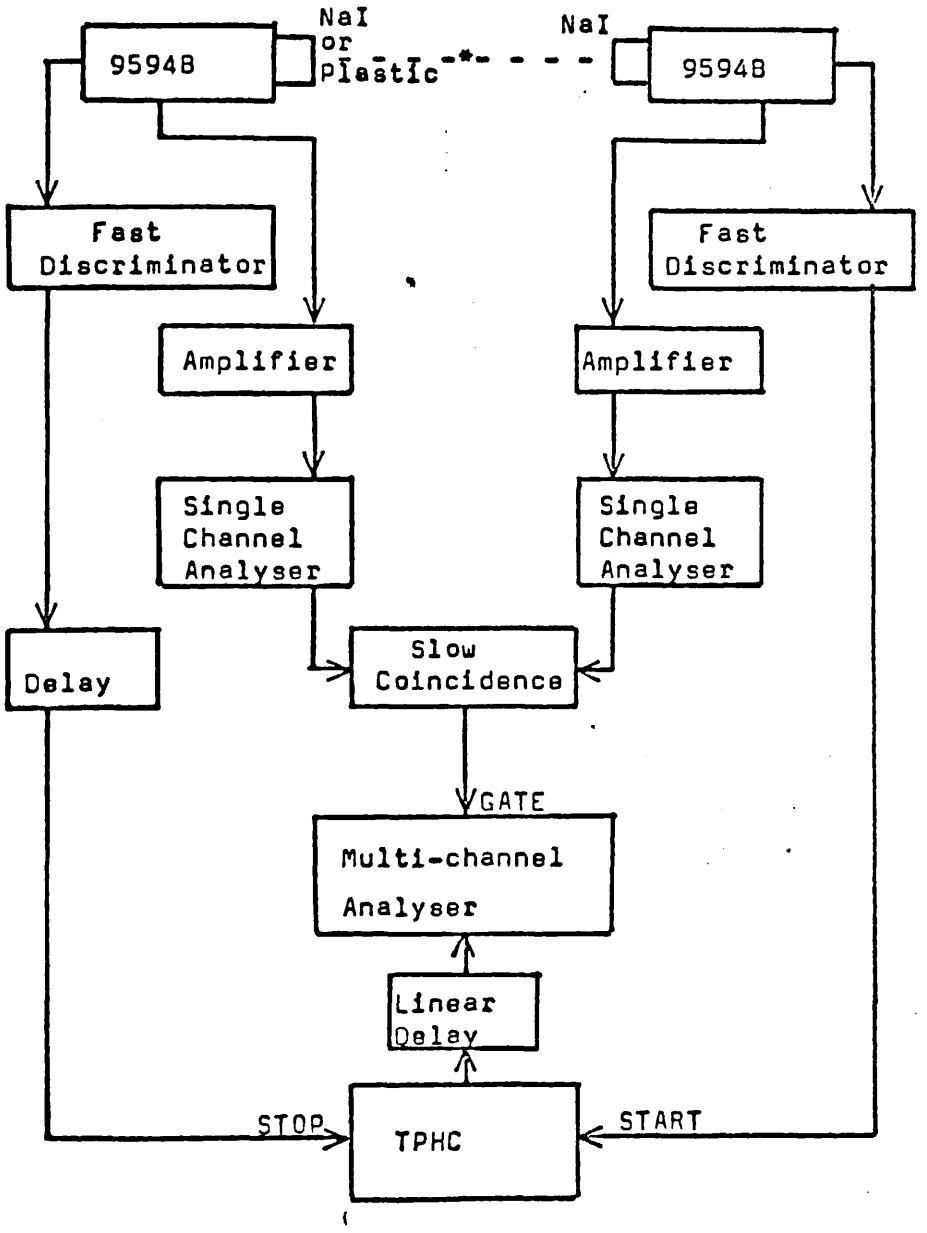

FIGURE 5.4 a Measurement of a time spectrum

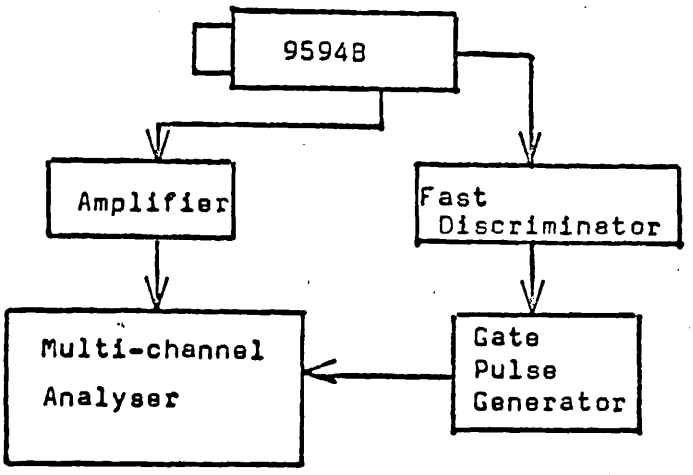

FIGURE 5.4 b Measurement of discriminator threshold

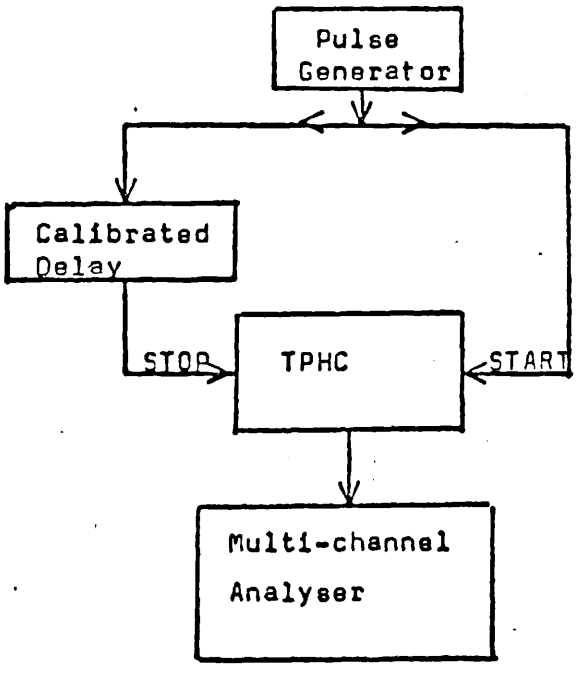

FIGURE 5.4 c Calibration of time-to-pulse height converter (TPHC)

Initial tests were made to check that the discriminator did not multiple trigger by taking the output of the fast discriminator to one channel of a coincidence unit and the output of a discriminator following the amplifier on the energy signal to the other channel. Scaler tests on these channels allowed the thresholds to be adjusted to give equal output rates. Provided that no multiple triggering occurred the coincidence rate between the two channels should then equal the singles rate. This was found to be satisfied.

The threshold of the discriminator was measured by gating the energy spectrum taken from the dynode and displayed on a MCA by the output of the fast discriminator. The minimum threshold was found to be (7 ± 2) keV.

The timing performance of the circuit was tested using the arrangement shown in figure 5.4. The output pulses from the fast discriminators were used to start and stop a time to pulse height converter.(TPHC) The output of the TPHC was analysed with the MCA and thus a time spectrum was obtained. The time spectrum was gated by pulses from a slow coincidence unit which satisfied the energy requirements set by the two single channel analysers. Thus the time spectrum corresponding to triggering pulses falling in a defined energy range was obtained. The triggering threshold set by the bias to the tunnel diode was adjusted using the

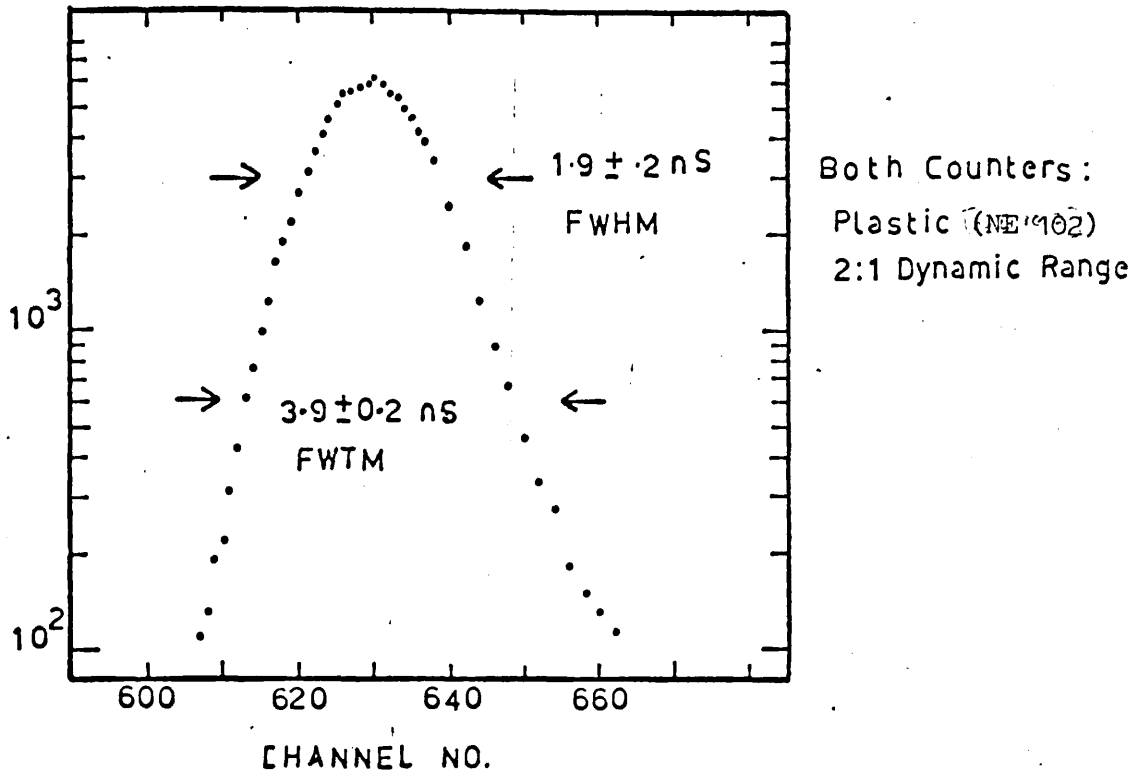

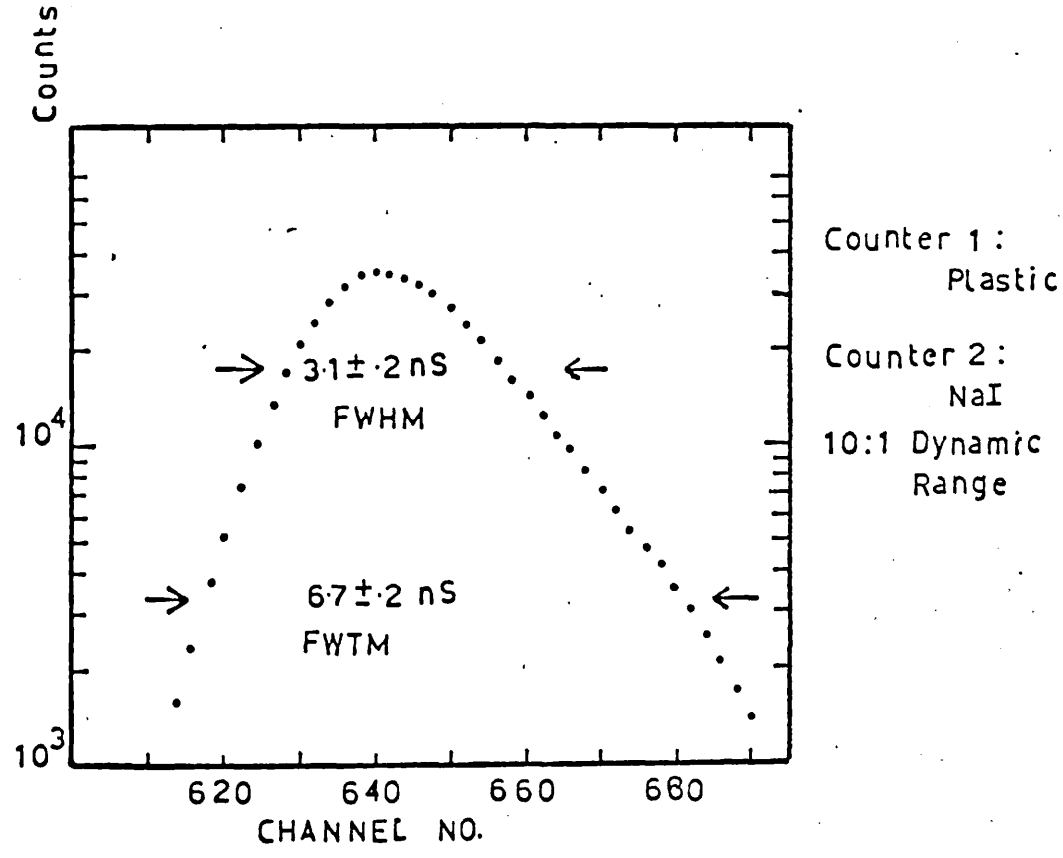

FIGURE 5.5 Performance of leading edge discriminator

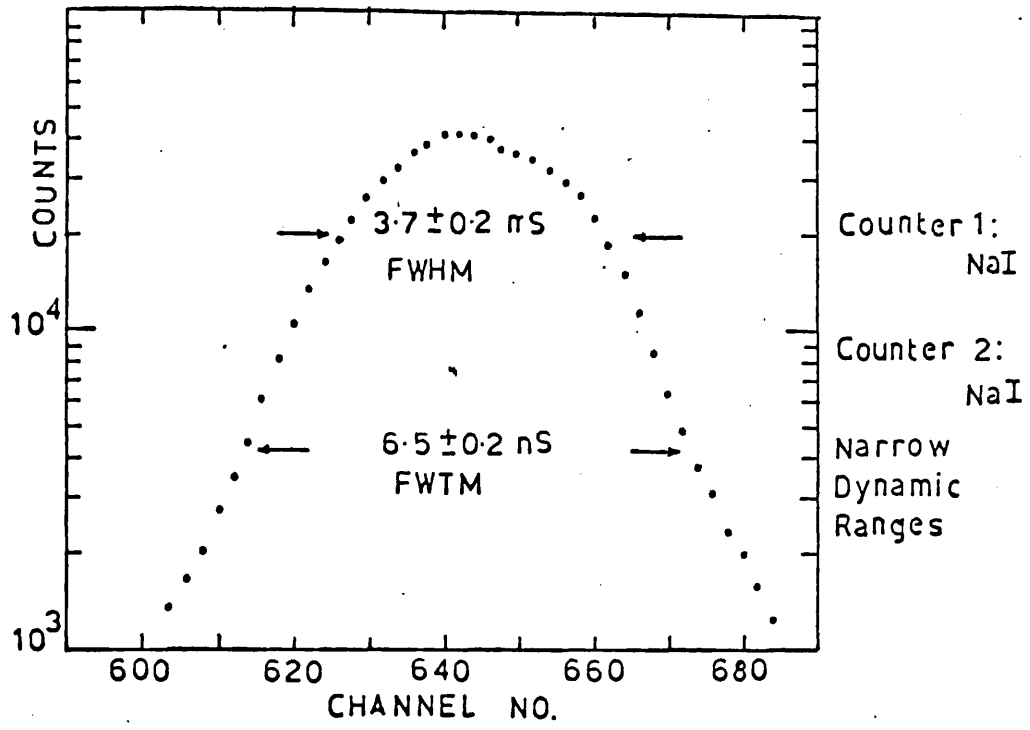

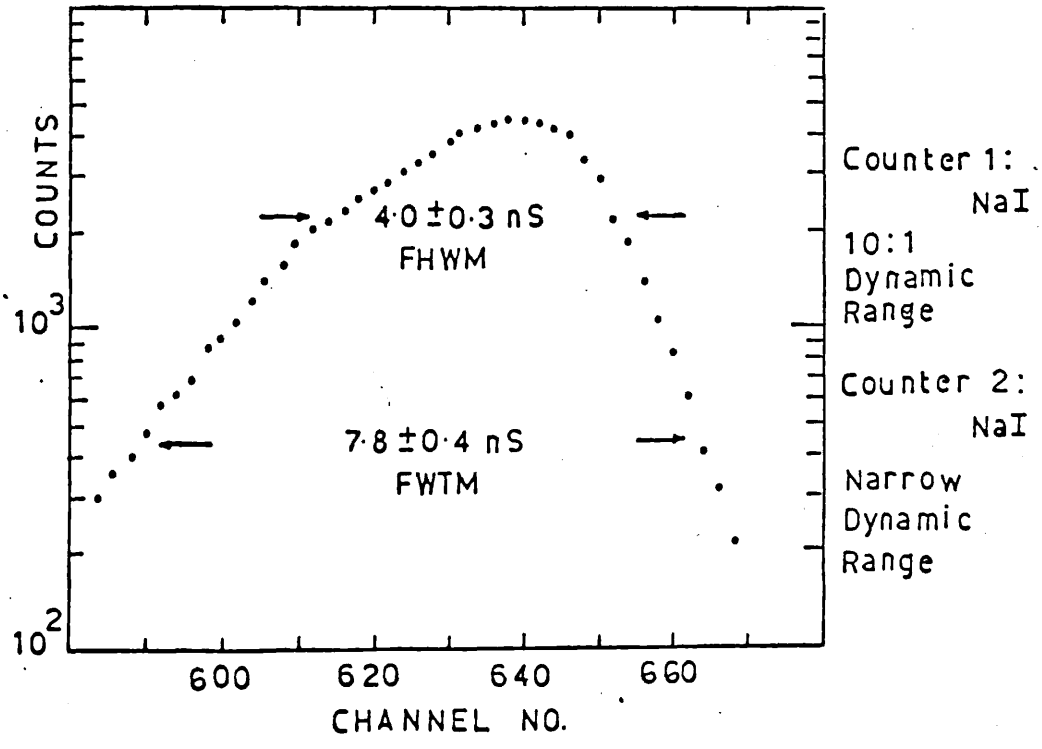

FIGURE 5.6 Performance of leading edge discriminator

arrangement shown in figure 5.4b. The TPHC was calibrated using the arrangement shown in figure 5.4c. The shift in the output amplitude from the TPHC was observed as the calibrated delay was changed and thus a calibration of nS per channel was obtained.

Examples of the performance obtained are shown in figures 5.5 and 5.6. Figure 5.5 shows the time spectrum obtained when one scintillation counter was equipped with a plastic scintillator and the other counter with a NaI crystal. Figure 5.6 shows the performance when both scintillation counters used NaI crystals.

5.4 Fast pulse shaper

This circuit was designed by the author to interface the Ortec model 260 time pick-off unit used with the Ge(Li) detectors to the Elron fast coincidence unit. Due to the long pulses produced by the Ge(Li) detectors it was necessary to adjust the time pick-off unit to produce a long (100 nS) output pulse as reduction in this pulse width caused multiple triggering to occur on the detector pulses. Since the correct operation of the fast coincidence unit required that the input pulse width should be less than the set resolving time, a circuit using a tunnel diode monostable with emitter follower output was designed.

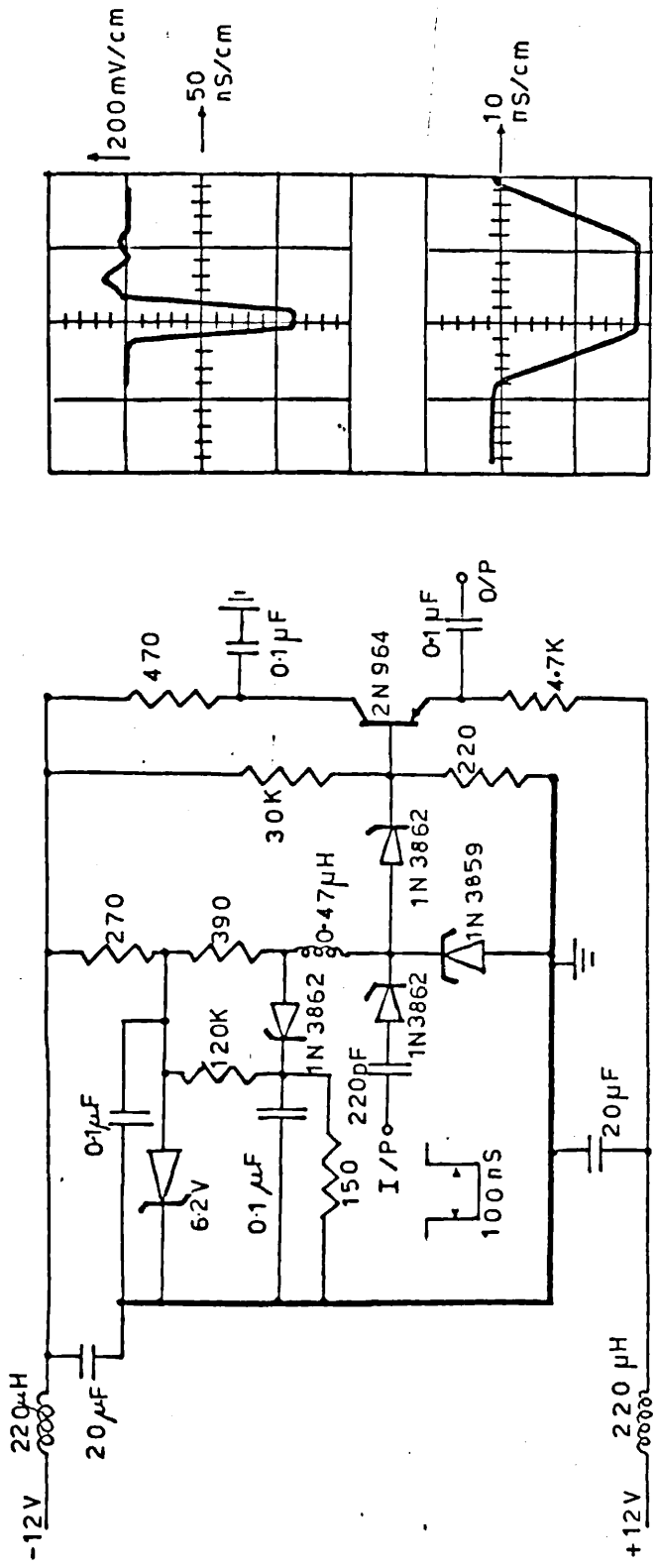

FIGURE 5.7 Fast pulse shaper and output pulse

The circuit diagram and the output pulse are shown in figure 5.7. The input pulse is heavily differentiated by C1 and the low input impedance of the tunnel diode (TD). The output pulse, taken from the emitter follower, has a width which is controlled by the inductance L and the forward resistance of TD. The circuit uses a back-diode (D1) to ensure that a fast switching action takes place on a small input current and a second back-diode (D2) ensures that the entire input current is directed to the tunnel diode which must switch over before the emitter follower can draw current.

The performance of the pulse shaper was measured and compared with that of the Ortec time pick-off discriminator used alone. The time response of the Ortec discriminators is shown in figure 5.8a for trigger pulses which just cross the discriminator thresholds and in figure 5.8b their performance is shown for pulses with an amplitude well above the thresholds. The corresponding time spectra with the fast pulse shapers placed after the Ortec discriminators are shown in figures 5.8c and 5.8d. It is seen that the performance with input pulses well above the threshold of the Ortec discriminator is unchanged by the pulse shaper. With input pulses which just cross the threshold of the Ortec discriminators an improvement is obtained when the pulse shapers are used. This is due to the fact that the tunnel diode monostable

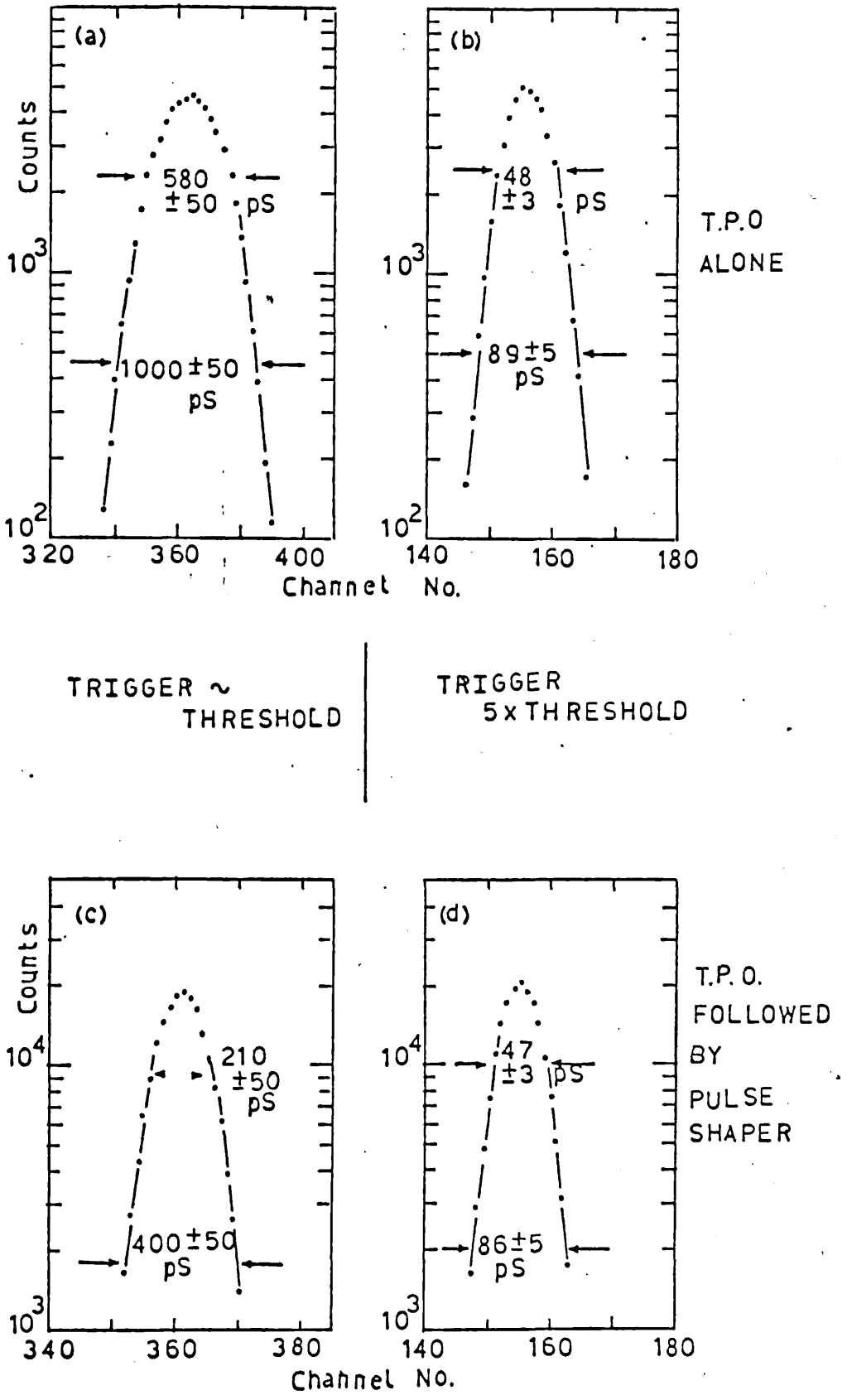

FIGURE 5.8 Performance of fast pulse shaper

circuit used in the Ortec discriminators is sensitive to the amount of overdrive applied to it and the time of output is poorly defined for pulses which just pass its threshold. The time spectrum seen by the TPHC is measured by discriminators at its input with thresholds of 150 mV (high for a 500 mV 'jittering' pulse). The addition of the constructed fast pulse shapers applies a much lower threshold to these pulses (a few mV) and thus improves the time spectrum as measured by the TPHC.

5.5 Electronic systems for the measurement of singles spectra from Ge(Li) detectors

The Ge(Li) detectors used were equipped with charge-sensitive pre-amplifiers with a cooled FET input stage. The output pulse from these pre-amplifiers was suitable for use with the pole-zero cancelling network of most commercial low-noise pulse amplifiers.

The main amplifier used in most of the present work was an Ortec 440A which was found to give good performance. The performance of the Ge(Li) detectors with counting rate suggested that they were not as good as some American rivals can produce (these are typically quoted as maintaining good resolution to 10 kHz or so) but it is unknown for a manufacturer to quote exactly where and how this counting rate has been

measured - a discriminator having a finite threshold.

The MCA system used a Northern Scientific 8192 channel ADC and a NS 630 4096 memory unit. A digital stabiliser was applied to the ADC which provided a high stability reference pulser (to set the zero of the conversion range) and a digital peak locking system. This meant that it was a comparatively easy task to maintain the same energy calibration over long counting periods or with widely varying counting rates. The use of a stabiliser which continuously corrects the conversion gain to maintain a set channel position for a specified peak necessarily degrades the intrinsic resolution of a detector - amplifier system but it can provide an improvement when long counting times are involved as the system, in the absence of the stabiliser, is sensitive to the laboratory temperature. Unfortunately the system, as provided by Northern Scientific, is not perfect and can not easily be adapted to coincidence counting when the coincidence gating is performed at the ADC as the ADC does not then 'see' the zero reference pulser from the stabiliser. This could be overcome by a suitable linear gate prior to the ADC but the only model which provides a sufficiently long 'gate open' time produced an intolerable distortion of the energy signal. The peak stabilisation was only effective on a fairly prominent peak and, since ideally this peak should

be near the high end of the ADC range used, this too had limitations especially in any coincidence study. For these reasons the stabiliser was only applied for singles spectra runs.

5.6 The electronic system and its adjustment for fast - slow coincidence measurements

The fast-slow coincidence systems used in this work were essentially of the type shown in figure 5.9. Some of the units employed required to be individually adjusted to suit the conditions of the particular experiment being conducted. These are described below:

a) Timing discriminators

The thresholds were adjusted using the time spectrum obtained with a TPHC (see section 4.3). For Ge(Li) timing discriminator systems it was also possible to use a pulser test facility to measure the threshold in keV. For the NaI counter discriminator the energy spectrum from the counter could be displayed on the MCA gated by the output of the discriminator applied to the ADC coincidence gate to measure the threshold.

b) Fast coincidence unit

When a TPHC was available the coincidence resolving time appropriate to the system could be quickly measured and set with the fast coincidence unit. A single 'delay' curve was

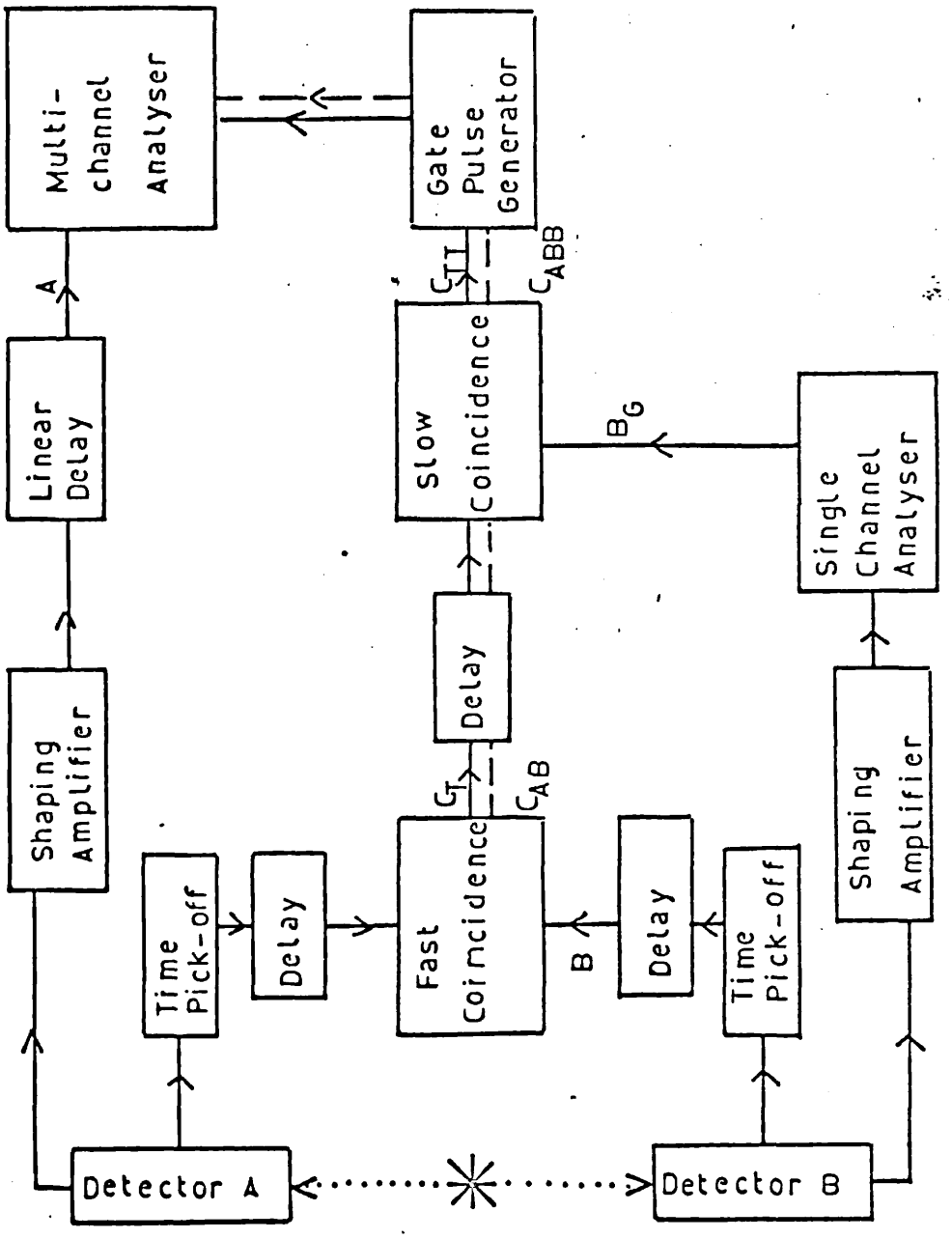

FIGURE 5.91 Fast - slow coincidence system

then sufficient to determine the necessary delays to record 'prompt' events at the fast coincidence unit.

Without a TAHC the resolving time suitable for a given system was determined by recording the true coincidence counting rate as a function of the resolving time imposed by the fast coincidence unit, given that the delays had been adjusted to record 'prompt' events.

Two different fast coincidence units were employed. The first was an ex-Harwell unit type 2035C. This unit used external clipping lines to set the resolving time by clipping the input pulses to the desired length. The fast coincidence detection stage consisted of a discriminator whose threshold could be adjusted to suit the amplitudes of the input pulses and the number of channels in use. This had to be set so that the discriminator did not respond to an individual (singles) input but only to genuine coincident inputs at the two inputs used. This was adjusted by observing the output counting rate of the unit as a function of the bias applied to the discriminator. The most severe limitation of this coincidence unit was that the operation of the clipping lines was only really useful up to a pulse length of about 20 nS. Above this length losses through the long cable resulted in a very poor pulse shape and unreliable operation. Thus the maximum resolving time usuable was about 40 nS. Another, less serious

disadvantage was its input requirements (minimum 2V) which were not met by the output of the commercial time pick-off units used with the Ge(Li) detectors (0.5V) so that a wide bandwidth amplifier was required between the time pick-off units and the fast coincidence unit.

A more modern fast coincidence unit was purchased (manufactured by Elron) which was a very versatile unit with internal delays which improved the performance of the timing channel. However, it was necessary to build a pulse shaper for use with this unit as its input requirements were that the input pulses should be shorter than the resolving time to be used. The outputs from the Ge(Li) time pick-offs could not be reduced in length without multiple triggering on the long detector signals. Two pulse shapers were constructed as described in section 5.4. The NaI discriminator output could be easily changed so that this could be used with the new coincidence unit.

c) Gating energy selection

In figure 5.9, detector B provides a gating signal whenever a pulse falls within a set energy range. This range is set with a timing single channel analyser. An Ortec timing single channel analyser was used in a mode such that the output signal was generated on the cross-over of a bipolar input signal. The output signal of this single channel

analyser (SCA) could be adjusted to have a walk of less than 20 nS over its full range (0.01 - 10V) provided that the input pulse rise time was less than about 500 nS. The timing performance of the SCA deteriorated with longer rise time input pulses so that even with the Ge(Li) detectors where good energy resolution demanded much longer shaping time constants (4 μS) it was more appropriate to reduce these to 0.25 μS or 0.5 μS as a compromise. These reduced time constants also reduced the delay necessary between the fast coincidence unit and the slow coincidence unit (and thus the linear delay in detector A energy signal to the MCA) as the time to the cross-over of the shaped gating signal was then only about 1 μS.

The energy range selected by the SCA could be adjusted easily for a NaI counter by the conventional method of plotting a differential spectrum. When detector B was a Ge(Li) detector this method did not hold as the resolution of the detector (0.5%) is far better than the smallest differential resolution obtainable with the SCA (4%). It was then necessary, either to plot time consuming integral spectra or to employ a different technique. If the energy spectrum from counter B was displayed on the MCA it was possible to gate this spectrum with the output from the SCA. The SCA window could then be adjusted to the desired energy region.

d) Slow coincidence unit and the MCA gate

The delays on the inputs to the slow coincidence unit were adjusted by plotting a delay curve as for the fast coincidence unit and a suitable resolving time was selected. For this work a resolving time of 200 nS was used. This was the minimum available and was probably larger than necessary as this resolving time is determined by the walk characteristics of the SCA employed or the fast coincidence resolving time; whichever is the greater.

The output of the slow coincidence unit was then used to gate the MCA (via a suitable pulse shaping unit constructed by the author and shown in figure 5.9A). For most systems it was necessary to delay the arrival of the energy signal from detector A until the gating signal from the slow coincidence unit had arrived to open the ADC linear gate to accept the energy signal. This delay must be linear and a commercial unit (Ortec 417) was used. The timing of the arrival of the gating signal to the ADC was set up with the aid of an oscilloscope. The delayed time base feature enabled the difference in time between the energy and gating signals to be adjusted to about 20 nS. This timing could be checked over the entire pulse amplitude range by observing the coincidence spectrum recorded on the MCA and comparing the position of a full-energy peak with its position in a singles

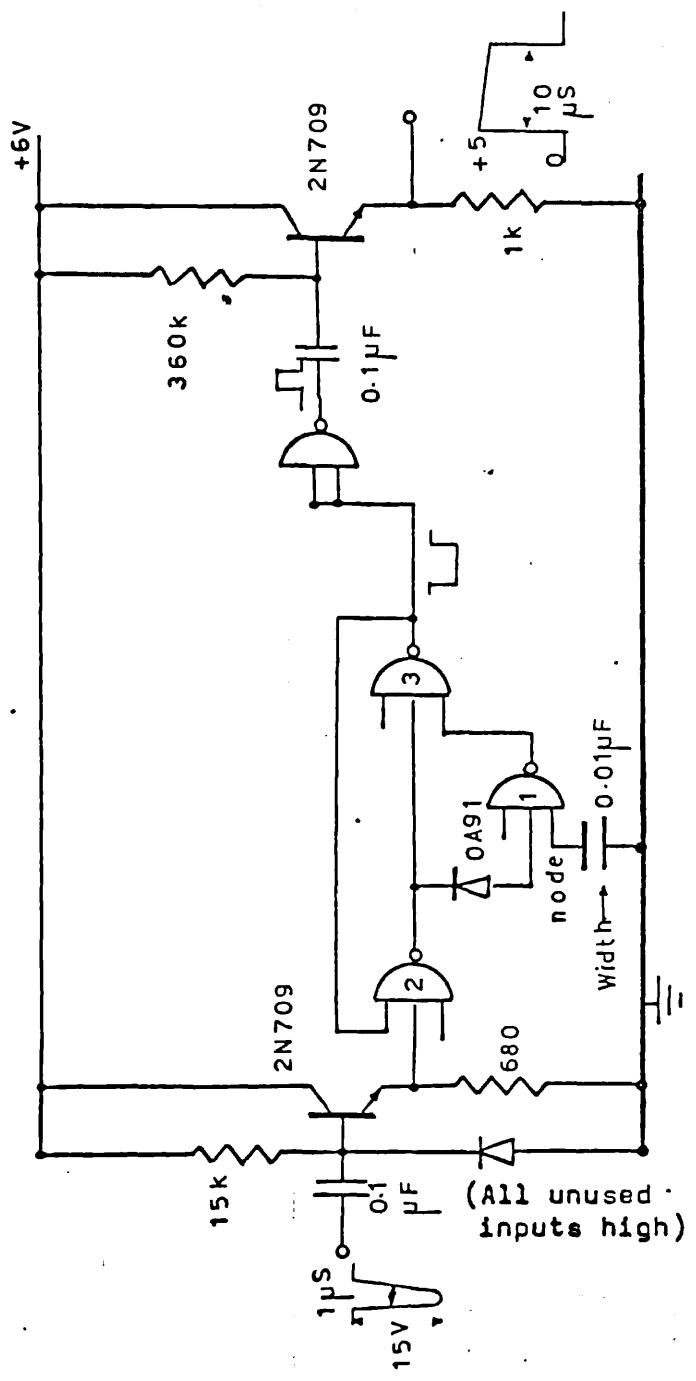

FIGURE 5.9A Gate - pulse generator

spectrum. If the adjustment is incorrect, a shift to lower channels occurs in the coincidence spectrum when the ADC gate is not opened early enough or closes too soon as the ADC fails to 'see' the correct pulse amplitude. This test assumes that the requirements for the length of the gating pulse are met.

These 'overall' delay adjustments are most easily made with a ^{22}Na source where possible as the coincidence counting rates for 180^{o} geometry are very good.

For each system used a test run was made with a source having well established coincident transitions so that the system could be checked.

5.7 The electronic system for sum-coincidence spectra

The electronic system used in the fast - slow coincidence measurements was employed in a modified form to record sum-coincidence spectra. This was used in the study of ^{207}Bi. The system used is shown in figure 5.10. The summing amplifier was used to sum the pulses from the two detector pre-amplifiers so that an energy selection gate could be placed on all pulses which satisfied both the fast coincidence requirement and which fell within a certain sum-energy window set by the SCA. This selection was achieved at the slow coincidence unit which was then used to gate the MCA. Since the fan-out load at the pre-amplifier of the

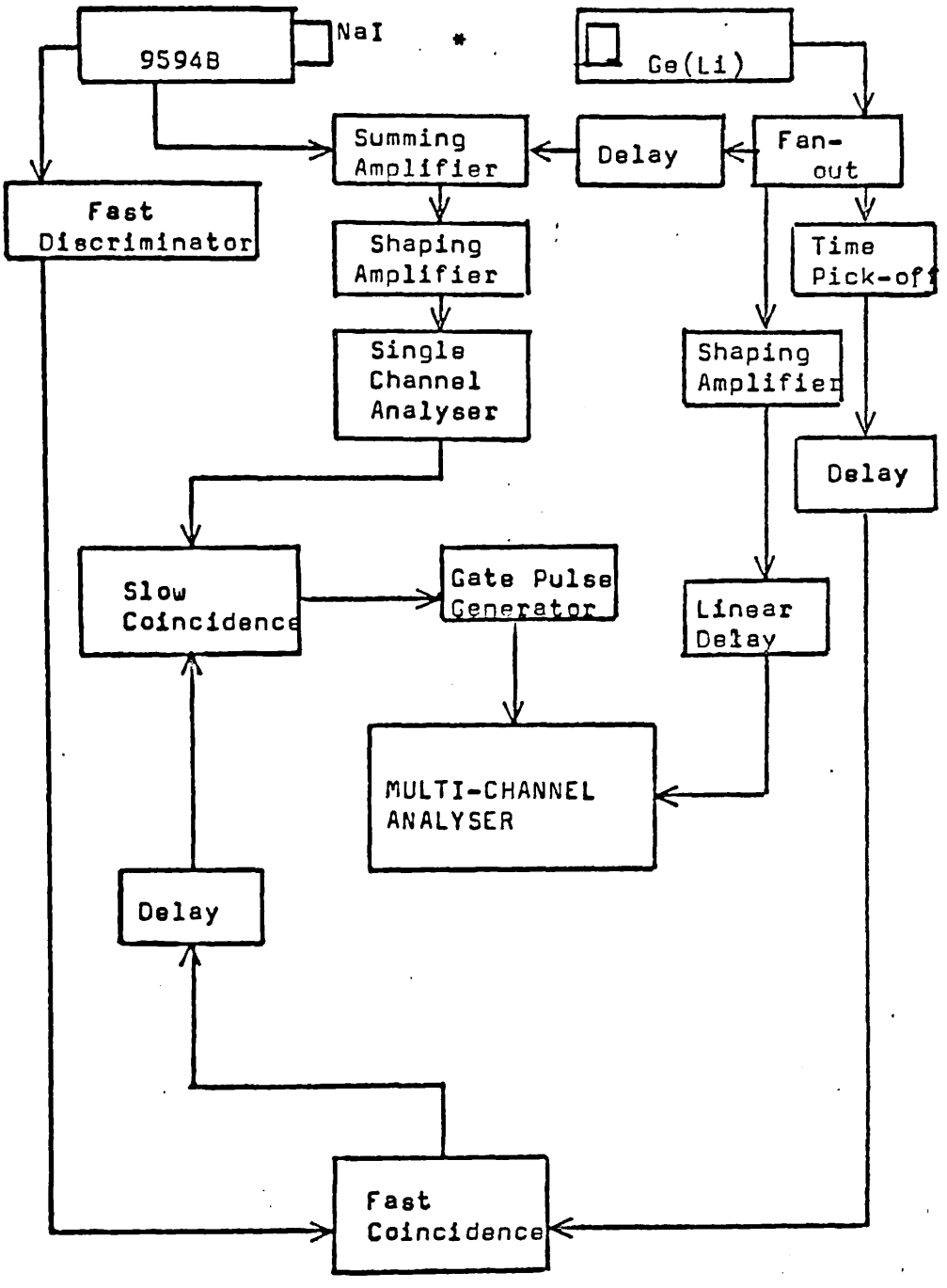

FIGURE 5.10 Measurement of Sum-Coincidence spectra

Ge(Li) detector was increased to three it was felt wise to use an isolating unit which was designed and constructed by Mr R.N.Thomas.

The setting up adjustments for this system were broadly similar to those used in section 5.6 with the addition of the requirement that the energy scales of the two detectors should be equal. This was achieved by adjusting the EHT on the NaI counter until the NaI spectrum seen through the summing-amplifier and the main amplifier matched that of the Ge(Li) detector measured in the same manner. The adjustment of the SCA window was made on a 'digital' basis by observing the summing-amplifier spectrum with the MCA and using the SCA output signal to gate the ADC. The window was then adjusted to cover the channels dictated by the constituent summing channels - this providing a more reliable setting which did not depend on the calibration of the NaI counter at high energies when non-linearities could occur.

The performance of the system was checked by setting it to record a spectrum of ^{22}Na with a sum-energy gate of 1022 keV (figure 5.11) and a spectrum of ^{60}Co in coincidence with a sum-energy gate of 2405 keV (figure 5.12).

The excellent performance of this system which totally removed Compton events from the spectrum in certain

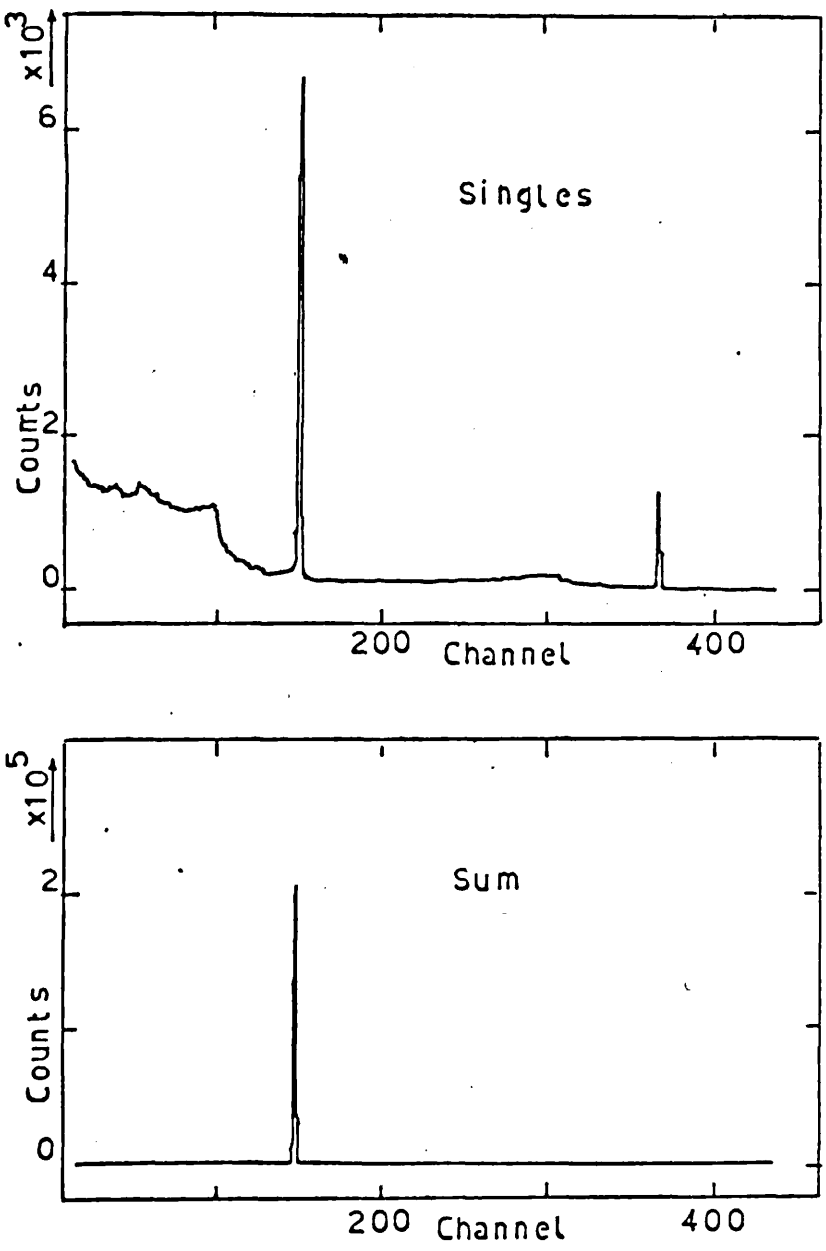

FIGURE 5.11 Sum - coincidence spectrum ^{22}Na

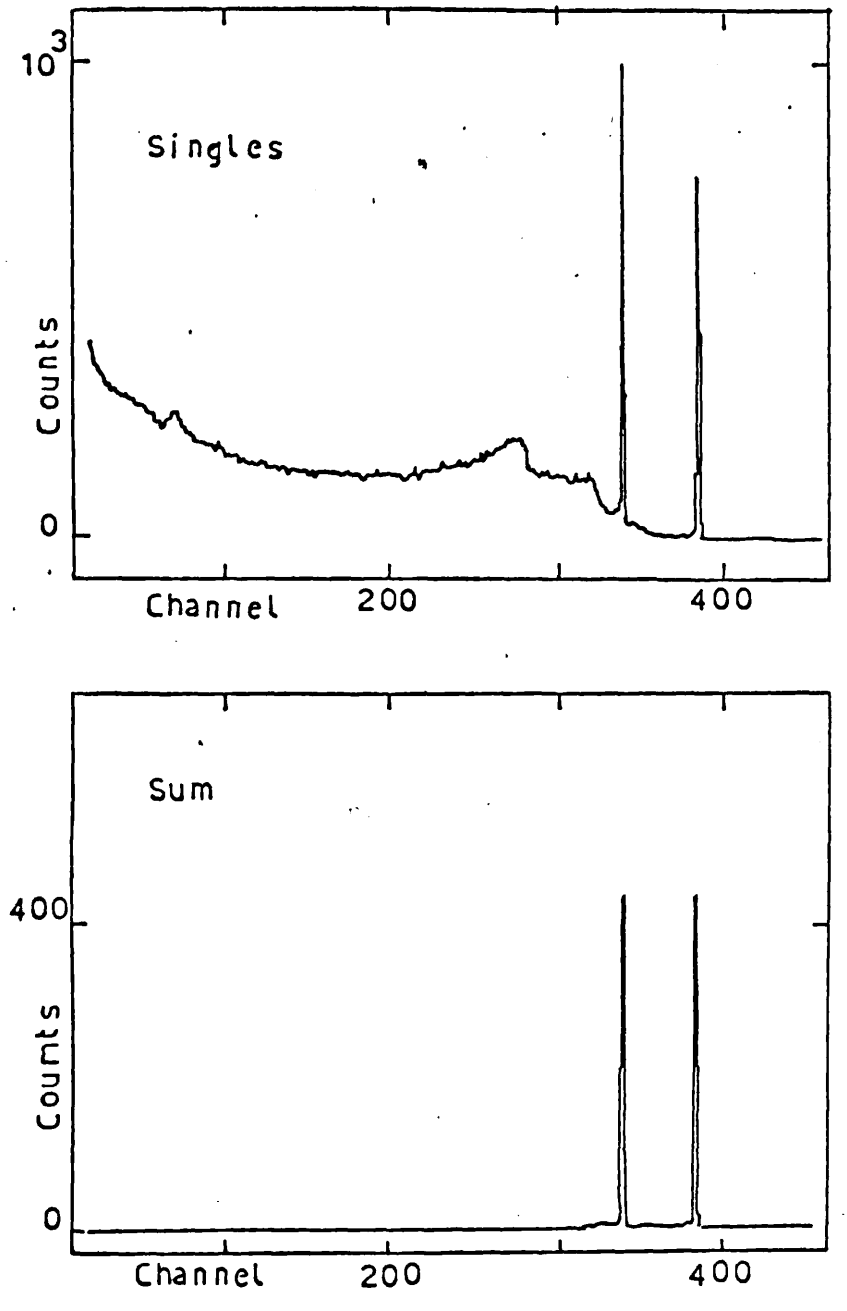

FIGURE 5.12 Sum - coincidence spectrum ^{60}Co

cases was found to be extremely useful for some types of coincidence investigations involving two gamma cascades. It can be extended to three or more gamma cascades with the addition of a NaI well-crystal.

CHAPTER 6 THE DECAY OF ^{75}Se

6.1 Introduction

The decay of $^{75}_{34}Se$ proceeds by electron capture to some of the excited states of $^{75}_{33}As$ with a half-life of 120.4 days[31]. $^{75}_{33}As$ is an odd proton nucleus which is considerably removed from neutron and proton closed shells and thus a simple shell model treatment of this nucleus does not provide a satisfactory description of the excited energy levels and their decay properties. The most successful theoretical model treatments of this nucleus have been developed by Imanishi et al.[32] and Scholz et al.[33]. These authors considered the motion of an unpaired quasi-particle which moves in Nilsson's deformed orbit and is coupled by a Coriolis force with the rotational motion of the core.

The main modes of gamma decay of the excited states of ^{75}As have been well established but there remain several possible decay modes of weak intensity and, since some of these are also of fairly low energy, their detection has proved difficult. It was felt that the superior energy resolution of the Ge(Li) X-ray detector, together with its advantage for this type of investigation of a rapidly decreasing efficiency for gamma photons above about 150 keV, might allow a confident identification and measurement of the relative intensities of these transitions and, by suitable coincidence

studies, confirm their places in the decay scheme.

6.2 Previous experimental work

Early authors [34, 35, 36, 37] studying the decay of ^{75}Se used beta-ray spectrometers and obtained most of the main modes of gamma decay by the measurement of their internal conversion lines and the measurement of their internal conversion coefficients gave an indication of the multipolarities of these transitions. Gamma-ray spectra taken with NaI scintillation detectors[35, 38, 39] again revealed the main transitions but failed to confirm two low energy transitions (24 keV and 81 keV) suggested by the internal conversion electron measurements. One, more recent, attempt by Pratt[40] with a NaI X-ray counter used graded absorbers to assess the contribution to the gamma spectrum in the region of 24 keV due to degraded high energy photons and, from this, obtained evidence for a photopeak at this energy. The development of Ge(Li) detectors inspired new studies by Raeside et al.[41] and by Paradellis and Hontzeas[42] which revealed some evidence for weak gamma-ray transitions at energies of 24 keV, 81 keV, 373 keV and 463 keV. Coulomb excitation experiments by Robinson et al.[43] also suggested gamma-rays of energy 308 keV, 293 keV and 374 keV in addition to the established 572 keV which de-excites the level at 572 keV. Following this work Pratt[44] used a Ge(Li) detector to investigate the

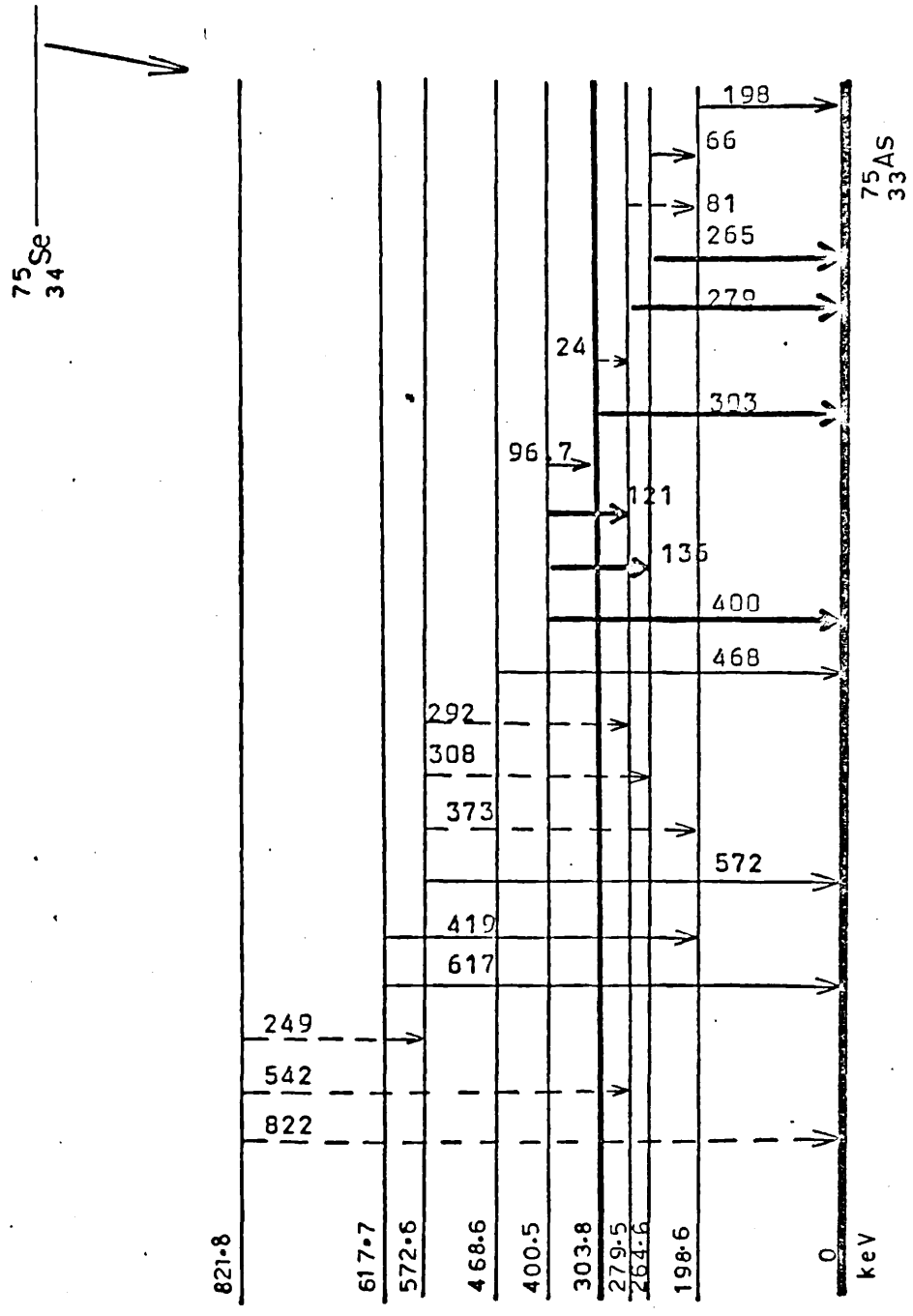

FIGURE 6.1 Decay scheme for ^{75}Se from previous authors

reported gamma-rays corresponding to transitions of energy 469.4 keV and 821.7 keV with intensities, relative to I(265keV) = 100, of $(5.4 \pm 1.8).10^{-4}$ and $(2.16 \pm 0.1).10^{-4}$ respectively. No mention was made of any of the other gamma-rays reported by Robinson et al. The decay scheme of ^{75}Se due to these previous authors is shown in figure 6.1 with the established transitions shown by solid lines and with transitions claimed by only a few authors shown by dashed lines. Table 6.1 gives a summary of the energies and intensities of the gamma transitions.

6.3 Experimental details of singles spectra

The isotope ^{75}Se was obtained from the Radiochemical Centre (Amersham) in the form of sodium selenite in aqueous solution. It was produced by the reaction $^{74}Se(n,\gamma)$ using a Se target. The only contaminants expected were ^{81m}Se and ^{81}Se which have half-lives of 57m and 18m respectively. Two separate purchases were made, one about one year after the other, to try to identify the origin of a gamma-ray of energy 634.1 ± 2 keV which appeared in the spectra taken with the first sample. From the stock solution several sources of differing activities were prepared in aluminium planchets and covered by a thin adhesive paper label.

ENERGY keV	INTENSITY (Relative to I(265)=100		
Present work	Present work	Ref. 42	Ref. 39
14.9 ± 0.5	$(34\pm6)10^{-3}$		
24.4 ± 0.2	$(63\pm8)10^{-3}$	$(44\pm6)10^{-3}$	$\leq 1\times10^{-3}$
66.0 ± 0.1	1.50±0.15	1.72±0.04	1.64±0.05
80.8 ± 0.1	$(11\pm3)10^{-3}$	0.1	
96.7 ± 0.1	5.4±0.4	5.12±0.1	5.33±0.16
121.1 ± 0.1	26.7±3.0	27.7±0.5	27.8±0.8
135.9 ±00.1	95.9±7.0	95.0±1.8	94.9±2.0
198.5 ± 0.1	2.59±0.2	2.38±0.07	2.28±0.05
264.6 ± 0.5	100	100	100
279.5 ± 0.6	42.1±0.8	42.0±0.8	43.0±0.9
303.9 ± 0.6	2.11±0.3	2.19±0.07	2.39±0.05
373.8	$\leq 5\times10^{-3}$	$\leq 6\times10^{-3}$	
400.7 ± 0.6	18.0±0.4	20.4±0.5	22.3±0.05
418.5 ± 0.5	$(17\pm3)10^{-3}$	$(23\pm2)10^{-3}$	$(32\pm6)10^{-3}$
468.8	$\leq 2\times10^{-3}$	$(10\pm5)10^{-3}$	
572.1 ± 0.2	$(48\pm5)10^{-3}$	$(63\pm2)10^{-3}$	$(64\pm1)10^{-3}$
617.5 ± 0.5	$(59\pm7)10^{-4}$	$(75\pm2)10^{-4}$	$(78\pm2)10^{-4}$
821.7	$\leq 2\times10^{-3}$		

TABLE 6.1 Energies and intensities of gamma-ray transitions in the decay of ^{75}Se

Singles spectra were recorded using both the Ge(Li) X-ray detector and the 25 cm^3 detector. The sources were placed on the axis of the detector concerned at 7 cm from the end window of the X-ray detector and at 20 cm from the end-window of the 25 cm^3 detector. These distances corresponded to those used in the measurements of the relative full-energy peak detection efficiency (see section 2.4).

The amplification system following the Ge(Li) X-ray detector was set to display energies up to 650 keV in 4096 channels of the MCA and the digital stabiliser was used to maintain the position of the 400 keV full-energy peak constant throughout. Three spectra were recorded using sources of different activities.

The 25 cm^3 Ge(Li) detector was used to obtain spectra up to 1 MeV with the amplification set so that, with a conversion gain of 4096 at the ADC, the first 2048 addresses contained the desired energy region. Again the digital stabiliser was set to maintain the position of the 400 keV full-energy peak. As several weak gamma-rays were expected in the energy region above 300 keV this region was recorded separately in two of the four runs taken. The lower energies (less than 300 keV) were rejected at the ADC input stage by the low level discriminator. This resulted in a significant reduction in the dead time of the MCA system and thus

effected a useful increase in the counting rate of pulses above 300 keV actually recorded without an increase in the total counting rate experienced by the preceding electronic system. The singles spectra were recorded for two sources which gave counting rates at the detector differing by a factor of five when they were placed at 20 cm from it. The resulting spectra when analysed were then used to identify only those gamma energies whose relative full-energy peak intensities were independent of this change in counting rate and thus both random summing and background radiations were eliminated.

6.4 Analysis of singles spectra

The resulting singles spectra (three from the X-ray detector and four from the 25 cm^3 detector) were analysed using the programme Sampo (see section 3.4). The peak shapes used in the analysis were obtained from the main ^{75}Se transitions and from spectra taken with ^{57}Co, ^{152}Eu and ^{182}Ta at the same distance from the detectors and with source strengths giving the same counting rates as used in the ^{75}Se spectra. The automatic peak searching routine was employed and, in addition, the spectra were searched by hand in the regions corresponding to all possible gamma-ray transitions between established and suggested energy levels. The final peak areas were obtained using the routine FITS. The intensities were calculated from the peak areas using the measured relative

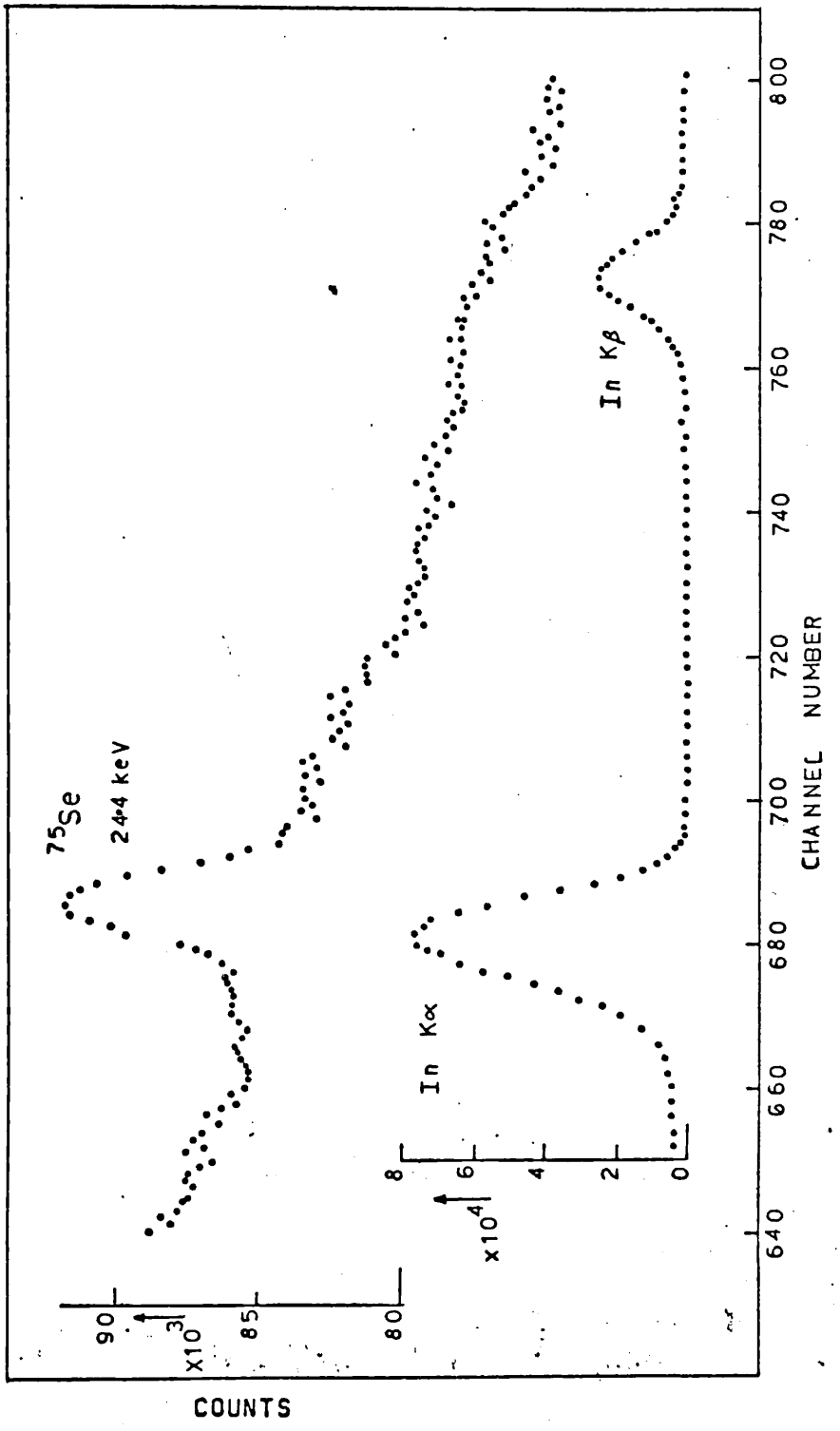

FIGURE 6.2 Portion of spectrum taken with the X-ray detector showing the 24.4 keV photopeak

full-energy peak detection efficiencies of the detectors. These intensities were then normalized to I(265keV) = 100. The final energies and intensities are given in table 6.1 and are the mean values obtained from these spectra.

Figures 6.2 and 6.3 show portions of the spectra from the X-ray detector and figure 6.4 shows the spectrum from the 25 cm^3 detector.

6.5 Discussion of the spectra below 100 keV

In addition to the previously established gamma-ray transitions at 66 keV and 97 keV and the Arsenic K X-rays, the spectra showed clearly the gamma-rays of energy 24.4 keV and 80.8 keV. In this investigation, particular importance was placed on establishing the existence of these two gamma-rays in view of the contradictions which have appeared in the work of previous authors. Both transitions have been observed in conversion electron spectra and the 24.4 keV transition was observed in a Ge(Li) detector spectrum and also in a scintillation counter investigation. However, the use of a Ge(Li) detector at low energies presents special difficulties in interpreting the nature of weak photopeaks. The Ge(Li) detector required to measure such low energies has a small volume (0.1 cm^3 in the present work and 0.4 cm^3 in the study made by Paradellis and Hontzeas[42]). In such a

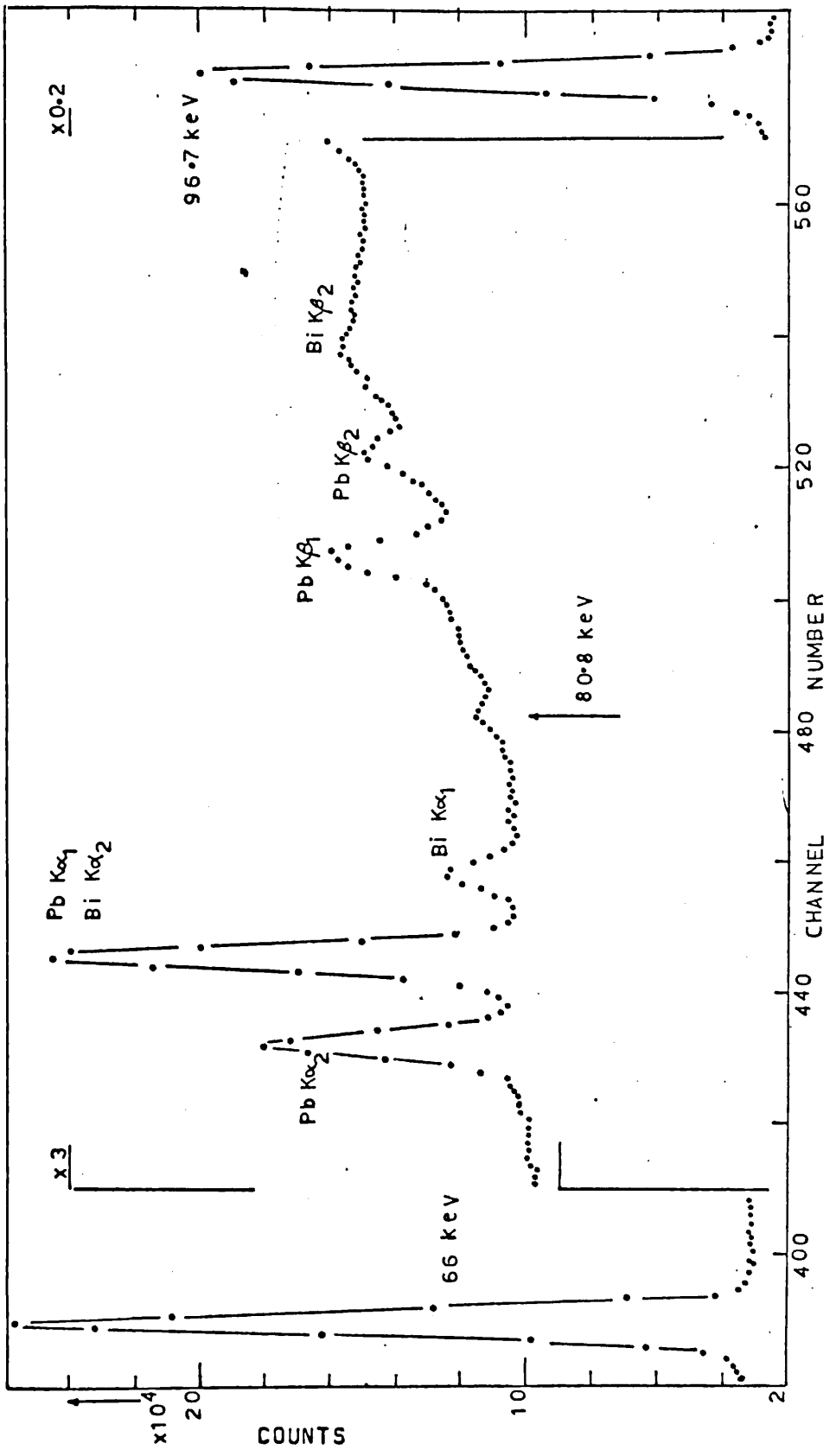

FIGURE 6.3 Portion of spectrum taken with the X-ray detector showing the 80.8 keV photopeak

detector the presence of comparable volumes of other materials used in the construction of the detector system in close proximity to the detector can give rise to fluorescent X-rays which are excited by photons from the source under investigation. The energies and intensities of the fluorescent photopeaks appearing in the low energy spectrum are dependent upon the individual detector used but commonly identified peaks include the Gold X-rays (Gold is used as a detector window) with energies between 67 and 80.1 keV and Indium (used to make electrical connections to the detector crystal) with energies of 24.00 keV ($K_{\alpha 2}$), 24.2 keV ($K_{\alpha 1}$) and 27.3 keV (K_{β}). In addition, the detector used in the present work exhibited fluorescent lead X-rays at 72.8 keV ($K_{\alpha 2}$), 74.97 keV ($K_{\alpha 1}$), 84.5 keV and 87.3 keV (K_{β}) and Bismuth X-rays from an unidentified origin within the detector cryostat. Thus the study of the decay of ^{75}Se was complicated by the possible presence of fluorescent peaks close to the two disputed transition energies of 24.4 keV and 80.8 keV.

Paradellis and Hontzeas[42] were clearly aware of the presence of fluorescent peaks in their X-ray detector system, for they identified the fluorescent Gold X-rays which prevented them from finding the predicted 80.8 keV gamma-ray. However, they did not mention the possibility of a 24.2 keV fluorescent peak from indium and attributed their peak at

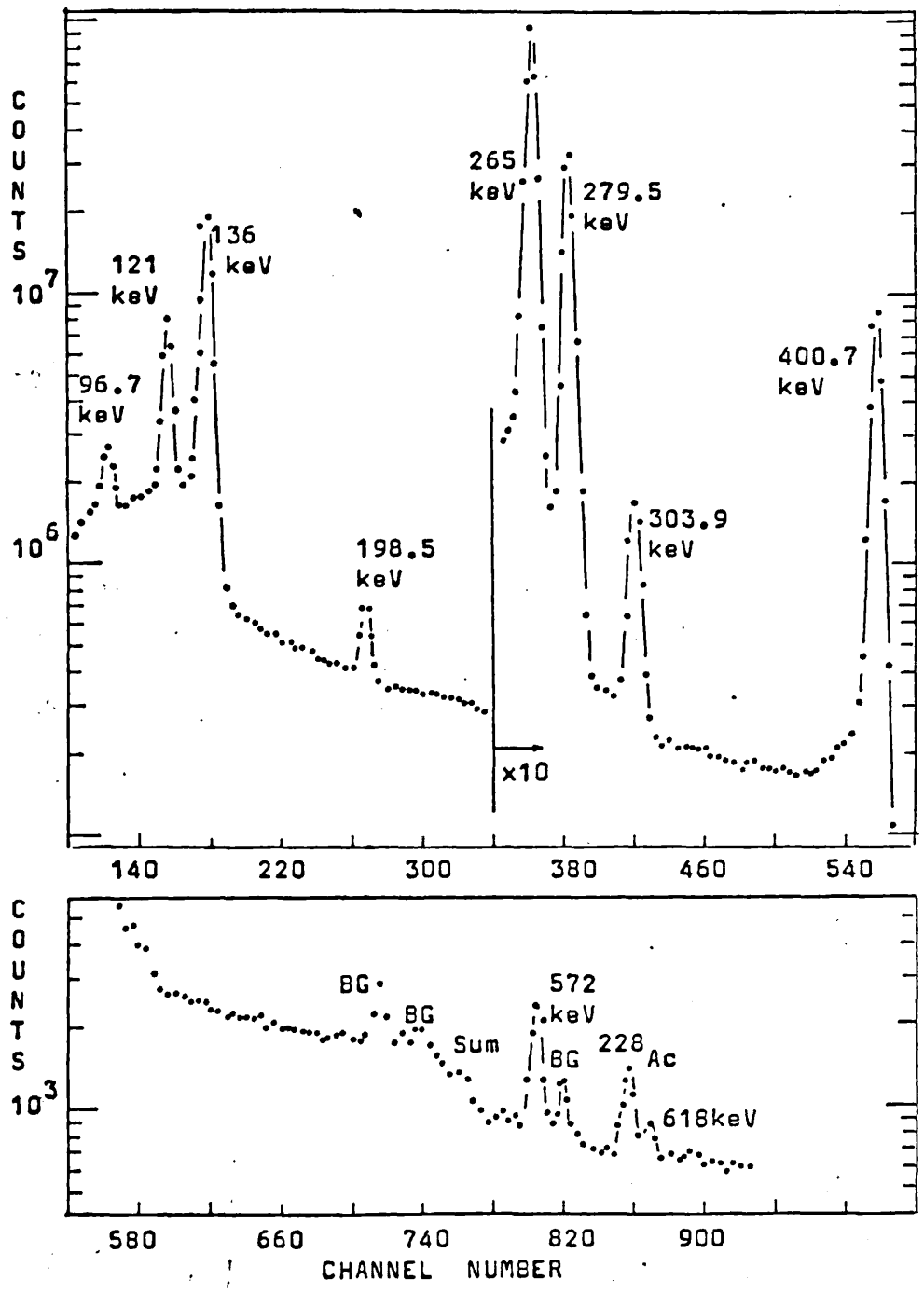

FIGURE 6.4 Singles spectrum of ^{75}Se above 100 keV taken with the 25cm^3 Ge(Li) detector

24.4 ± 0.1 keV unambiguously to the decay of ^{75}Se.

The question of indium fluorescence did not arise in the case of the measurements made by Pratt[40] on the 24.4 keV gamma-ray using a NaI scintillation counter, but the technique of measurement utilised with difference measurements employing selected absorbers was less direct than a straightforward measurement with a high-resolution detector and more liable to be affected by systematic errors.

Consequently, the present measurements were made with a view to establishing directly the existence and intensity of these low energy transitions and with suitable precautions taken to avoid confusion between the ^{75}Se gamma-rays and any spurious photopeaks.

Previous experience with the Ge(Li) X-ray spectrometer used for these measurements indicated that the fluorescent peaks to be expected were the prominent X-rays of lead and weakly excited peaks corresponding to bismuth and indium. This detector had not given rise to noticeable gold fluorescence and the indium lines were not usually strongly excited.

The low energy spectrum in the region of the 24.4 keV gamma-ray (figure 6.2) shows the well defined gamma photopeak and its position in relation to indium X-rays

obtained from the decay of ^{113}Sn. The high resolution of the X-ray detector together with the computer analysis of the results clearly distinguished the ^{75}Se gamma-ray from the indium $K_{\alpha 2}$ X-ray; a result which is confirmed by the results of the coincidence measurements.

The energy spectrum in the region of the 80.8 keV gamma-ray (figure 6.3) clearly showed the presence of this previously unseen transition although the fluorescent lead X-rays were very prominent in the spectrum. The intensities of this and the 24.4 keV gamma-ray are given in table 6.1.

The spectra taken with the X-ray detector also revealed some evidence for a transition of energy 14.9 keV with intensity $3.4 \pm 0.6 \times 10^{-2}$ relative to I(265) = 100 which was on the borderline of the statistical significance test (see section 2.6). This gamma transition would fit energetically between the level at 279.5 keV and the level at 264.6 keV

6.6 Discussion of the spectra above 100 keV

The spectra (figure 6.4) failed to reveal gamma-rays of energy 373 keV[45] or 468 keV[42, 43, 44]. Also it was not possible to detect gamma-rays of energies 249 keV, 292 keV, 308 keV, 542 keV and 822 keV seen in Coulomb excitation[43] of ^{75}As. The gamma-ray at 419 keV was only

just of significant intensity in these spectra but it was included as its intensity agreed with that found by several other authors and this was considered sufficient evidence for its existence. The spectra taken with the first set of sources and the 25 cm^3 detector showed a gamma-ray of energy 834 $\pm$ 2 keV but this was thought to be of sufficient intensity for its presence to be reported by other authors and so a second source solution was purchased. This failed to confirm the presence of a gamma-ray at 834 keV and thus it was concluded that the first source solution must have been contaminated!

The spectra, carefully searched by hand in the regions corresponding to possible gamma-ray transitions, were used to establish the maximum intensities of the gamma-rays reported by previous authors and which were not seen in these spectra. From the minimum detectable peak areas in a given region of the spectra it was possible to estimate the counting time required to improve the counting statistical accuracy to a level at which the intensities of the 822 keV and 469 keV gamma-rays reported by Pratt[44] could be 'seen'. Since the spectra already recorded had taken up to 12 days each and their extensions to reach the levels reported would have involved counting times increased by a factor of eight, this study was not considered feasible. These estimates do not

agree very well with the figures reported by Pratt who claimed to have recorded spectra for periods up to 240 hours. However, no mention was made of the ADC resolution used or of the system counting rate.

6.7 Coincidence studies

Several of the gamma-ray transitions can be placed in the decay scheme of ^{75}Se by observing coincidence spectra between well established transitions and those of interest. In particular, it was thought wise to confirm the results of the analysis of the singles spectra by coincidence work where this was possible.

The gamma-gamma fast - slow coincidence system was set up using the 25 cm^3 detector to gate the spectrum from the X-ray detector. The resolving time used was fairly long (100 nS) as the threshold of the time pick-off discriminator on the X-ray detect r, although at its minimum level, was at about 6-8 keV. This meant that the low energy region around the K X-rays (11 keV) showed a severe time walk with respect to the higher energy regions resulting in the need for a long fast coincidence resolving time.

The energy gate of the 25 cm^3 detector was adjusted to pass energies in the range 275 keV to 285 keV (279.5 keV peak). The resulting coincidence spectrum,

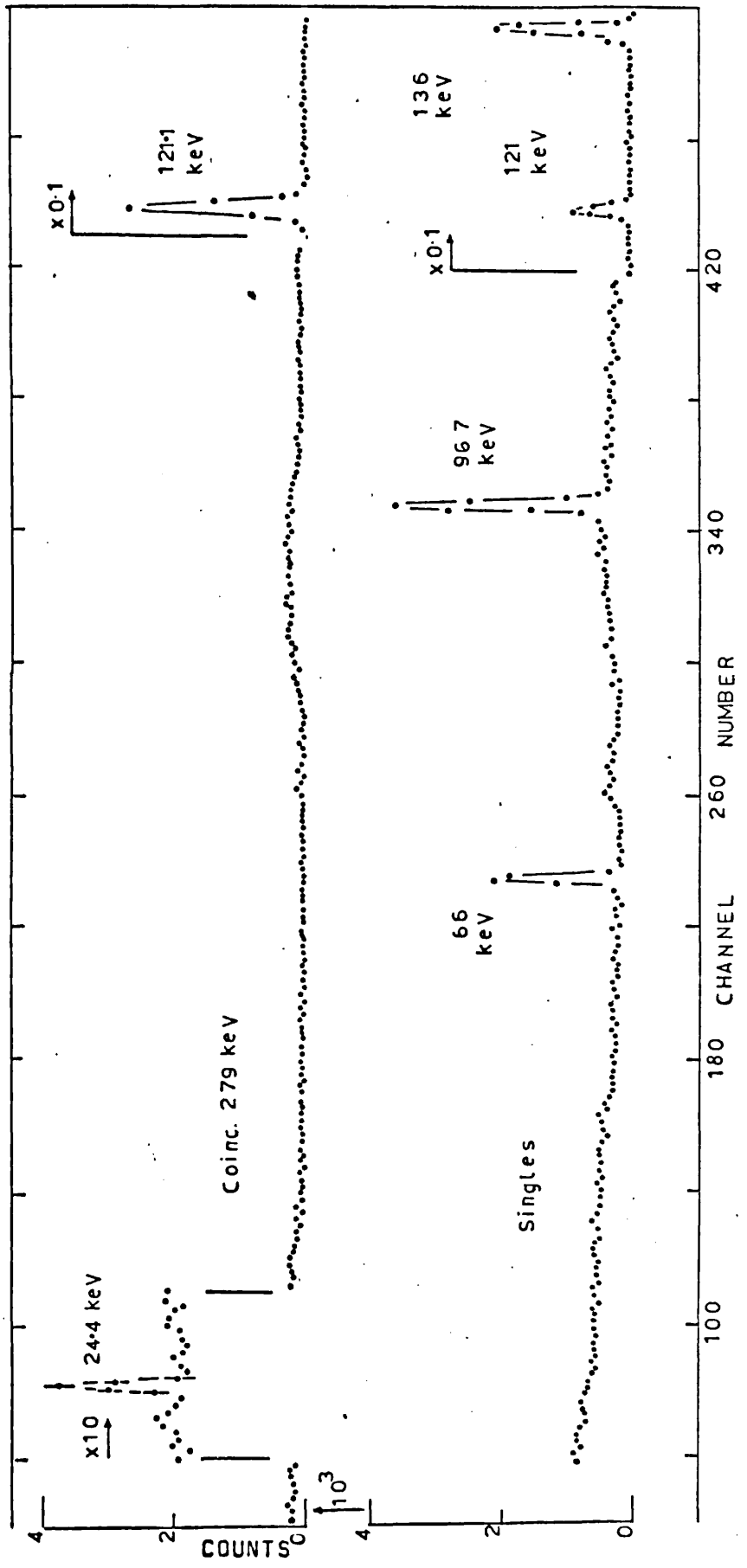

FIGURE 6.5: Coincidence spectrum: Gate 279 keV

corrected for chance contribution, is shown in figure 6.5. The 24.4 keV gamma-ray was thus shown to be coincident with the 279.5 keV gamma-ray. Its intensity was deduced from the coincidence spectrum by comparison with the 121 keV gamma transition. Its value of 0.058 $\pm$ 0.01 (relative to I(265)=100) is consistent with that measured from the singles spectrum.

The energy gate of the 25 cm^3 detector was moved to the 198.5 keV peak, again passing about 5 keV on either side of the centre of the peak. The resulting coincidence spectrum obtained from the X-ray detector is shown in figure 6.6. This showed that the 80.3 keV gamma-ray was in coincidence with the 198.5 keV gamma-ray. Its intensity was deduced by comparison with the 66 keV gamma transition and was found to be 0.011 $\pm$ 0.002 relative to I(265) = 100. This was in good agreement with the intensity measured from the singles spectrum.

The 265 keV photopeak was selected by the 25 cm^3 detector and the system was used to search for a possible 15 keV transition. This investigation was not completed as the counting time predicted by section 4.8 was 2×10^7 seconds.

The coincidence system was set up with a 5 cm^3 Ge(Li) detector in coincidence with the 25 cm^3 Ge(Li) detector. The energy gate was selected by the 5 cm^3 detector to pass the 198.5 keV photopeak. It was hoped that this study might reveal the 373 keV gamma-ray reported[45] but no evidence was

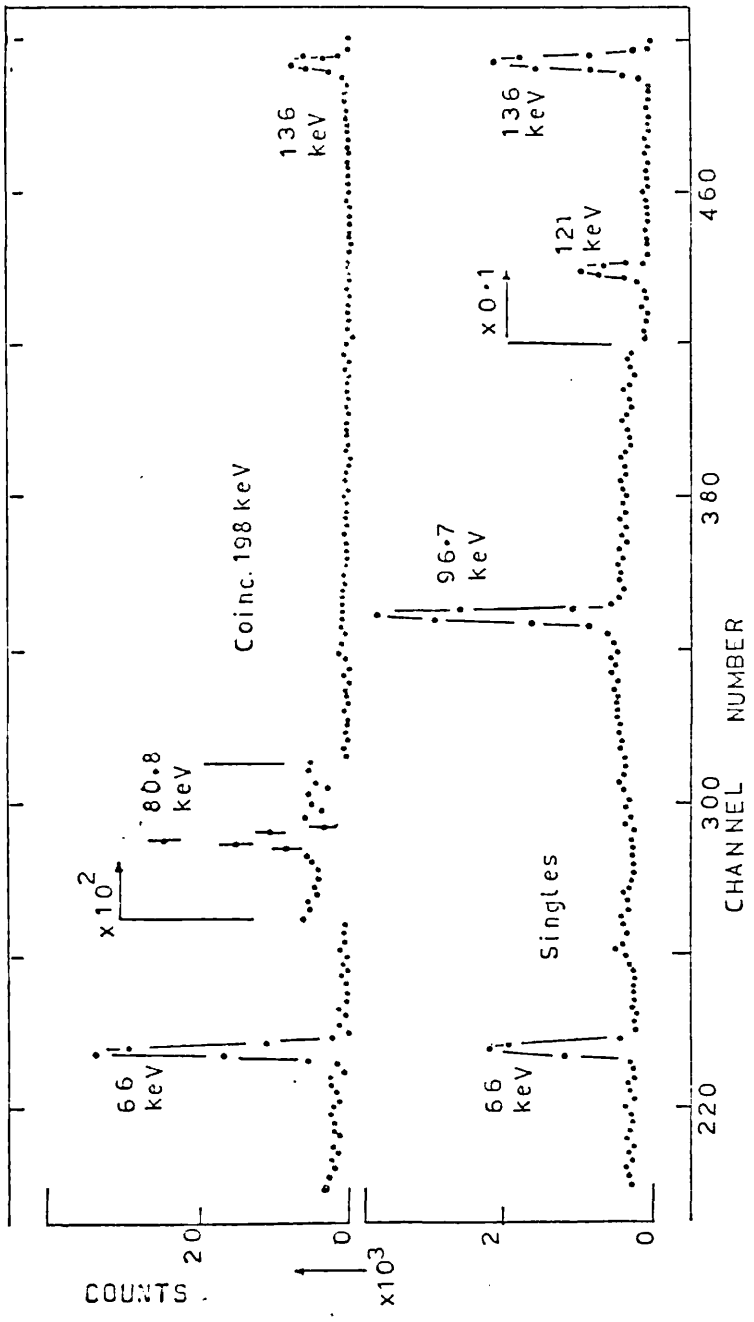

FIGURE 6.6 Coincidence spectrum: Gate 198 keV

found for coincidences between the 198.5 keV gamma-ray and such a transition.

6.8 Reduced transition probabilities

Coulomb excitation studies by Robinson et al.[43] have been used to measure experimentally the B(E2) and B(M1) values for the main ^{75}Se transitions of these multipolarities. From the present work it is possible to estimate an experimental value for the B(E2) value for the 81 keV transition and the B(M1) value for the 15 keV transition by assuming the mixing ratio and the B(E2) value for the 280 keV transition as measured by these authors.

The calculation gives a B(E2) value for the 81 keV transition of 10 ± 3 wu and a B(M1) value in units of $10^2/(e\hbar/2Mc)^2$ of 4 ± 2 from the relative transition intensities measured in this work.

6.9 Conclusions

A detailed study of ^{75}Se has confirmed the presence of two gamma-rays of 24 keV and 81 keV previously suggested and has supported their positions in the decay scheme. The study failed to detect some of the weaker modes of decay seen by some other authors but as most of these were found by Coulomb excitation their detection from the straight decay of ^{75}Se

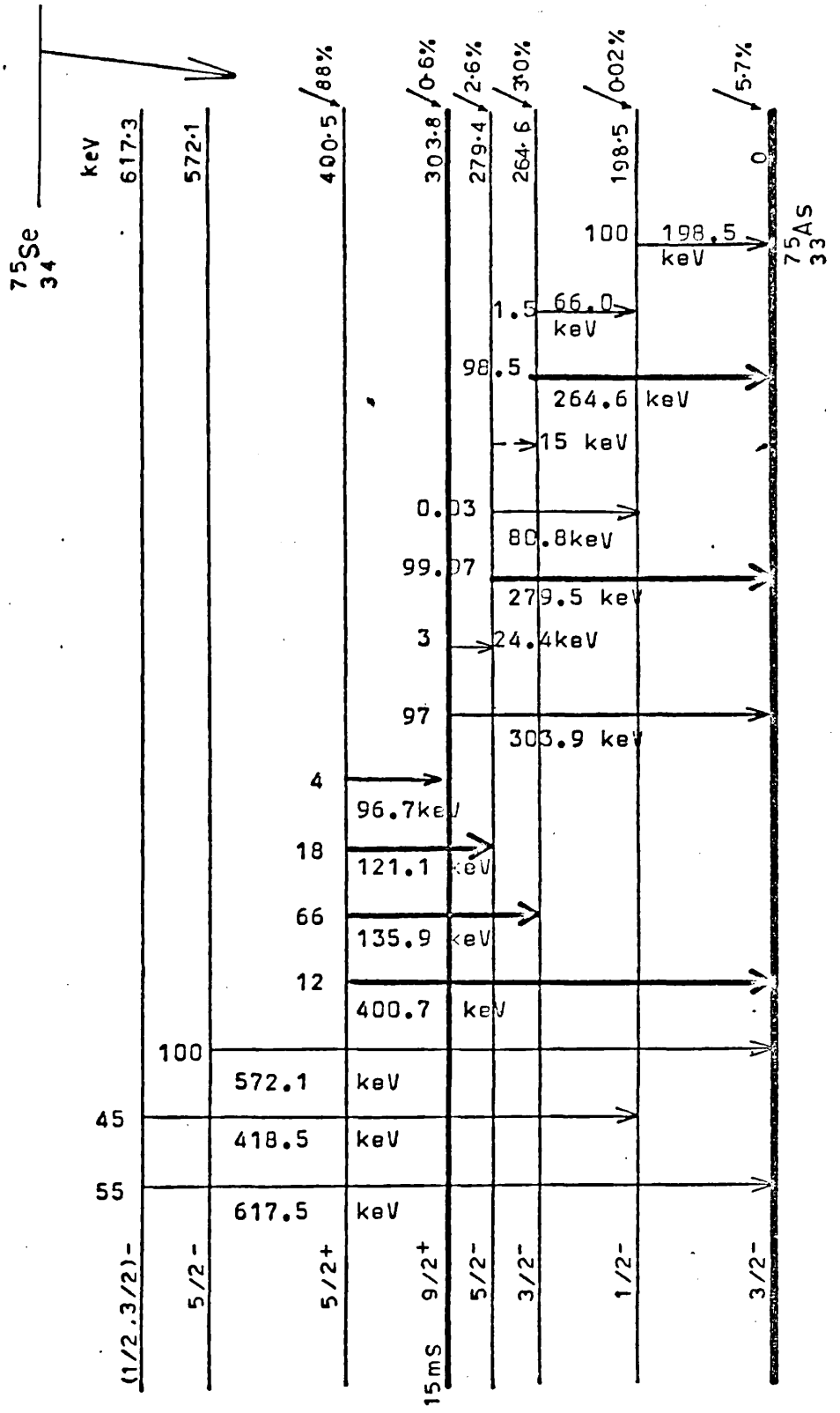

FIGURE 6.7 Decay scheme for ^{75}Se from the present work

is not as likely. The presence of a gamma-ray of energy 14.9 keV is thought to be just detected in the spectra obtained.

The decay scheme as measured in this study is shown in figure 6.7 together with the gamma-ray transition branching ratios.

CHAPTER 7 THE DECAY OF ^{207}Bi

7.1 Introduction

The main gamma-ray transitions following the decay of $^{207}_{83}Bi$ by electron capture to $^{207}_{82}Pb$ have been extensively studied. The energies and intensities of these transitions have been measured from studies of internal conversion lines made by Alburger et al.[46] and by Brady et al.[47]; external conversion spectra[48] and by gamma spectra taken with NaI detectors by Lazar and Klema[49] and by Prescott[50]. Further investigations by Chilosi et al.[51] into the weaker transitions used NaI counters and sum-coincidence techniques. The good energy resolution of the Ge(Li) detector has been used by Robinson et al.[52] for the precise determination of the energies of the two most prominent gamma-rays.

The gamma decay of the excited states of ^{207}Pb is of particular interest as the independent particle model has been applied by Pryce[53] to this isotope to predict its energy levels and spins corresponding to the single particle (hole) states.

Although the main gamma transitions (see figure 7.7) have been well established the observation of the weaker modes of de-excitation has proved difficult. The branching ratio of the $f_{7/2}$ level at 2340 keV has previously been studied

by Chilosi et al.[51] but this work assumed that the 898 keV level ($p_{3/2}$) decays straight to the ground state with no branching to the $f_{5/2}$(570 keV) level. The possibility of a gamma-ray transition between the $p_{3/2}$(898keV) and the $f_{5/2}$ (570 keV) levels was considered by Alburger et al.[46] who placed an upper limit on the intensity of the K-conversion line corresponding to a transition of energy 328 keV.

Such a transition should be M1 in character but the extreme single particle shell model predicts that the M1 gamma-ray matrix element vanishes for transitions of this type where the orbital angular momentum would change. Transitions of this type where $J_i - J_f = L$ and $l_i - l_f = L + 1$ are known as 'l-forbidden' gamma-ray transitions.

Recently the M1 transition probabilities in the Pb region have been studied by Klemt and Speth[54] and by Harada and Pittel[55]. Both studies calculated theoretical transition probabilities for the l-forbidden gamma transition from the 898 keV to the 570 keV levels. The transition probabilities for the other M1 transitions in ^{207}Pb, based on these models, have been compared by these authors with experimental values; recent experimental data for the 898 keV level having been obtained by Klapdor et al.[56] and by Häusser et al.[57].

This present study was undertaken to identify and measure the weaker modes of gamma decay. It was felt that the use of coincidence techniques might well aid the search for these transitions.

7.2 Experimental details and analysis of the singles spectra

A 50 μCi source of ^{207}Bi was obtained from the Radiochemical Centre (Amersham) and the spectra used in these measurements were recorded two years after production of the isotope. Spectra were also recorded from a five year old ^{207}Bi source and the results obtained did not differ from those obtained with the newer source, thus eliminating the possibility of any effects from contamination of the source.

The spectra were taken with the 25 cm^3 Ge(Li) detector and the position of the 1770 keV full-energy peak was maintained with the digital stabiliser. The system was calibrated for energy and relative efficiency with standard sources as described in chapter 2 and the spectra were analysed using the programme Sampo (see section 3.4).

A typical spectrum showing the main ^{207}Pb gamma-ray transitions and the positions of the two gamma-rays of interest is given in figure 7.1. The full-energy peaks corresponding to the two weak transitions occur at awkward positions in this spectrum relative to the strong lines and

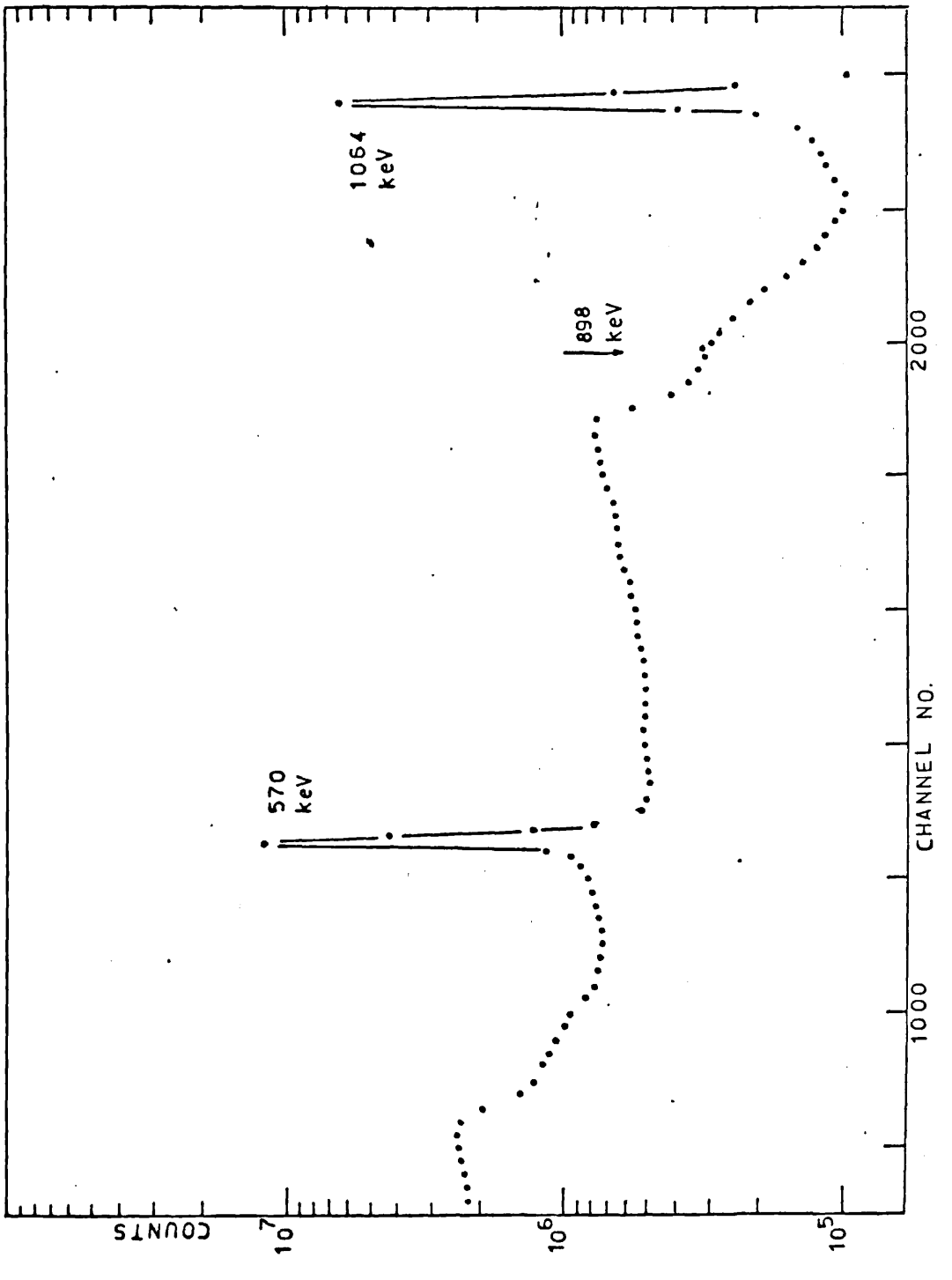

FIGURE 7.1 Singles spectrum ^{207}Bi

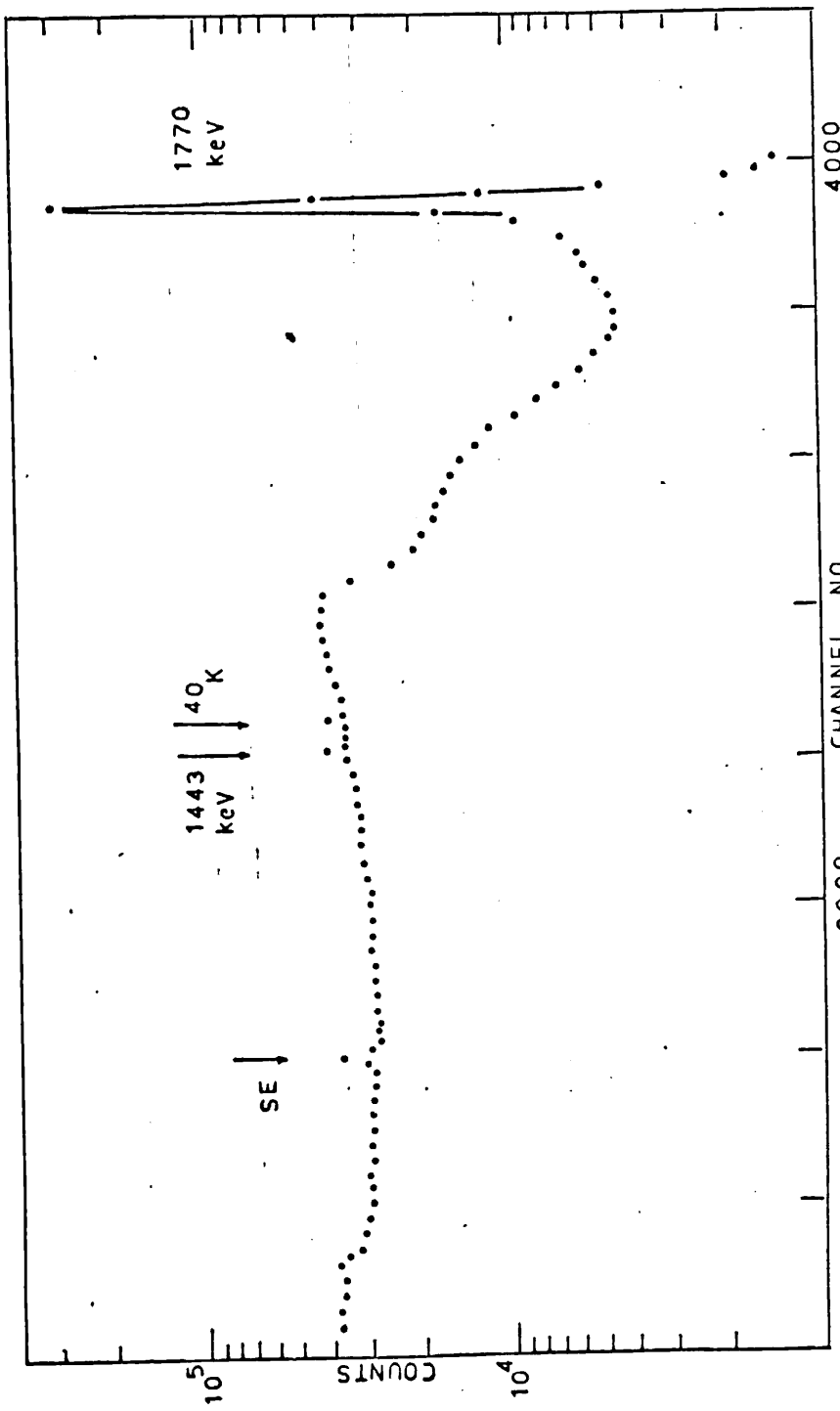

FIGURE 7.1 (cont)

SPIN CHANGE	ENERGY keV	GAMMA INTENSITY This work	Ref.46	TRANSITION INTENSITY
$p^-_{3/2}-f^-_{5/2}$	328.0 ±0.5	0.014 ±0.008		0.017 ±0.01
$f^-_{5/2}-p^-_{1/2}$	570.7 ±0.2	100	100	100
$p^-_{3/2}-p^-_{1/2}$	898.7 ±0.2	0.121 ±0.007	0.146 ±0.006	0.121 ±0.007
$i^+_{13/2}-f^-_{5/2}$	1064.1 ±0.3	76.5 ±4.1	79.6 ±1.6	85.7 ±4.5
$f^-_{7/2}-p^-_{3/2}$	1443.2 ±0.2	0.141 ±0.007	0.178 ±0.007	0.138 ±0.007
$f^-_{7/2}-f^-_{5/2}$	1770.3 ±0.5	8.2 ±0.4	7.23 ±0.03	8.1 ±0.4

TABLE 7.1 Energies and intensities of the gamma-ray transitions in ^{207}Bi

the natural background radiation from ^{40}K in the laboratory. The 898 keV full-energy peak occurs on the Compton edge of the 1064 keV transition and the 1443 keV full-energy peak is about 20 keV from the ^{40}K full-energy peak. Any attempt made to increase the system counting rate from the source in order to decrease the relative contribution of the ^{40}K full-energy peak unfortunately caused a deterioration in the resolution of the system and the consequent broadening of the two weak peaks under observation would have made the measurement of their energies and intensities difficult.

7.3 Results derived from the singles spectra

Figures 7.2 and 7.3 show the regions of interest expanded from a typical spectrum. The energy of the gamma transition from the $p_{3/2}$ level to the ground state was found to be 898.7 ± 0.2 keV and that of the transition from the $f_{7/2}$ level to the $p_{3/2}$ level was measured as 1443.2 ± 0.2 keV. This places the $f_{7/2}$ level at 2341.0 ± 0.3 keV and the $p_{3/2}$ level at 898.7 keV using the data for the other transitions as shown in table 7.1.

The two weak gamma transitions were found to have gamma-ray transition intensities of 0.121 ± 0.007 for the 898 keV gamma and 0.141 ± 0.007 for the 1443 keV gamma, normalized to a gamma transition intensity of 100 for the

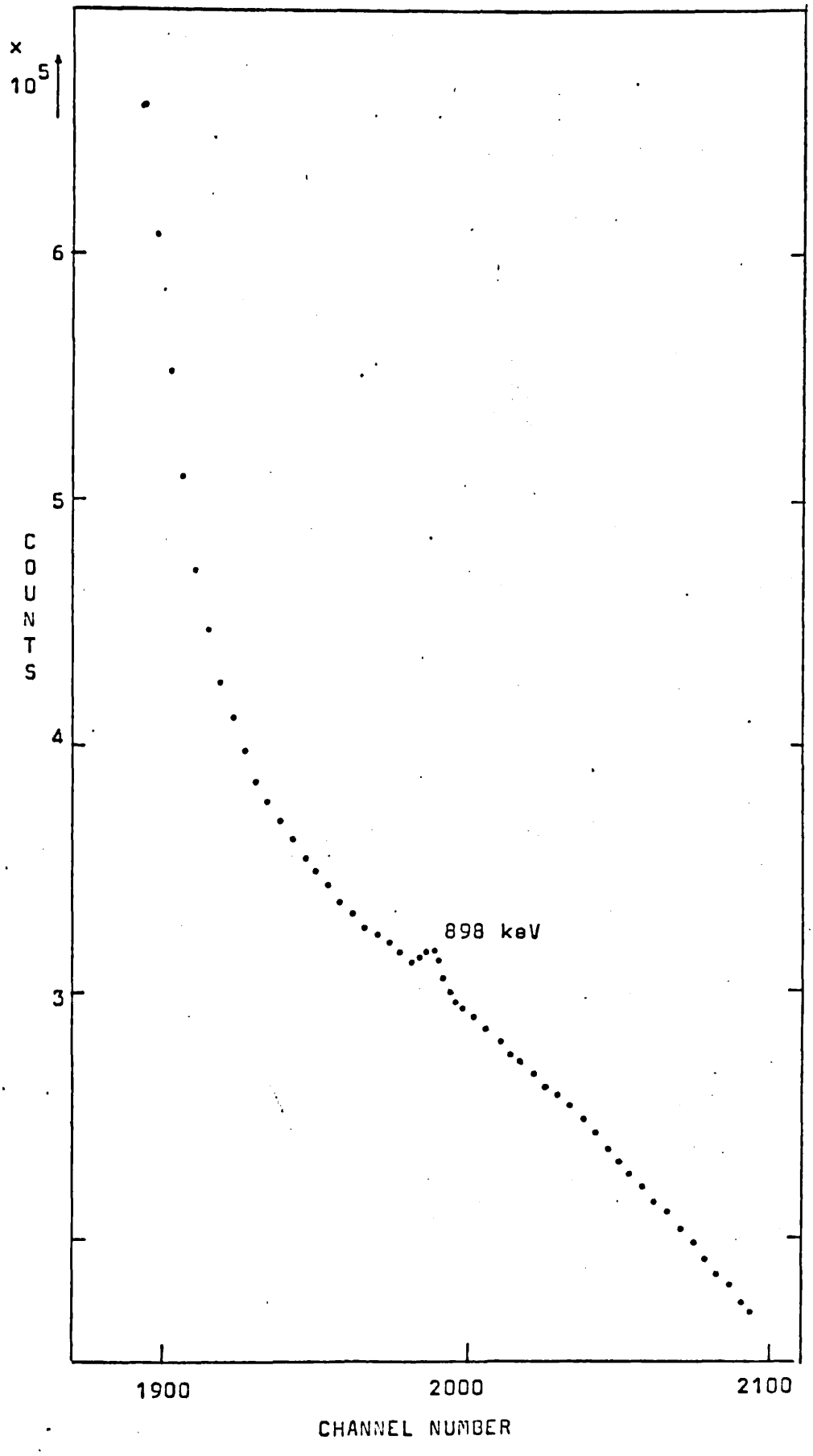

FIGURE 7.2 898 keV Transition

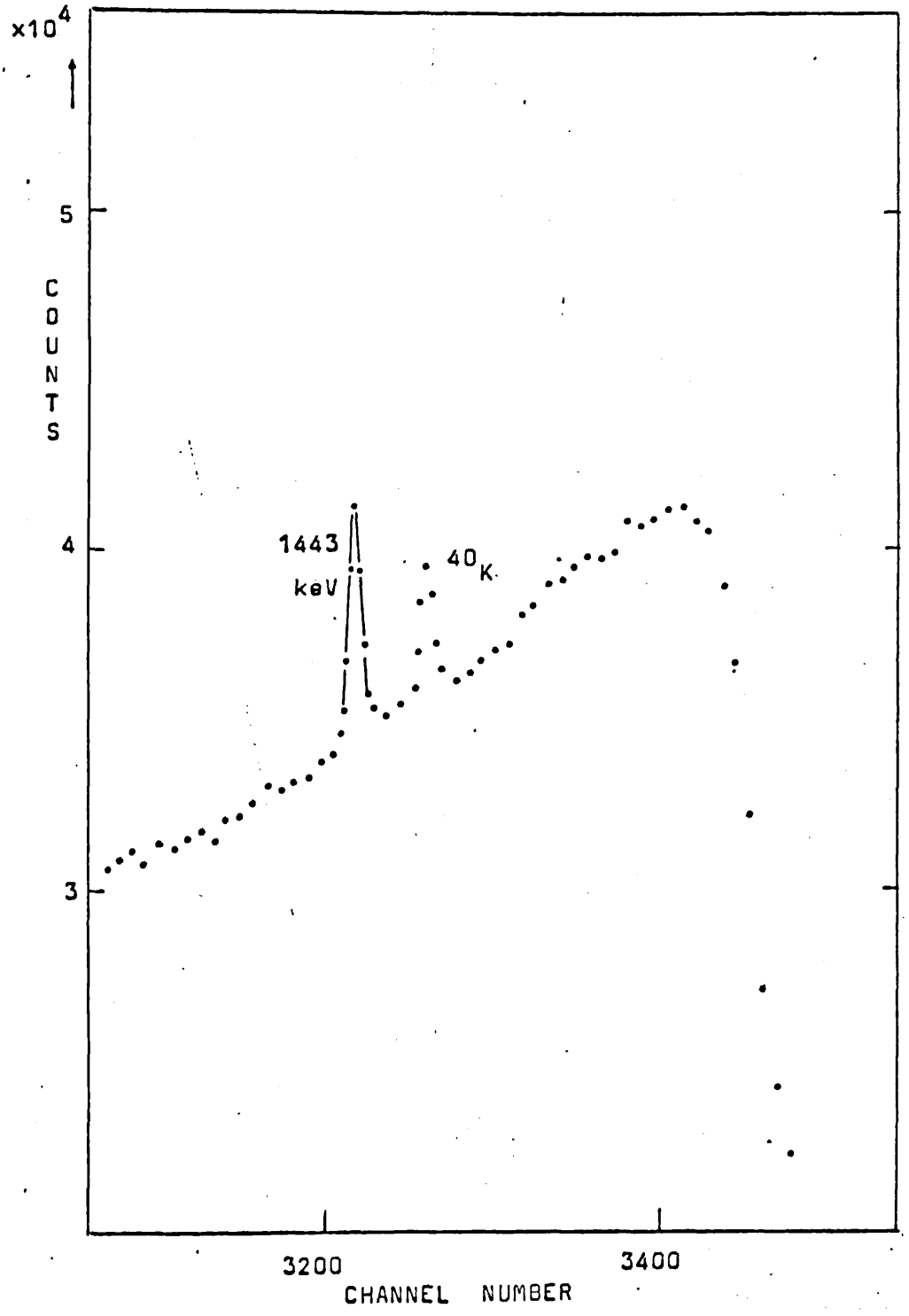

FIGURE 7.3 1443 keV Transition

570 keV gamma-ray. Table 7.1 gives the gamma transition intensities for ^{207}Pb based on the analysis of these singles spectra and also the transition intensities using experimentally determined values for the internal conversion coefficients taken from data published by Alburger et al.[46] and Lazar et al.[49]. The branching ratio of the 1443 keV and 1770 keV transitions from the 2341 keV level is 1.7 ± 0.1 from this data which is reasonably consistent with the experimental values of 2.3 ± 0.2 and 2.0 ± 0.6 found by previous workers [51, 46].

The interesting difference of 0.017 ± 0.010 between the transition intensities for the $f_{7/2}$ - $p_{3/2}$ (1443 keV) and the $p_{3/2}$ - $p_{1/2}$ (898 keV) transitions is an indication of the possibl. intensity of the 'l-forbidden' transition between the $p_{3/2}$ (898 keV) and the $f_{5/2}$ (570 keV) levels which would have an energy of 328 ± 0.5 keV. An upper limit of 0.014 ± 0.008 (relative to $I_\gamma(570) = 100$) for the intensity of gamma radiation of this energy can be evaluated from this figure for the transition intensity by assuming pure M1 radiation and a theoretical internal conversion coefficient of 0.23 from the tables of Sliv and Band[58]. An unsuccessful search was made in the appropriate region of the spectra for any indication of this transition but this region is seriously affected by Compton scattering from higher energy gamma-rays. An upper limit of 0.04 ± 0.01 was found for the intensity of this

transition from the spectra.

The measurement of the branching ratio of the 2341 keV level can be combined with the value (measured by Lazar and Klema[49]) of δ^2 (see section 1.2) for the 1770 keV transition to estimate the ratio of 1443 keV E2 radiation to 1770 keV E2 radiation. These experimental results give a value of 2.4 ± 0.5. This value is somewhat lower than the value obtained by Chilosi et al.[51] and can be compared with the value deduced from a single particle model for ^{207}Pb which is 3.221 ± 0.005 based on the measured energies and assuming constant charge density in the nucleus. Values of 2.82 ± 0.07 and 2.74 ± 0.07 are quoted by Chilosi et al.[51] for the harmonic oscillator potential and by Blomqvist and Wahlbern[59] for the diffuse potential respectively.

The extreme single particle model suggests that the transition $p_{3/2}$ to $f_{5/2}$ (328 keV) is 'l-forbidden' but experimental observations on many isotopes exhibiting transitions of this type by Govil and Khurana[60] indicate finite transition intensities. Several attempts have been made to account for these finite transition intensities and it is interesting to compare the predictions of recent theoretical calculations[55, 56] with the experimental result obtained here. Harada and Pittel[55] considered the effects of magnetic dipole core polarization on M1 dipole moments in ^{207}Pb and calculated that the 'l-forbidden'

(328 keV) transition should be hindered by a factor of about 100 relative to the 898 keV transition. This figure implies that the ratio of the gamma-ray intensities seen in the singles spectrum should be about 0.001.

The experimental results obtained need to be combined with the appropriate mixing ratio for the 898 keV transition to yield the experimental ratio of 328 keV M1 gamma radiation to 898 keV M1 gamma radiation. Using the value of δ (E2,M1) = -0.31 ± 0.06 obtained by Häusser et al.[51] the experimental values yield a ratio of about 0.16 ($\pm$60%). This is at least a factor of 10^2 larger than the theoretically predicted ratio.

7.4 Sum - coincidence studies

The technique of sum-coincidence spectra has been outlined in section 5.7. To confirm the 1443 keV - 898 keV cascade and to search for the 328 keV transition the system was set up using one NaI counter and the 25 cm^3 Ge(Li) detector.

The spectrum obtained with the sum energy window set to cover the range 2280 keV to 2360 keV is shown in figure 7.4. This revealed, in addition to the prominent 1770 keV - 570 keV cascade, the much weaker 1443 keV - 898 keV cascade.

The idea was then to move the sum energy window to 1770 keV in the hope of revealing a cascade composed of 1443 keV and 328 keV gamma-ray transitions. However, this sum energy

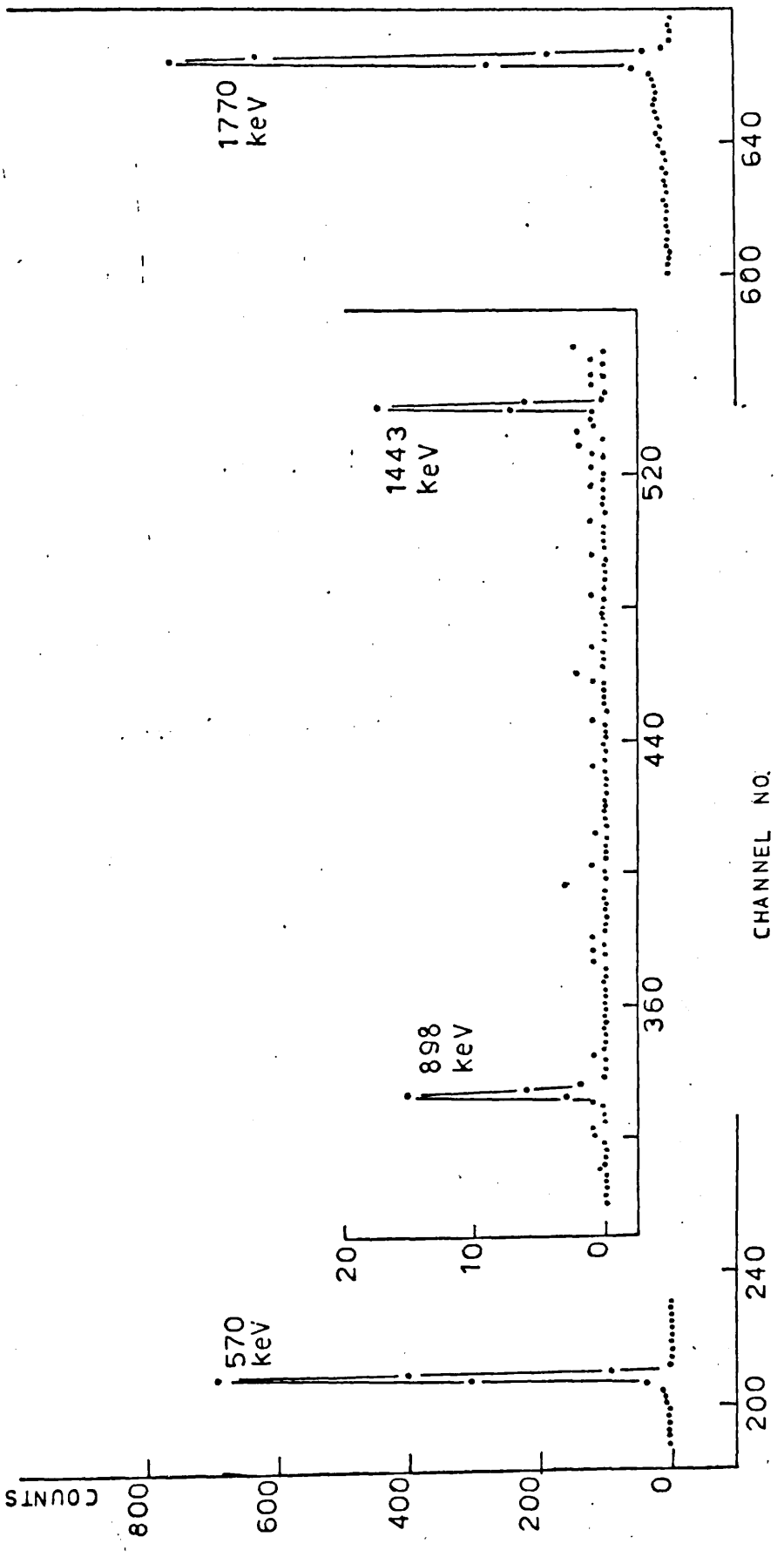

FIGURE 7.4 ^{207}Bi Sum-coincidence spectrum
sum energy 2340 keV

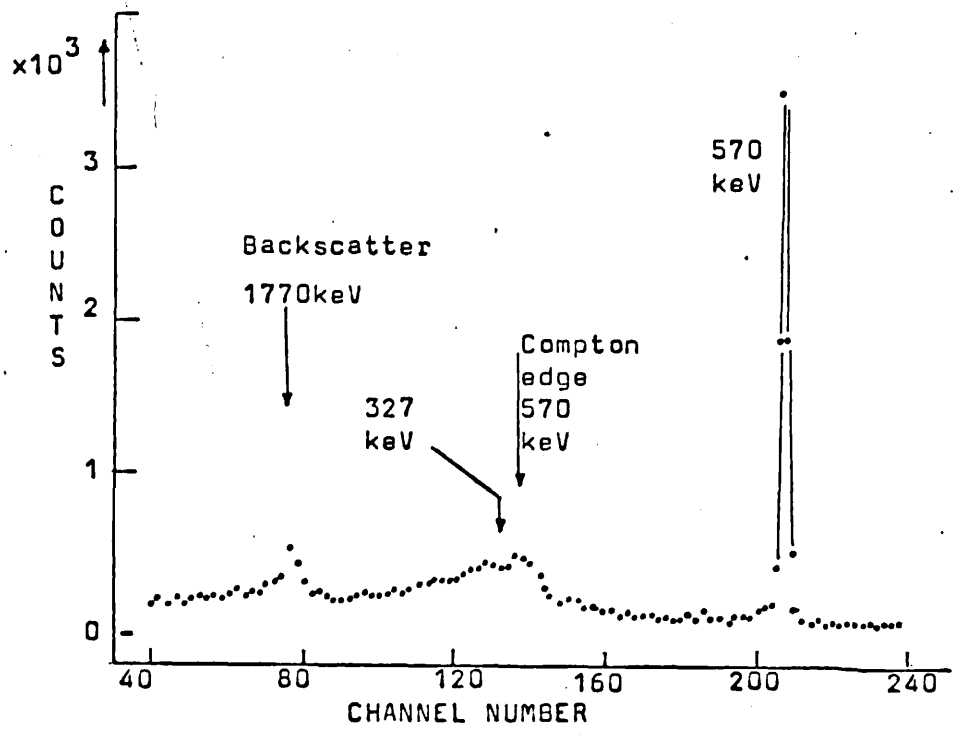

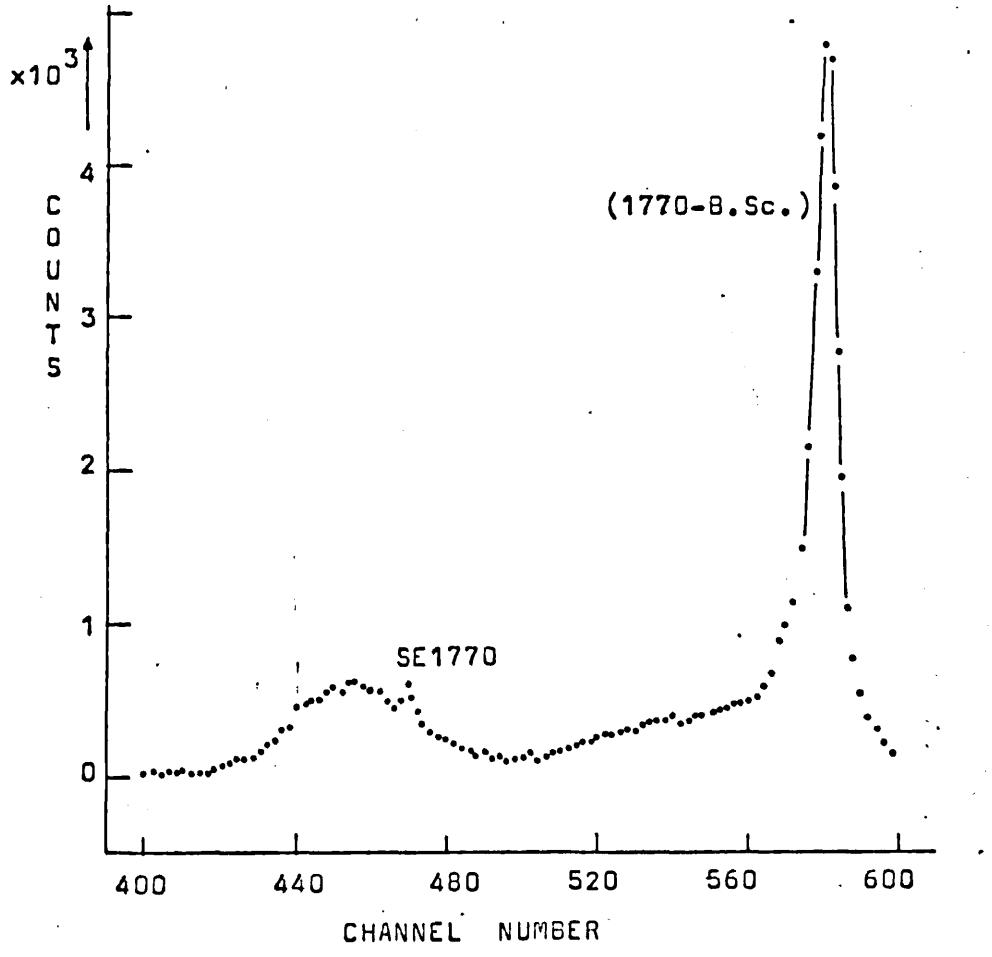

FIGURE 7.5 ^{207}Bi Sum -coincidence spectrum

Sum Energy 1770 keV

can also be reached by gamma interactions due to a 570 keV full-energy event summing with a Compton event due to a 1770 keV decay or by Compton events from 570 keV and 1770 keV transitions. In addition, the seriousness of intercounter scattering was well demonstrated and the resulting spectrum (figure 7.5) indicates clearly the two broad scattering distributions due to the backscattering of a 1770 keV gamma-ray in either counter entering the second counter to produce a sum energy satisfying the gate requirements. Any evidence for the 328 keV transition would be completely masked by these effects.

7.5 Coincidence studies

A gamma-gamma coincidence system was set up using a resolving time of 44 nS with the NaI counter gated on the region covering 1400 keV to 1480 keV. The spectrum recorded in the Ge(Li) detector is shown in figure 7.6 and again confirms the coincident 898 keV transition. It did not reveal any indication of the 328 keV transition. This was possibly masked by the high level of 570 keV Compton interactions detected in coincidence with the NaI counter gate which necessarily passed Compton interactions originating from 1770 keV gamma-rays.

From the spectrum, it was possible to determine an upper limit for the intensity of the 328 keV gamma transition. This was found from the area of the 898 keV full-energy peak

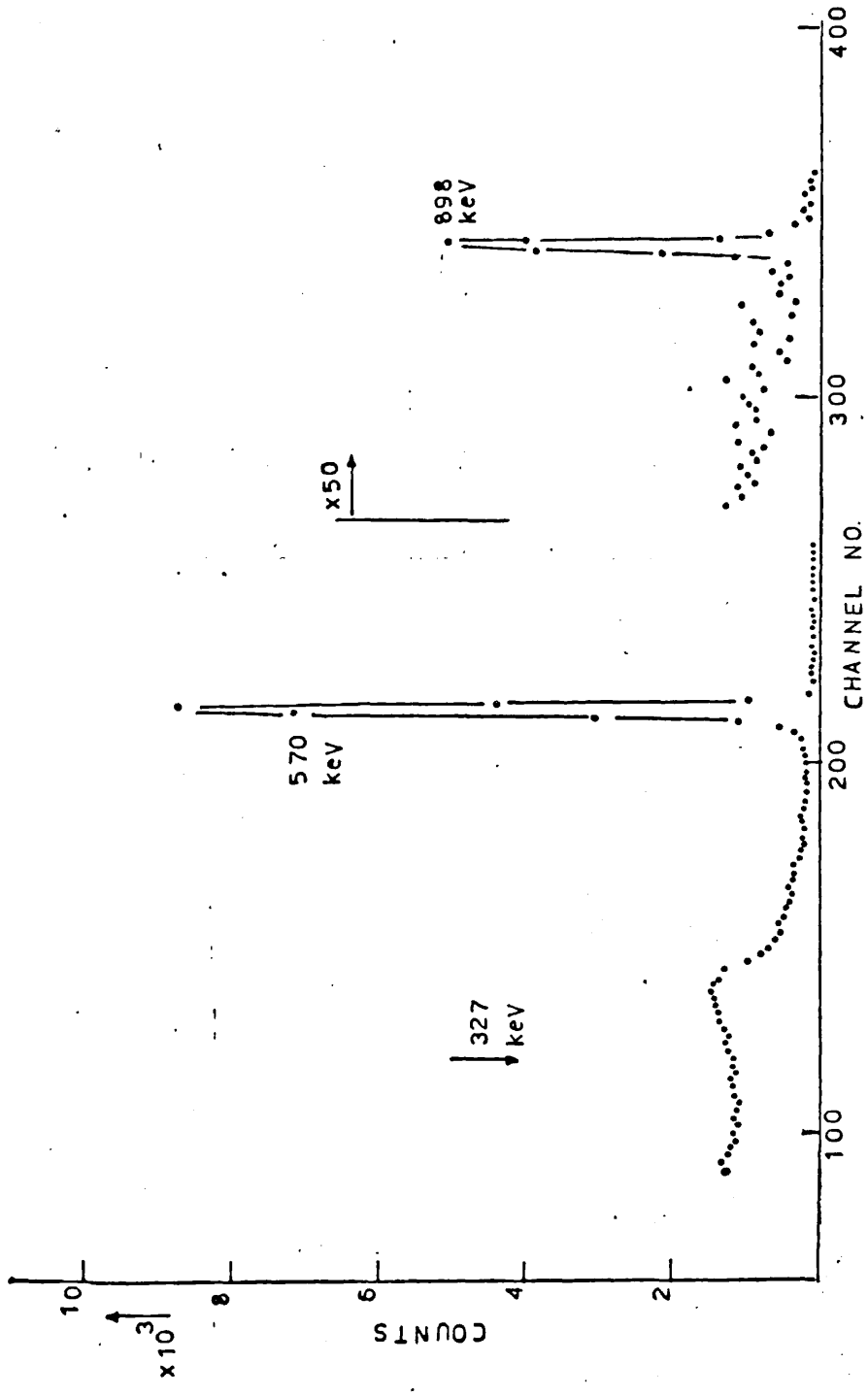

FIGURE 7.6 $^{207}_{83}Bi$ coincident with 1443 keV region

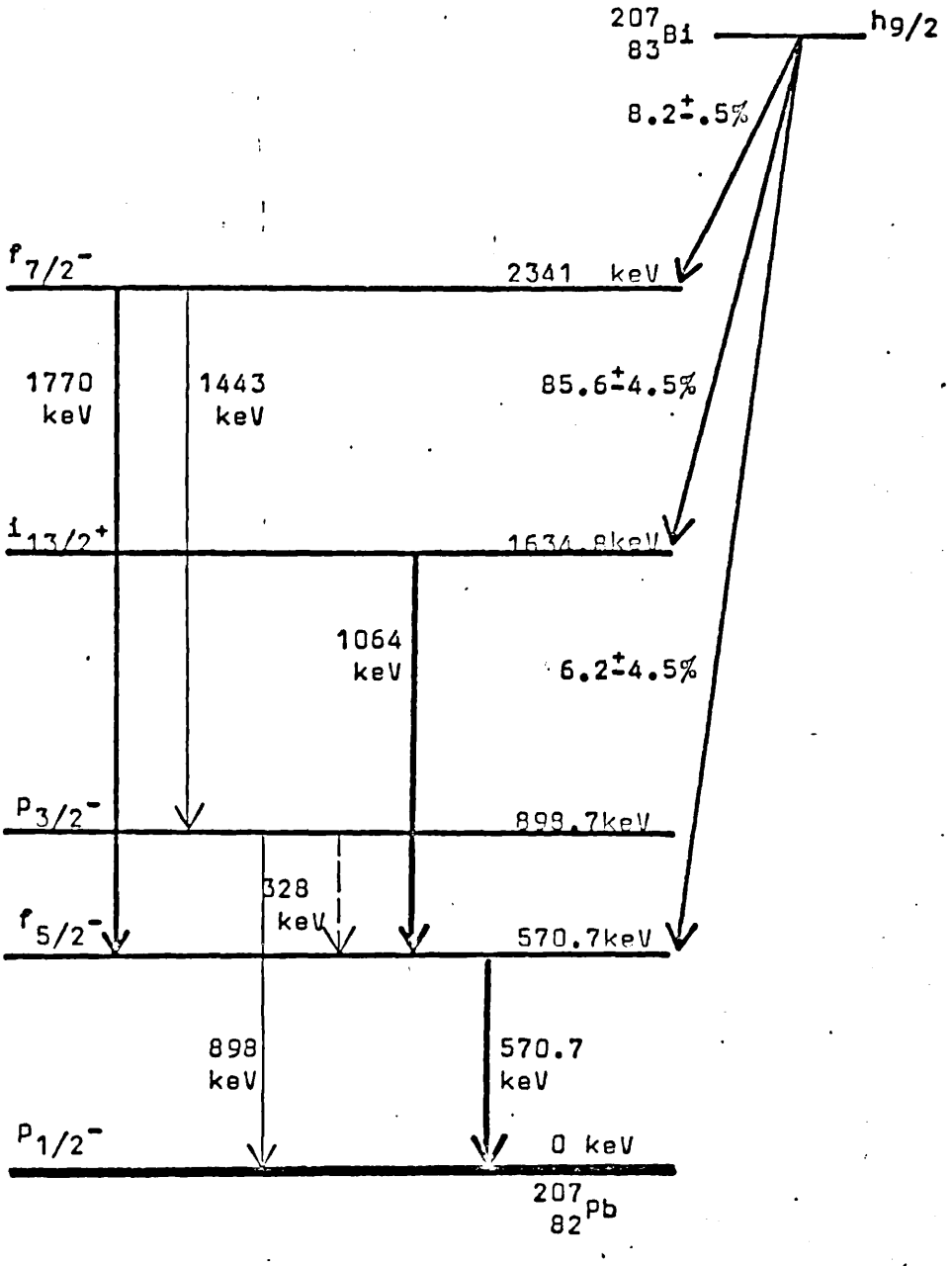

FIGURE 7.7 Decay scheme for ^{207}Bi

and using the criterion given in section 2.6. The coincidence spectrum gave a value for $I_\gamma(328)$ of less than 0.036 on the $I_\gamma(570) = 100$ scale. This is at least consistent with the estimate from the singles spectrum and indicates that a counting time of at least five months would be required with the system used to detect this gamma transition.

7.6 Conclusions

The results of singles spectra taken are sufficient to give some indication of the intensity of the 'l-forbidden' gamma transition of energy 328 keV and to suggest that it is not significantly hindered compared to the M1 component of the transition of energy 898 keV. However, the coincidence experiments failed to detect this transition. It is possible that an anti-Compton shield for the Ge(Li) detector might enable it to be 'seen' in a singles spectrum by reducing the 570 keV Compton continuum.

The final decay scheme for ^{207}Bi with electron capture intensities to ^{207}Pb based on these measurements is shown in figure 7.7.

CHAPTER 8 THE GAMMA DECAY OF ^{76}As

8.1 Introduction

The beta and gamma decay modes of $^{76}_{33}As$ have been the subject of frequent examination using bent crystal[61], double-focussing[62] and magnetic spectrometers[63, 64, 65] and NaI detectors[66, 67]. The obviously complex nature of the decay scheme has lent itself to several investigations using Ge(Li) detectors[68 - 74]. Several of these studies[70, 71, 72, 73, 74] have used coincidence techniques in an attempt to establish the various gamma cascades.

The fairly short half-life (26 hours) of the decay, coupled with the complexity of the decay, has resulted in a wide variety of variations in the gamma-rays reported and in their positions in the decay scheme. The purpose of this work was to further the knowledge of this decay, paying particular attention to the discrepancies in the previous work on this isotope.

8.2 Experimental procedure for singles spectra

The sources of ^{76}As were prepared by neutron irradiation of As_2O_3. The main contaminant present produced ^{124}Sb with a half-life of 60 days. Since the gamma energies expected from ^{76}As were all above 100 keV, the 25 cm^3 Ge(Li) detector was used throughout the study. The time required to search

for the weaker modes of decay necessitated the use of a source over several half-lives. For a fixed geometry this meant a rapid fall-off in counting rate with changes in resolution and possible pulse height drifts. The use of the digital stabiliser could correct for this but only with a considerable loss in energy resolution. Since it was not possible to replenish the source at intervals more frequent than one week, a control system was developed[75] to move the source towards the detector in order to compensate for the decay and so maintain a constant detector counting rate. Provided that this movement occurred over a limited range it did not affect the relative efficiency calibration (see section 2.4). The source was mounted on a toy railway engine whose position was controlled by suitable electrical pulses. The detector counting rate was monitored by a simple ratemeter whose output triggered the driving pulses to the train whenever the counting rate fell below a preset threshold. A counting rate constant to 1% was thus obtained.

Three runs of singles spectra were recorded at different counting rates. Each run consisted of one spectrum taken to determine the positions of the main peaks followed by a longer run to accumulate sufficient statistical significance to search for the weaker peaks. The system was stabilised on the 1787 keV full-energy peak and was calibrated before and after the runs. The energy calibrations were used

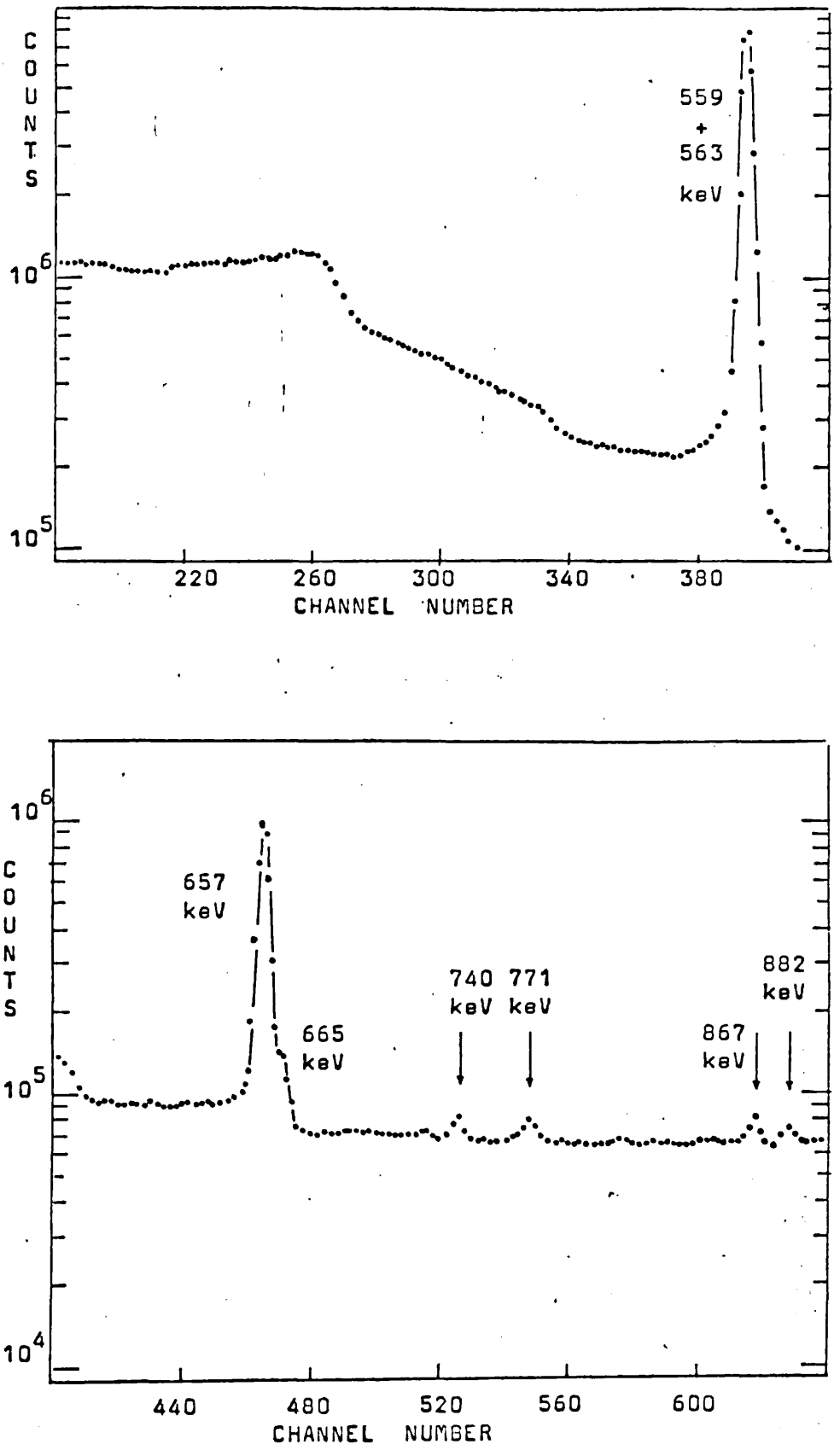

FIGURE 8.1 Singles spectrum of ^{76}As

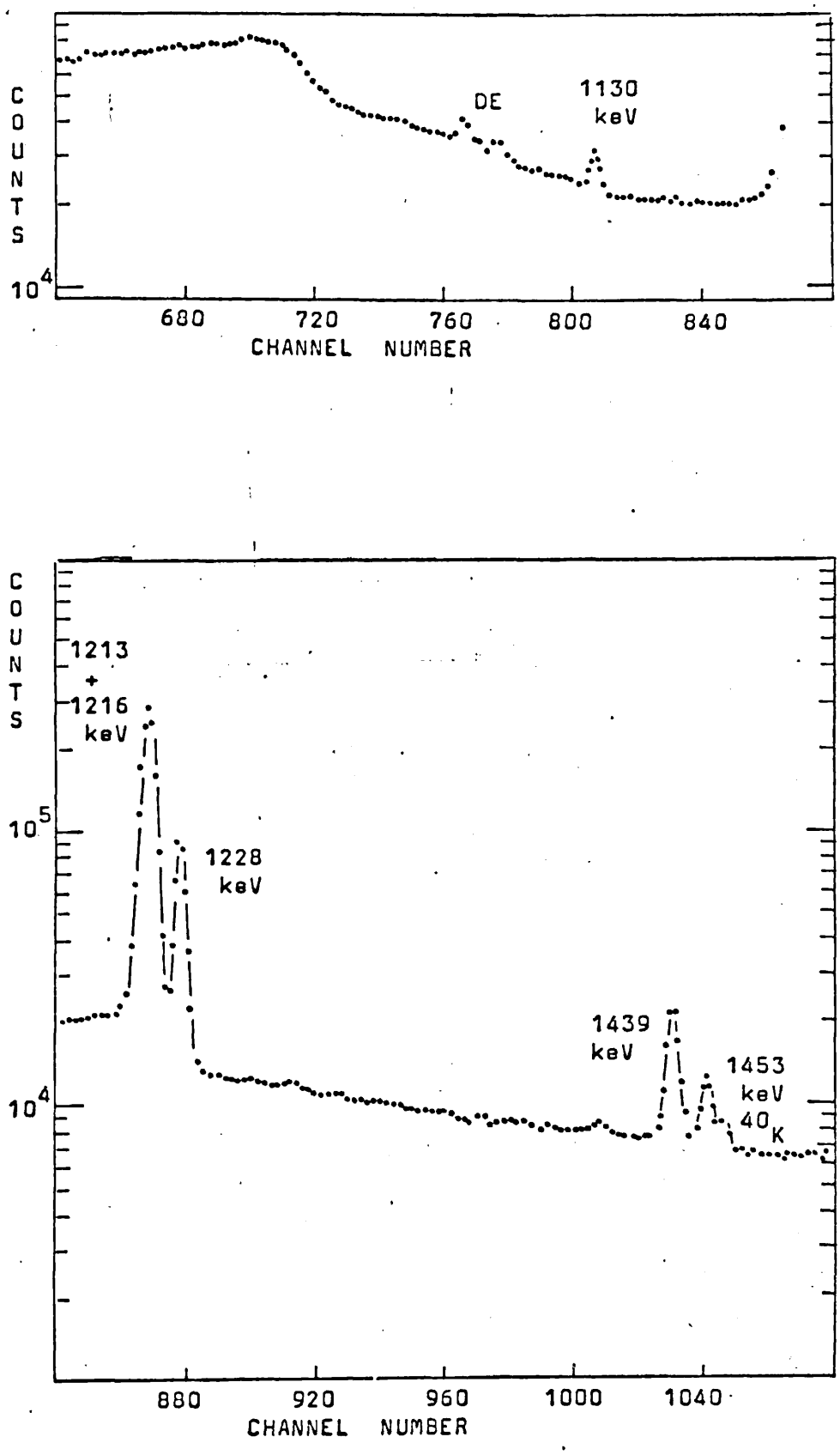

FIGURE 8.1 (continued)

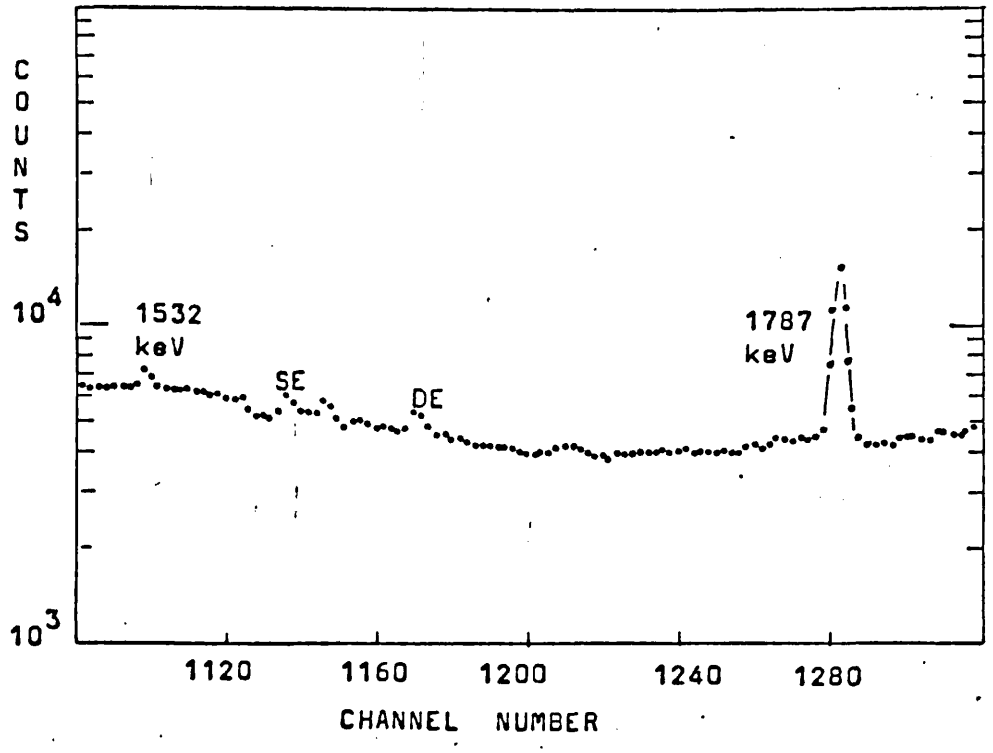

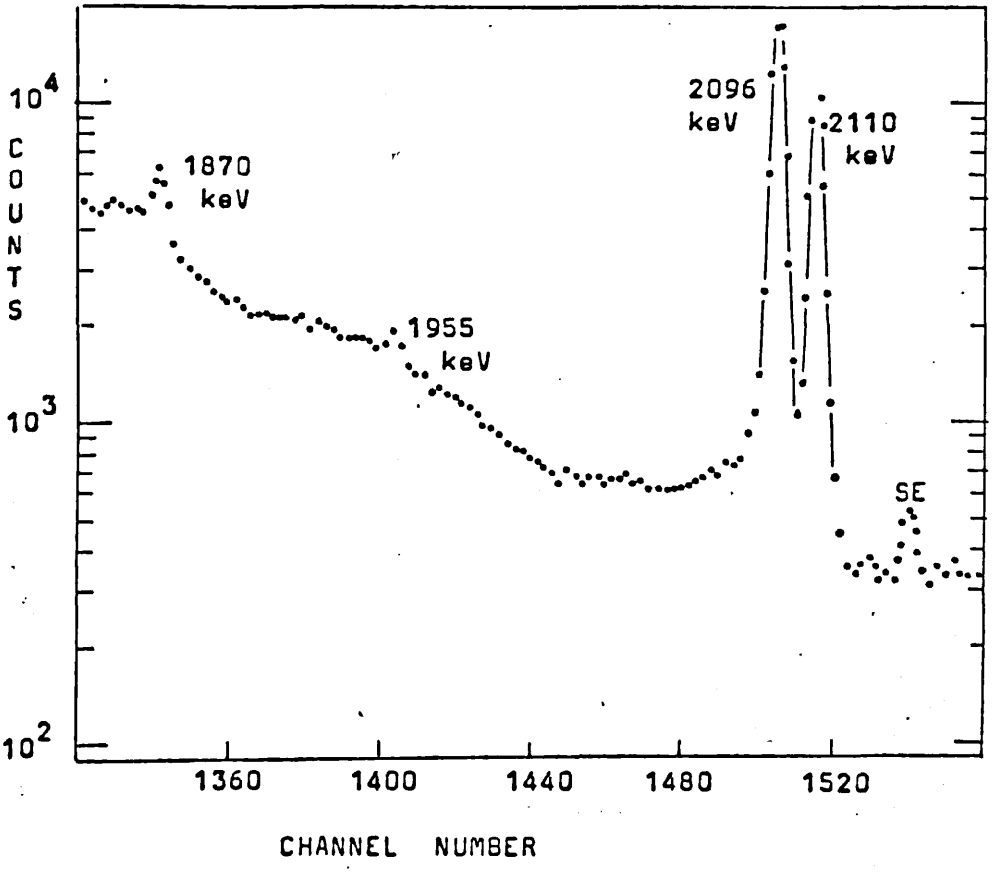

FIGURE 8.1 (continued)

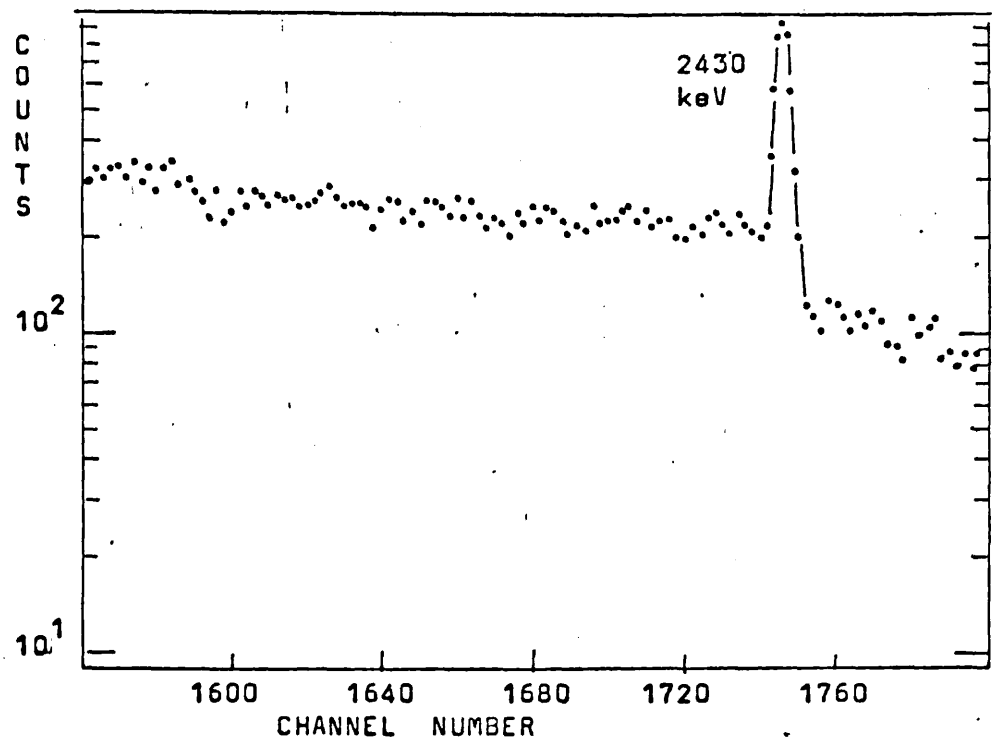

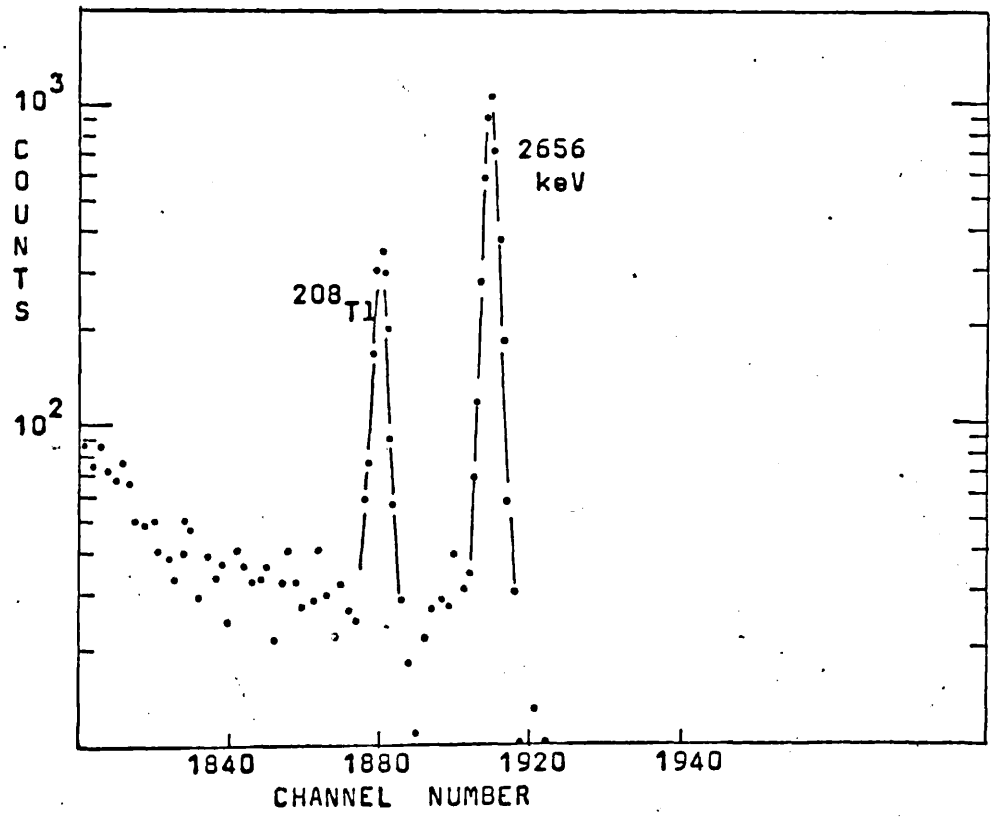

FIGURE 8.1 (continued)

to measure the energies of the main peaks in the ^{76}As spectrum and these were then used as internal standards to determine the energies of the weaker peaks. From the three runs it was possible to eliminate contaminant radiations and background gamma-rays. Also a check was made for summing effects and for double and single escape peaks.

The spectra were analysed using the programme Sampo and the routine FITS to find the areas of the full-energy peaks. In addition, the spectra were searched by hand in the appropriate regions to establish maximum intensities for transitions reported by previous authors but not detected in these spectra.

8.3 Results of singles spectra

The mean energies and intensities of the gamma-rays revealed by this study are given in tables 8.1 and 8.2 together with the results of some previous workers. A typical singles spectrum is shown in figure 8.1.

8.4 Experimental procedure for coincidence spectra

A fast-slow coincidence system using a NaI counter as the energy gate and the 25 cm^3 Ge(Li) detector was set up with a resolving time of 44 nS to investigate the more prominent gamma cascades. To obtain reasonable coincidence statistics it was necessary to pay some attention to the problem of source decay during the counting period.

ENERGY keV Ref. 71	ENERGY keV Ref. 73	ENERGY keV Ref. 72	ENERGY keV This work
			220±1.5*
301.3±.8	301.7±7	300.3±.3	303.4±.5
			316.6±.5
402.7±.5	403.0±.6	404 ±1	403.8±.4
456.7±.4	456.8±.6	456.0±.6	457.1±.5
472.9±4	472.8±.5	475.0±.1	471.8±.5
559.0±.2	558.9±.3	559.3±.1	559.1±.5
563.0±.3	563.0±.3	563.4±.1	562.7±.7
571.1±.3	570.8±.3	572.4±.1	572.0±1.5
575.2±.3	575.1±.3	576.8±.1	
639 ±1*		639*	
656.9±.2	656.9±.3	657.2±.1	657.1±.5
665.3±.2	665.2±.3	665.4±.1	665.2±.5
695.3±.6	695.0±.4	695.7±.5	693.8±.5
726.4±.5	726.9±.5	727.0±.1	726.4±.5
740.0±.3	739.9±.4	740.4±.1	739.6±.5
755.2±1	755.0±.7	754.8±.6	
771.0±.3	771.6±.4	772.1±.1	771.4±.5
797.0±1			
809.3±1	809.7±.4	809.9±.1	809.4±.5
863.3±1	863.6±.7		
867.5±.3	867.5±.6	868.1±.1	867.3±.5
882.0±.3	881.9±.4	882.8±.5	881.5±.5
		955.0±2	
980.7±.4	980.8±.7	981.7±.1	980.6±.5
		1051	1052.0±1*
	1098.1±1	1101±3	

* from coincidence measurements

TABLE 8.1 Energies of ^{76}As gamma-ray transitions

ENERGY keV Ref. 71	ENERGY keV Ref. 73	ENERGY keV Ref. 72	ENERGY keV This work
	1117.2±.9		
1129.5±.3	1129.6±.4	1131/2	1129.6±.5
1212.6±.3	1212.7±.4	1213.3±.1	1212.5±.5
1215.9±.2	1215.9±.4	1216.5±.1	1215.7±.5
1228.4±.2	1228.3±.4	1228.8±.1	1228.2±.5
1393.0±2			
1439.1±3	1439.2±.5	1439.1±.2	1438.7±.5
1453.7±.3	1453.7±.5	1453.6±.2	1453.2±.5
1532.7±.5	1533.0±.5	1532.9±.2	1532.4±.5
1567.6±1	1568.2±.5	1568.0±.2	1567.4±.5
1611.5±1	1611.6±.5	1611.0±2	1610.7±.5
1787.7±.3	1787.9±.6	1787.1±.3	1787.1±.5
		1807.0±.6	
1870.1±.3	1870.0±.6	1869.2±.4	1869.4±.5
		1907.5±.3	
1955.5±.5	1955.5±.6	1954.2±.5	1955.1±.5
2096.2±.3	2096.2±.6	2095.7±.5	2095.9±.5
2110.0±.3	2110.7±.6	2110.2±.5	2110.4±.5
2126.5±1	2127.0±.8		
2429.0±.3	2429.3±.6	2429.4±.6	2429.0±.5
2655.1±.3	2655.6±.5	2657.0±.5	2655.6±.5
2670.0±.5			

TABLE 8.1 (continued)

ENERGY keV	RELATIVE INTENSITY Ref. 71	Ref. 73	Ref. 72	This work
303	0.02±.005	0.02	0.07±.02	0.020±.004
317				0.015±.003
404	0.06±.01	0.06±.03	Weak	0.033±.007
457	0.07±.01		0.07±.02	0.08 ±.02
472	~0.1	0.11±.03	0.13±.03	0.18 ±.03
559	100	100	100	100
563	2.71±.13	2.8 ±.3	3.0 ±.2	3.6 ±1.1
572	0.34±.02	0.32±.06	0.48±.04	0.16 ±.12
575	0.14±.01	0.15±.03	0.13±.01	
657	13.8±.7	13.7±1.4	12.7±.7	13.9 ±.3
665	0.95±.06	0.93±.09	1.1 ±.05	0.97 ±.03
694	0.02	0.019±.004	0.014±.007	0.027±.007
726	0.06±.01	0.039±.007	0.027±.007	0.045±.002
740	0.27±.02	0.26±.04	0.18±.02	0.28 ±.02
755	0.016±.004	~0.01	0.001	≤ 0.005
771	0.29±.02	0.25±.04	0.21±.02	0.25 ±.02
797	0.017±.01			≤ 0.005
809	0.040±.004	0.039±.007	0.028±.008	0.038±.008
863	0.03±.01	0.02±.01		
867	0.30±.03	0.30±.04	0.25±.02	0.31 ±.05
882	0.15±.01	0.14±.03	0.09±.01	0.13 ±.02
995			0.015±.01	
981	0.11±.01	0.10±.03	0.10±.01	0.10±.02
1051			Weak	≤ 0.005
1098		0.008±.002	0.016±.008	≤ 0.005

TABLE 8.2 Intensities of ^{76}As gamma-ray transitions

ENERGY keV	RELATIVE INTENSITY Ref. 71	Ref. 73	Ref. 72	This work
1117		0.012±.003		≤ 0.005
1130	0.33 ±.02	0.32 ±.04	0.25 ±.02	0.31 ±.04
1213	3.64 ±.2	3.6 ±.4	3.2 ±.2	3.4 ±.5
1216	8.86 ±.5	8.4 ±.8	8.0 ±.4	7.8 ±1.0
1228	3.17 ±.15	3.0 ±.3	2.7 ±.5	2.7 ±.4
1439	0.73 ±.03	0.71 ±.07	0.52	0.65 ±.1
1453	0.29 ±.02	0.28 ±.03	0.19 ±.01	0.25 ±.04
1532	0.071±.007	0.060±.006	0.051±.008	0.058±.010
1567	0.014±.002	0.020±.003	0.006	0.010±.002
1611	0.017±.002	0.020±.003	.0063±.0004	0.014±.002
1787	0.75 ±.04	0.78 ±.08	0.56 ±.03	0.73 ±.1
1807			0.04	≤ 0.005
1870	0.14 ±.01	0.14 ±.01	0.11 ±.01	0.14 ±.02
1907			Weak	≤ 0.005
1955	0.025±.002	0.026±.003	0.020±.006	0.024±.004
2096	1.48±.08	1.5 ±.1	1.16±.06	1.4 ±.2
2110	0.87 ±.04	0.9 ±.09	0.60 ±.03	0.8 ±.1
2127	0.003	0.003±.004		≤ 0.005
2429	0.088±.006	0.09 ±.01	0.071±.007	0.083±.01
2656	0.10 ±.01	0.13 ±.01	0.106±.008	0.11 ±.02
2670	0.006±.001			≤ 0.001

TABLE 8.2 (continued)

At first sight it seemed that the source could be positioned and controlled by the system described in section 8.2 but when consideration was given to the chance rate obtained with this variable geometry (see section 8.5) it emerged that it was preferable to keep the source position fixed (at good coincidence geometry) and to tolerate the fall in counting rate as it decayed. However, the time required to collect reasonable spectra with this arrangement was prohibitive so the control system was modified so that it fed a new source to the counting position (kept constant) whenever the NaI detector singles rate fell below a set threshold. The source was then replaced by a series of sources, all irradiated once a week, but with masses calculated so that the source changed at half a half-life to a new one which restored the singles rates to their original levels. Thus the coincidence system counted a decaying source for about 13 hours when its counting rate fell below the threshold and initiated the feeding of a new source from a shielded enclosure above the equipment and the rejection of the old source to a shielded enclosure below the equipment. The singles counting rate was used to control the sources and was also monitored with a pen recorder to give a record of the counting rate and time of source change for the purpose of calculating the chance spectrum. With this system the coincidence counting rate could be maintained at an acceptable level.

Four coincidence runs were made using energy gates set with the NaI detector around 559 keV, 657 keV, 772 keV and 1787 keV.

8.5 Analysis of coincidence spectra

The alternative modes of operation and their respective true to chance rates were evaluated as follows.

8.5.1 Source stationary

Let N_{so} be the initial strength of the source which is positioned between the two detectors such that their respective absolute efficiencies are e_{as} and e_{bs}. Considering the true coincidences recorded, N_{Ts}, in time t_c.

$$N_{Ts} = \int_0^{t_c} e_{as} e_{bs} N_{so} e^{-\lambda t} dt$$

where $\lambda = \frac{\ln 2}{\tau_{\frac{1}{2}}}$ and $\tau_{\frac{1}{2}}$ = half-life of decay

so $$N_{Ts} = \frac{e_{as} e_{bs} N_{so} (1 - e^{-\lambda t_c})}{\lambda} \quad \ldots\ldots \quad 8.1$$

The chance coincidence counts recorded, N_{Cs}, are given by

$$N_{Cs} = \frac{2\tau_F e_{as} e_{bs} N_{so}^2 (1 - e^{-2\lambda t_c})}{2\lambda} \quad \ldots\ldots \quad 8.2$$

where $2\tau_F$ = resolving time of fast coincidence unit

thus the true to chance ratio is given by G_s as:

$$G_s = \frac{(1 - e^{-\lambda t_c})}{2\tau_F N_{so}(1 - e^{-2\lambda t_c})} \quad \ldots\ldots\ldots\ldots \quad 8.3$$

8.5.2 Source moving

Assuming that N_{so} is the maximum source strength that can be used as in 8.5.1 to satisfy the singles counting rate limitations (see section 4.8) then the alternative approach is to start with a stronger source, N_{mo}, which is positioned so that the detector efficiencies are e_{amo} and e_{bmo} respectively and then move the source inwards towards the detectors as it decays.

If the source is positioned so that it reaches a position such that the detector efficiencies are e_{as} and e_{bs} when the source strength is N_{so} after a time t_c, then:

$$N_{so} = N_{mo} e^{-\lambda t_c} \quad \ldots\ldots\ldots\ldots \quad 8.4$$

the detector efficiencies vary so that at any time, t, they are given by:

$$e_{am} = e_{amo} e^{\lambda t}$$

$$e_{bm} = e_{bmo} e^{\lambda t}$$

and the source strength is given by:

$$N_m = N_{mo} e^{-\lambda t}$$

then, since the singles rates are maintained constant:

$$e_{am}N_m = e_{amo}N_{mo} = e_{as}N_{so}$$
$$e_{bm}N_m = e_{bmo}N_{mo} = e_{bs}N_{so} \quad \ldots\ldots\ldots 8.5$$

thus $$e_{am} = e_{as}N_{so}/N_m = \frac{e_{as}N_{mo}e^{-\lambda t_c}}{N_m}$$

so $$e_{am} = e_{as}\exp(\lambda(t - t_c))$$

and $$e_{bm} = e_{bs}\exp(\lambda(t - t_c)) \quad \ldots\ldots\ldots 8.6$$

The true coincidence counts, N_{Tm}, recorded in a time t_c are given by:

$$N_{Tm} = \int_0^{t_c} e_{am}e_{bm}N_{mo}\exp(-\lambda t)\,dt$$
$$= \int_0^{t_c} e_{as}e_{bs}N_{so}\exp(-\lambda t)\exp(\ t)\,dt$$

or $$N_{Tm} = \frac{e_{as}e_{bs}N_{so}(1 - e^{-\lambda t_c})}{\lambda} \quad \ldots\ldots\ldots 8.7$$

The chance coincidence counts, N_{cm}, recorded in time t_c are given by:

$$N_{cm} = \int_0^{t_c} 2\tau_F e_{am}e_{bm}N_{mo}^2\exp(-2\lambda t)\,dt$$
$$= \int_0^{t_c} 2\tau_F e_{as}e_{bs}N_{so}^2\,dt$$

or $$N_{cm} = 2\tau_F e_{as}e_{bs}N_{so}^2 t_c \quad \ldots\ldots\ldots 8.8$$

the true to chance ratio, G_m, is:

$$G_m = \frac{(1 - e^{-\lambda t_c})}{2\tau_F N_{so} \lambda t_c} \quad \ldots\ldots\ldots\ldots\ldots\ldots 8.9$$

Equations 8.1 and 8.7 show that the true coincidences recorded in the two cases are identical but the number of chance coincidences as given by equations 8.2 and 8.8 are far higher in the case of the moving source. This illustrates the general principle that it is preferable to maximise the coincidence geometry and to take the source correspondingly weaker; even if this means that the source decay causes a rapid fall off in counting rate.

The ratio of the chance coincidences recorded in the two cases is:

$$\frac{N_{cm}}{N_{cs}} = \frac{t_c\, 2\lambda}{(1 - e^{-2\lambda t_c})}$$

which for $t_c = n\, \tau_{\frac{1}{2}}$ gives:

$$N_{cm} \doteq 2N_{Cs} \quad \text{for } n = 1$$

and $$N_{cm} \doteq 1.4\, N_{Cs} \quad \text{for } n > 3 \text{ or } 4$$

8.5.3 Calculation of the chance coincidence spectrum

The coincidence spectra finally recorded for ^{76}As were taken with the source feeding system described in section 8.4. Thus the chance spectrum was evaluated from a singles spectrum taken at the beginning of the run. The singles counting rates satisfied the requirements in section 4.8.

The chance counts recorded in a time t are given essentially by equation 8.2:

$$N_{Cs} = \frac{2\tau_F \, e_{as} N_{so} \, e_{bs} N_{so} \, (1 - e^{-2\lambda t})}{2\lambda}$$

where $e_{as}N_{so} = A$ and represents the initial counting rate in the Ge(Li) detector

$e_{bs}N_{so} = B_G$ and represents the initial energy gate counting rate

The final chance spectrum was calculated for each source from the singles spectrum taken at the beginning of the complete run and the values of B_G and t for the sources fed to the detectors during the run. The values of B_G and t were measured from the monitoring pen recorder plot.

8.5.4 Treatment of coincidence spectra

Each coincidence spectrum was corrected for chance contributions and the corrected spectra were analysed using

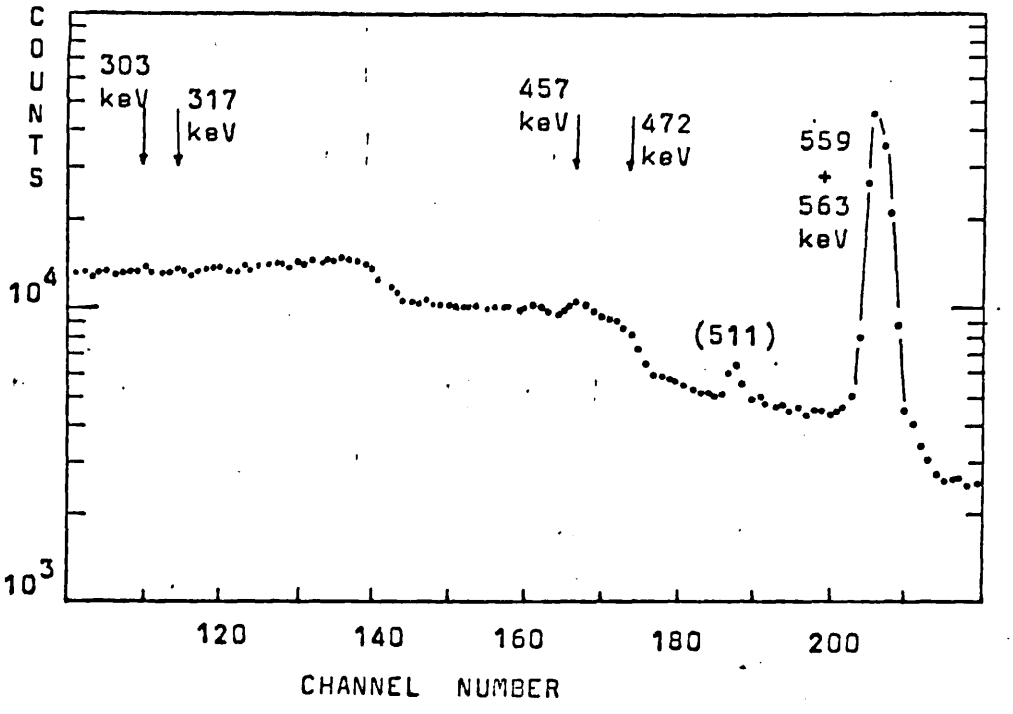

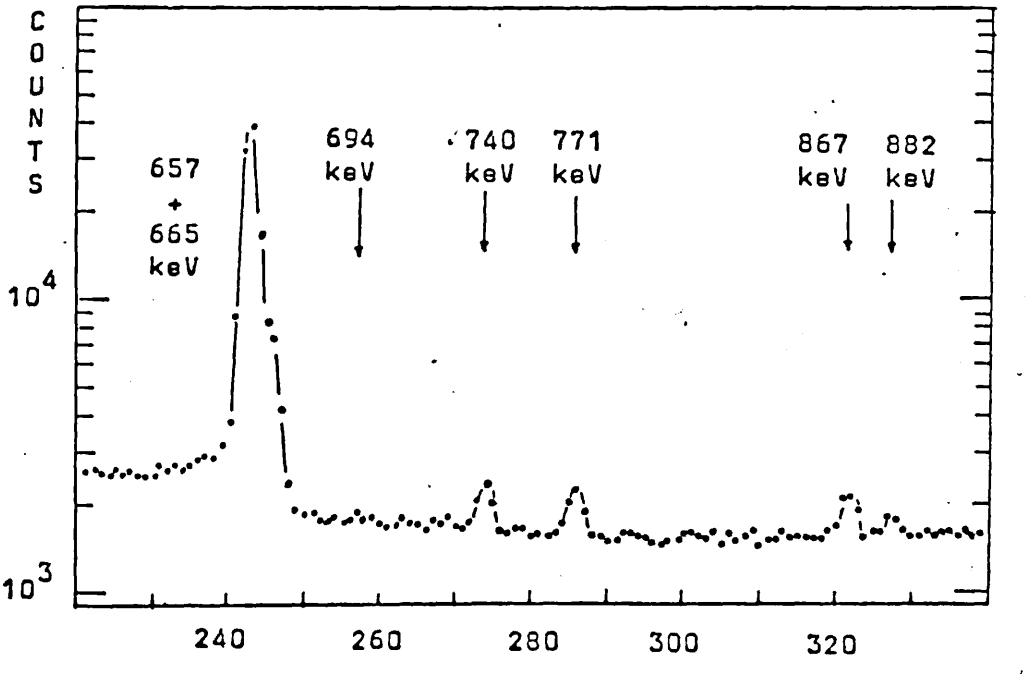

FIGURE 8.2 ^{76}As coincident with 559keV region

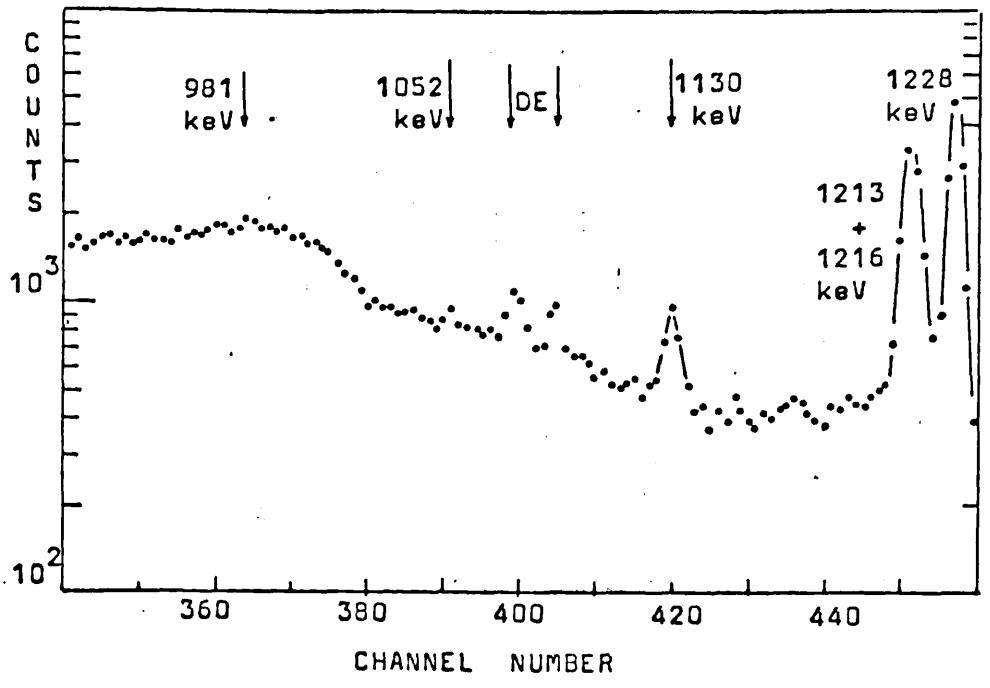

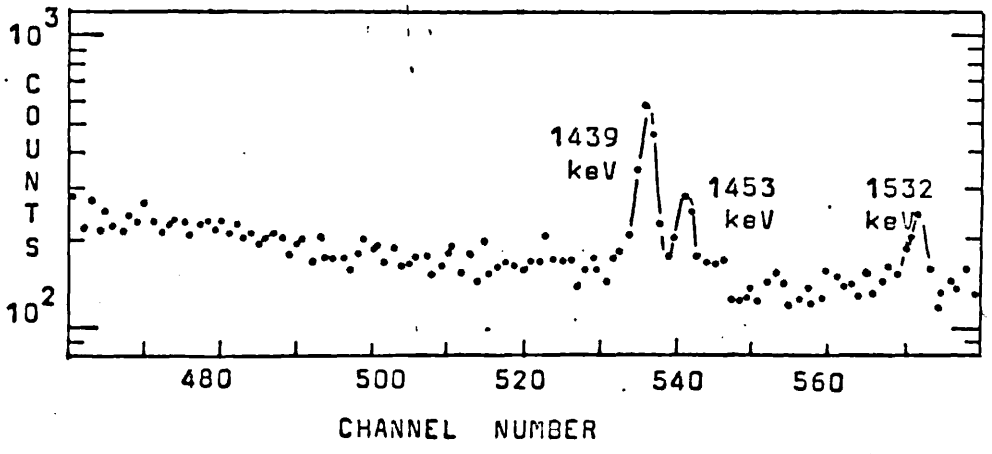

FIGURE 8.2 (cont.)

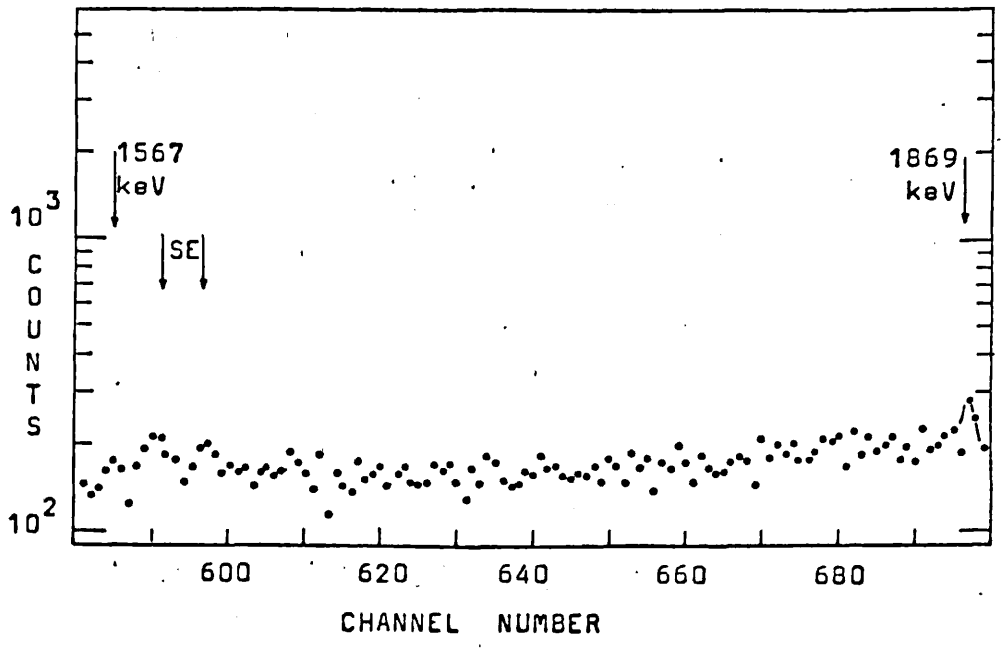

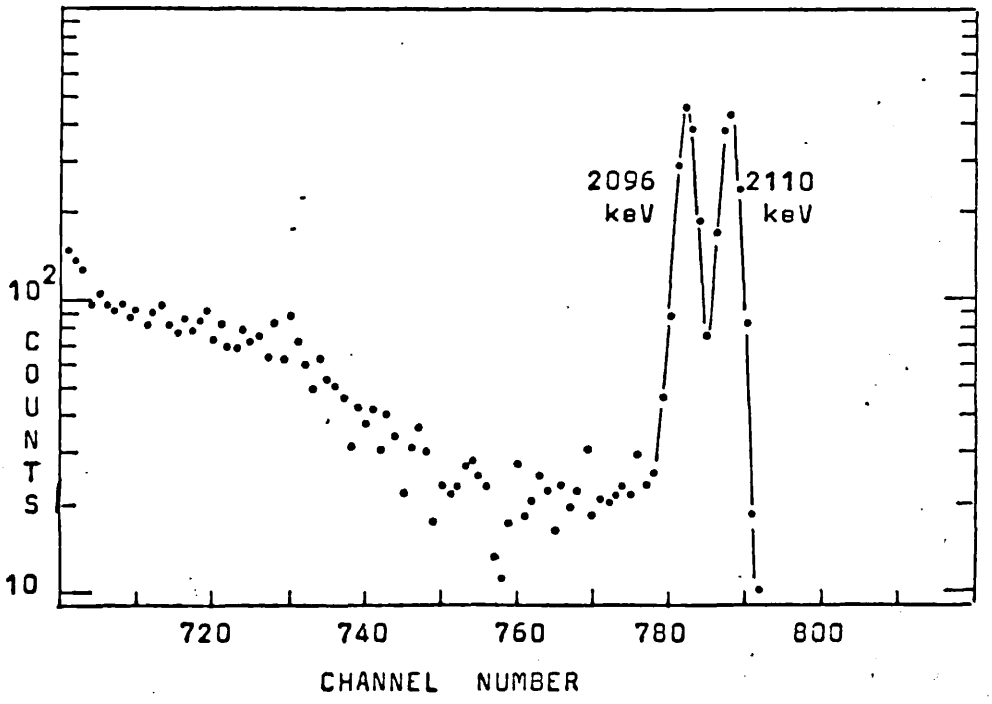

FIGURE 8.2(cont.)

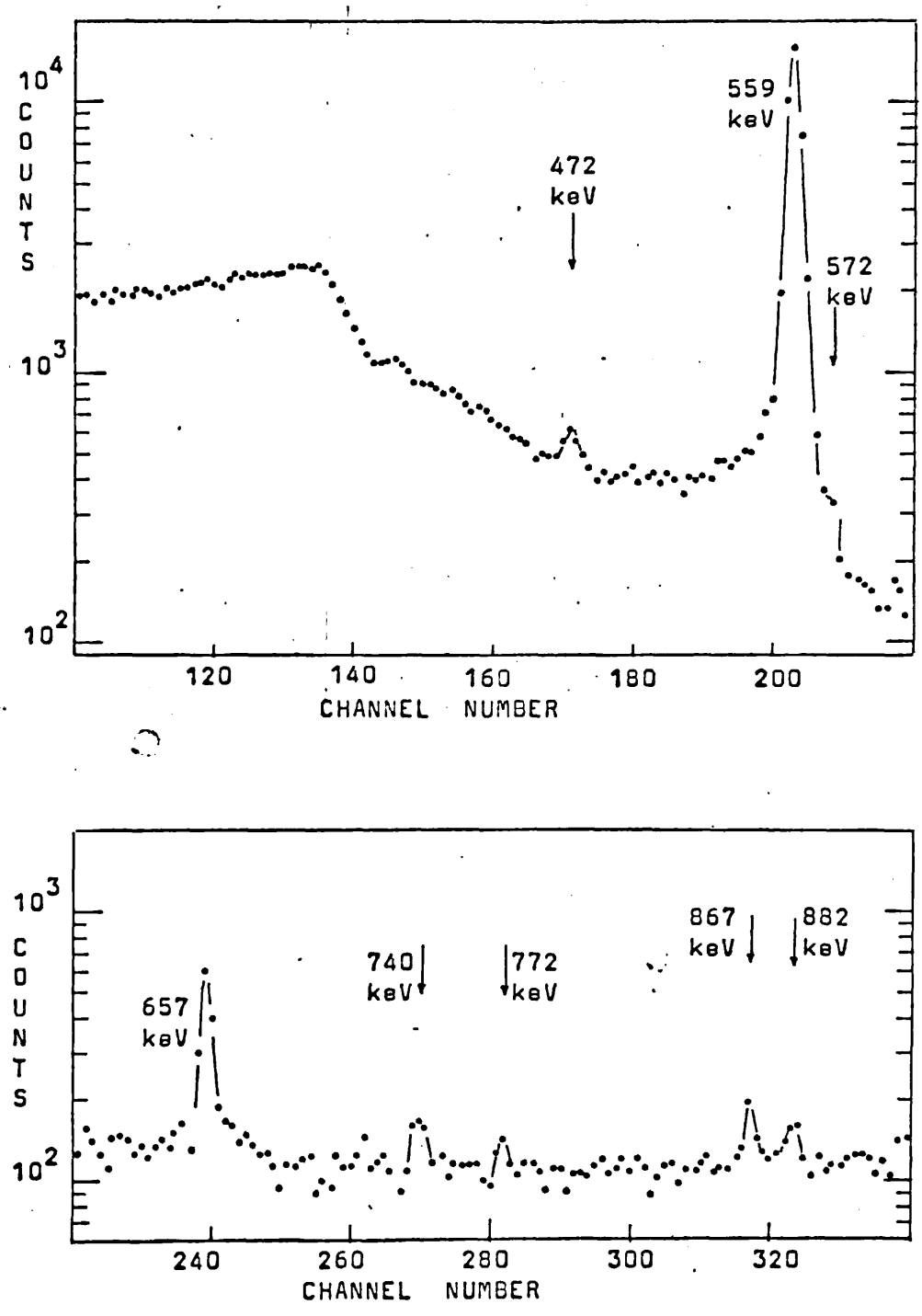

FIGURE 8.3 ^{76}As spectrum coincident with 657 keV region

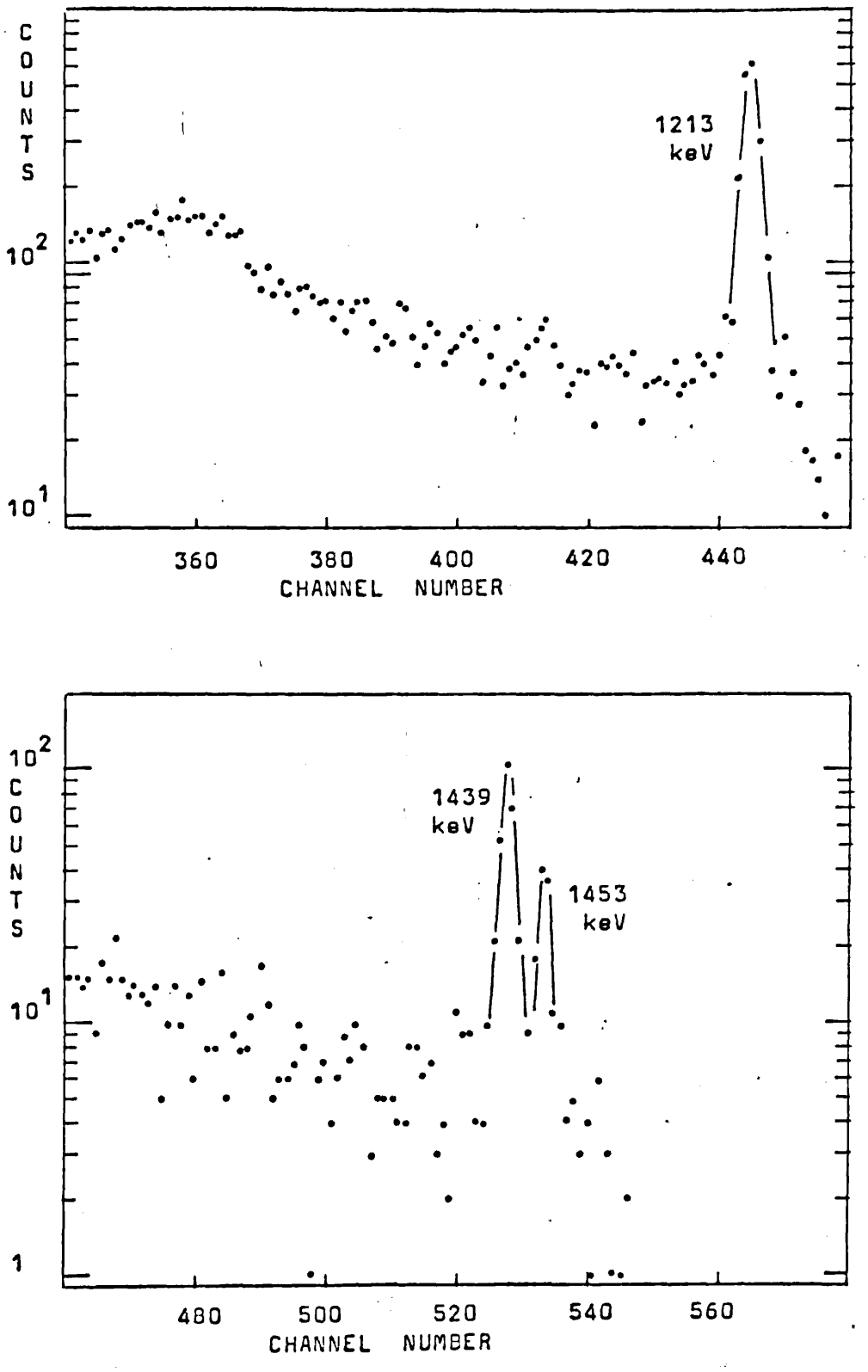

FIGURE 8.3 (continued)

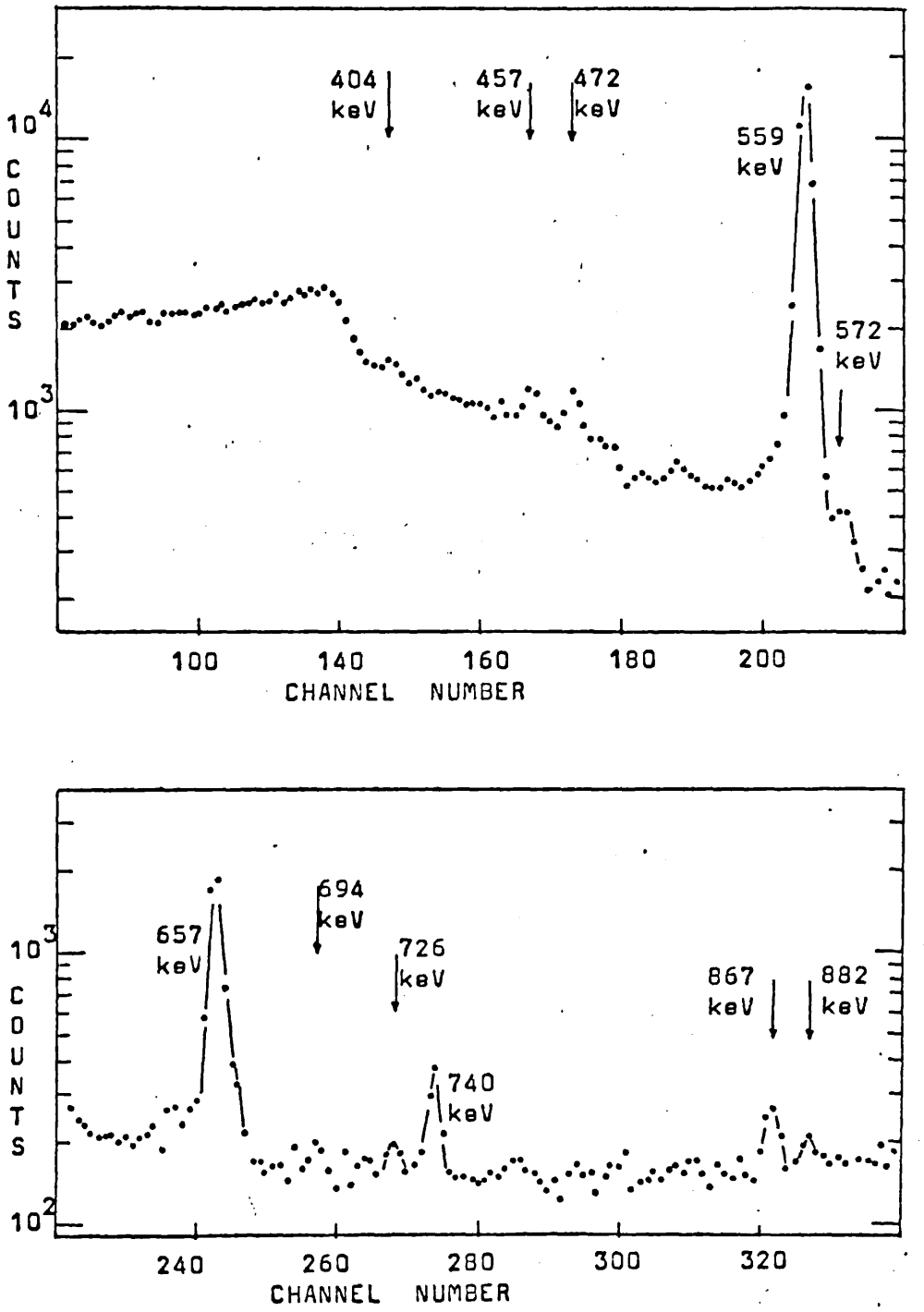

FIGURE 8.4 ^{76}As spectrum coincident with 772 keV region

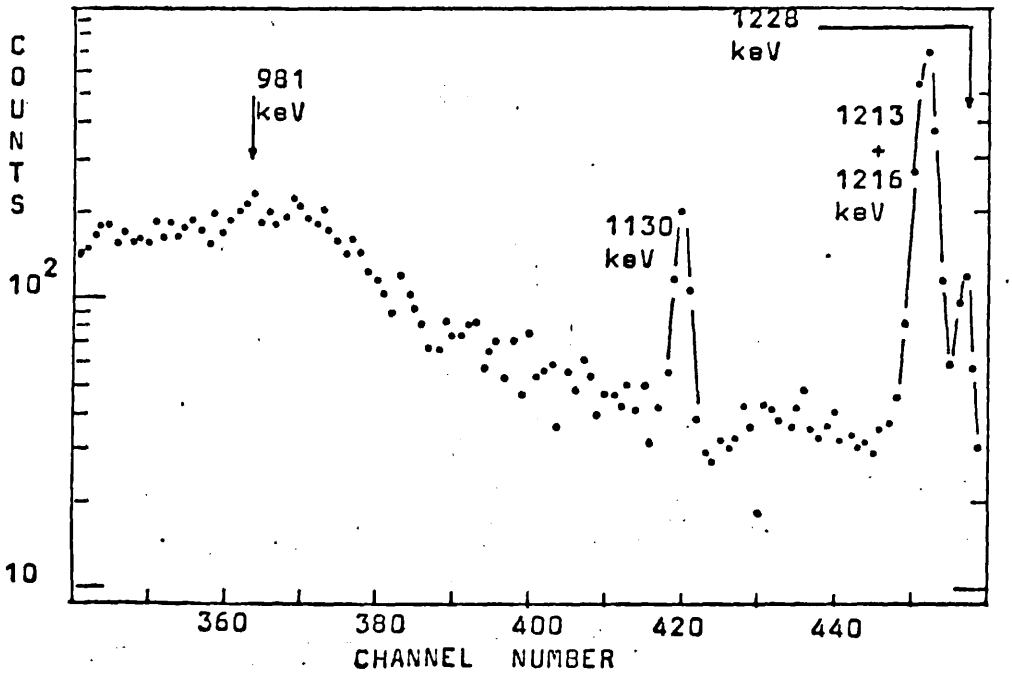

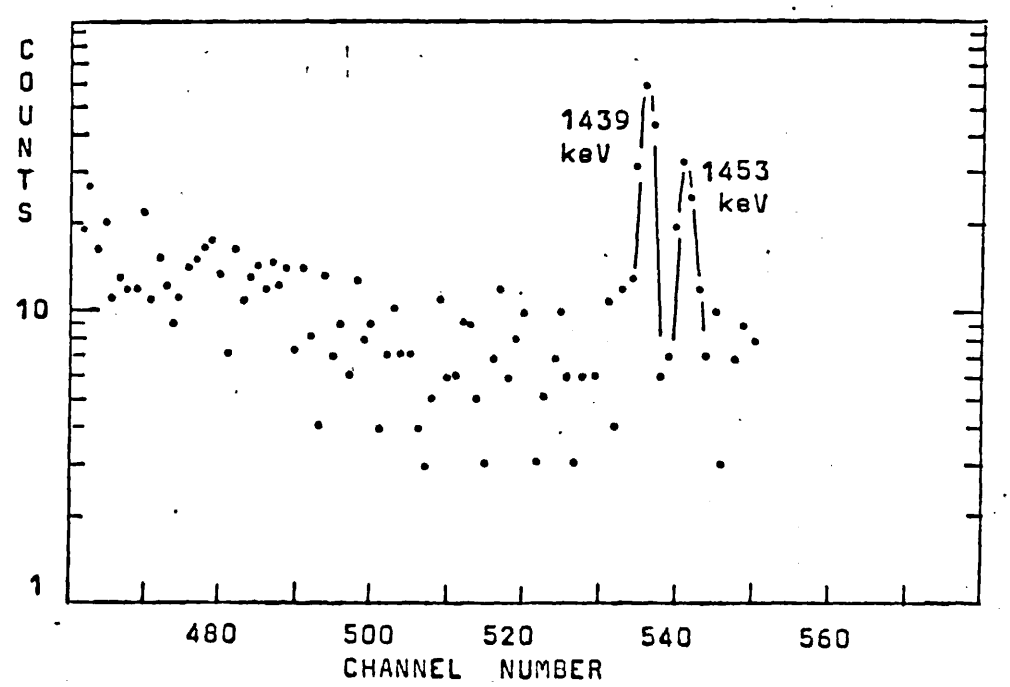

FIGURE 8.4 (continued)

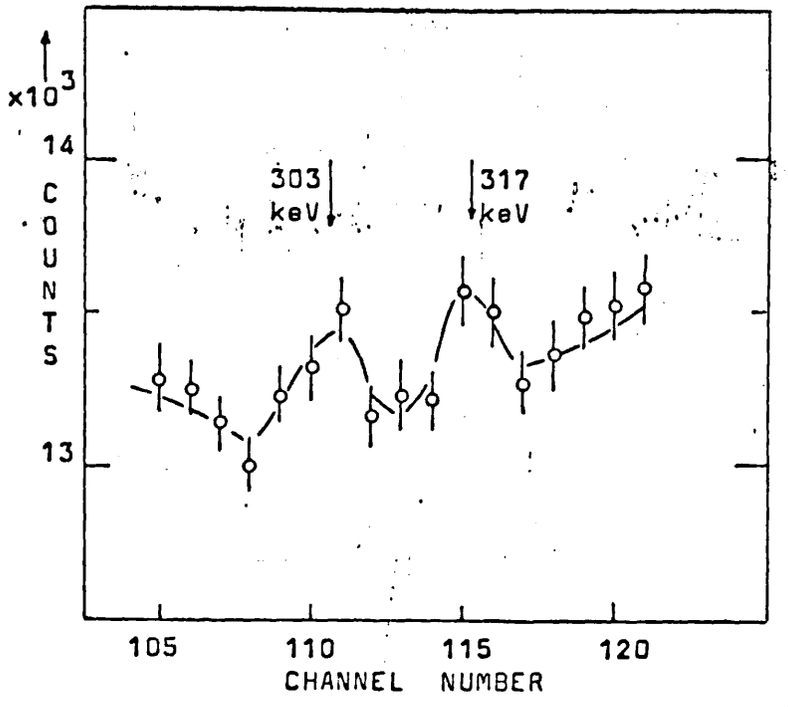

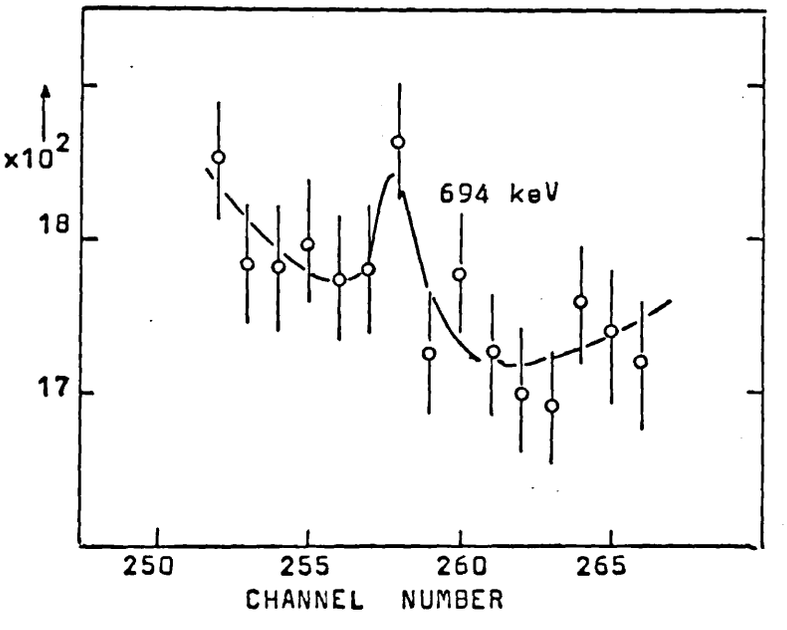

FIGURE 8.5 Portion of spectrum coincident with 559keV region

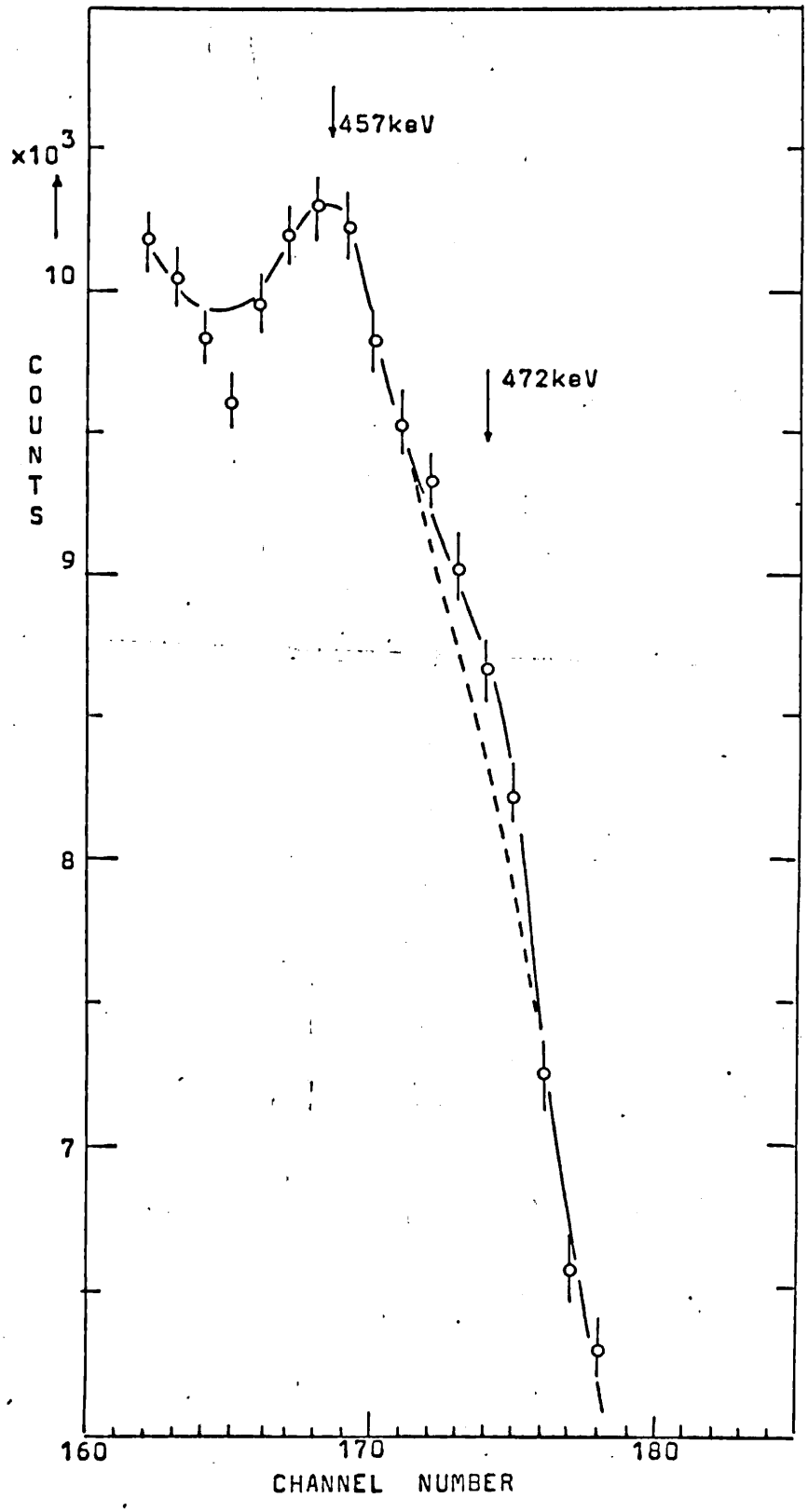

FIGURE 8.6 Portion of ^{76}As spectrum coincident with 559keV region

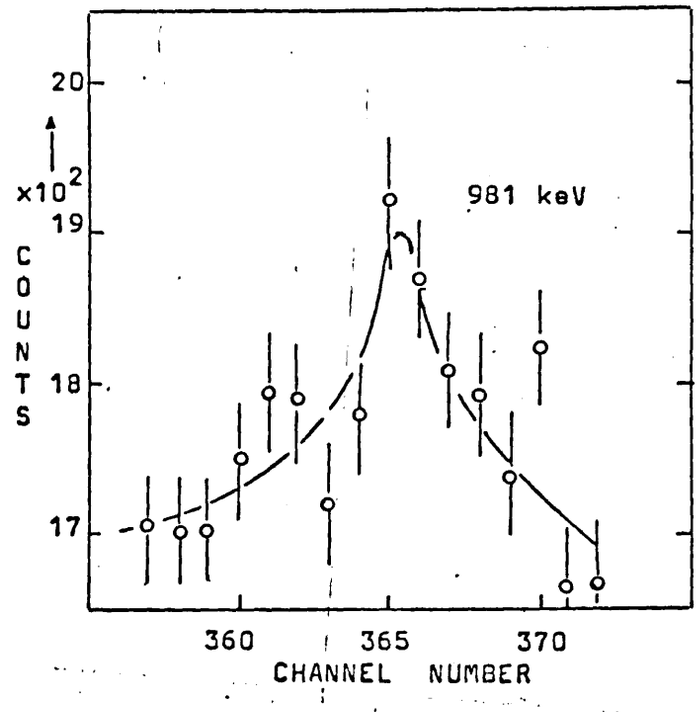

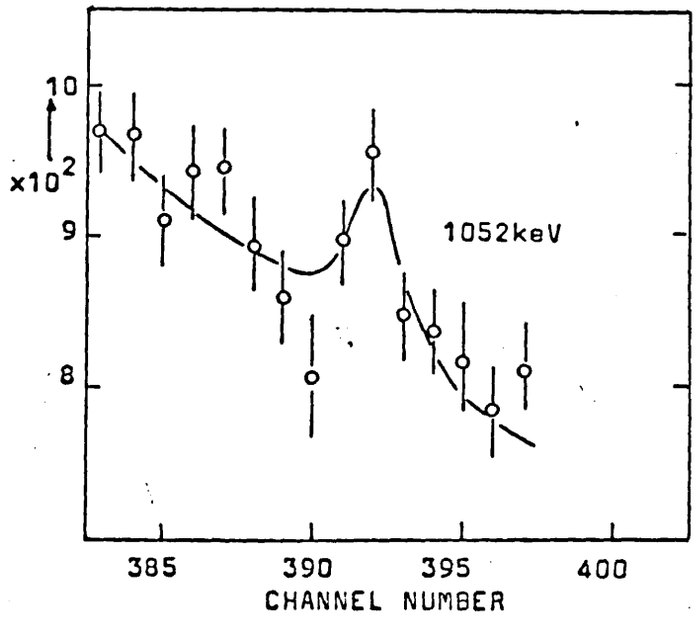

FIGURE 8.7 Portion of ^{76}As spectrum coincident with 559keV region

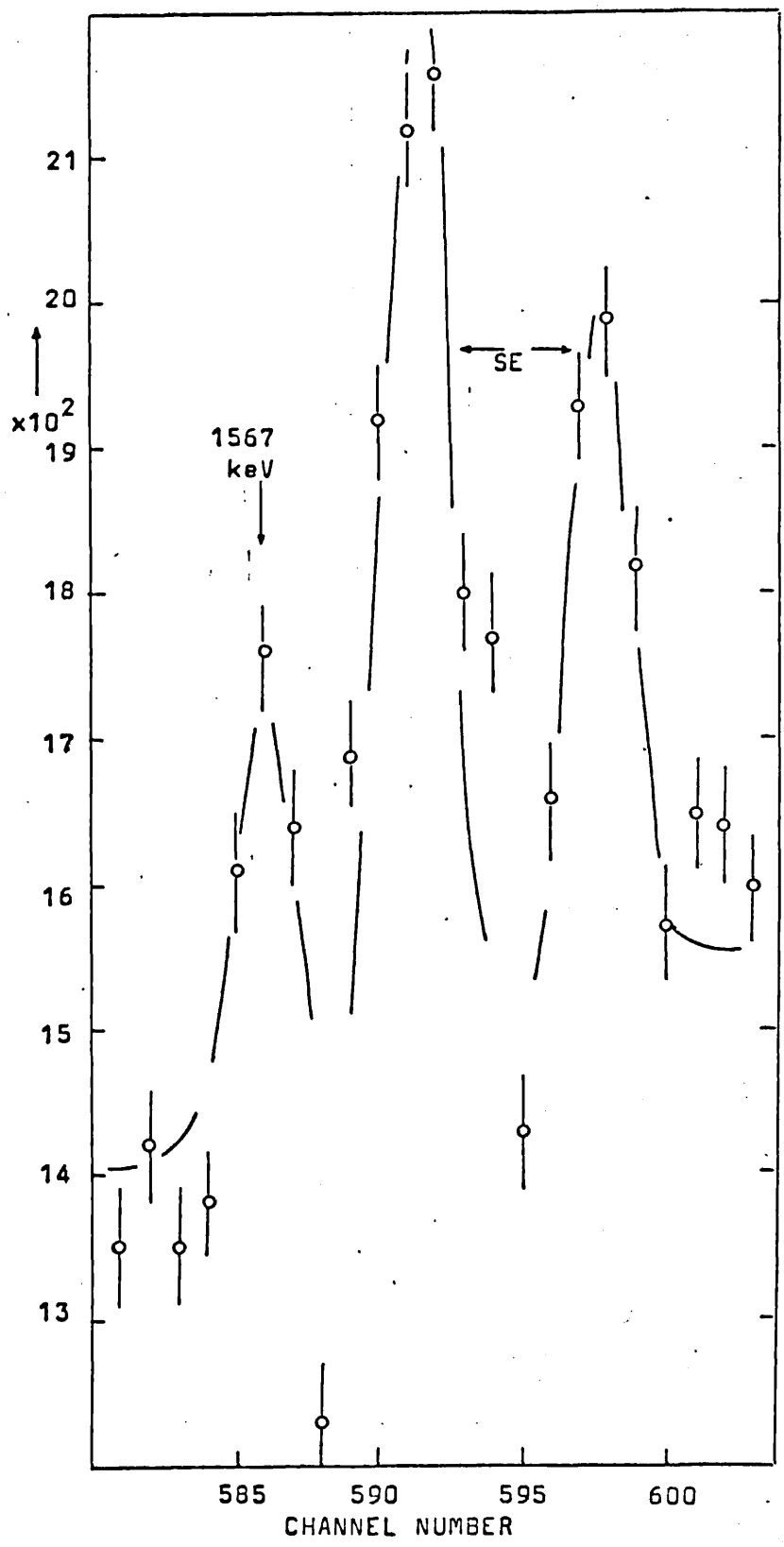

FIGURE 8.8 Portion of ^{76}As spectrum coincident with 559keV region

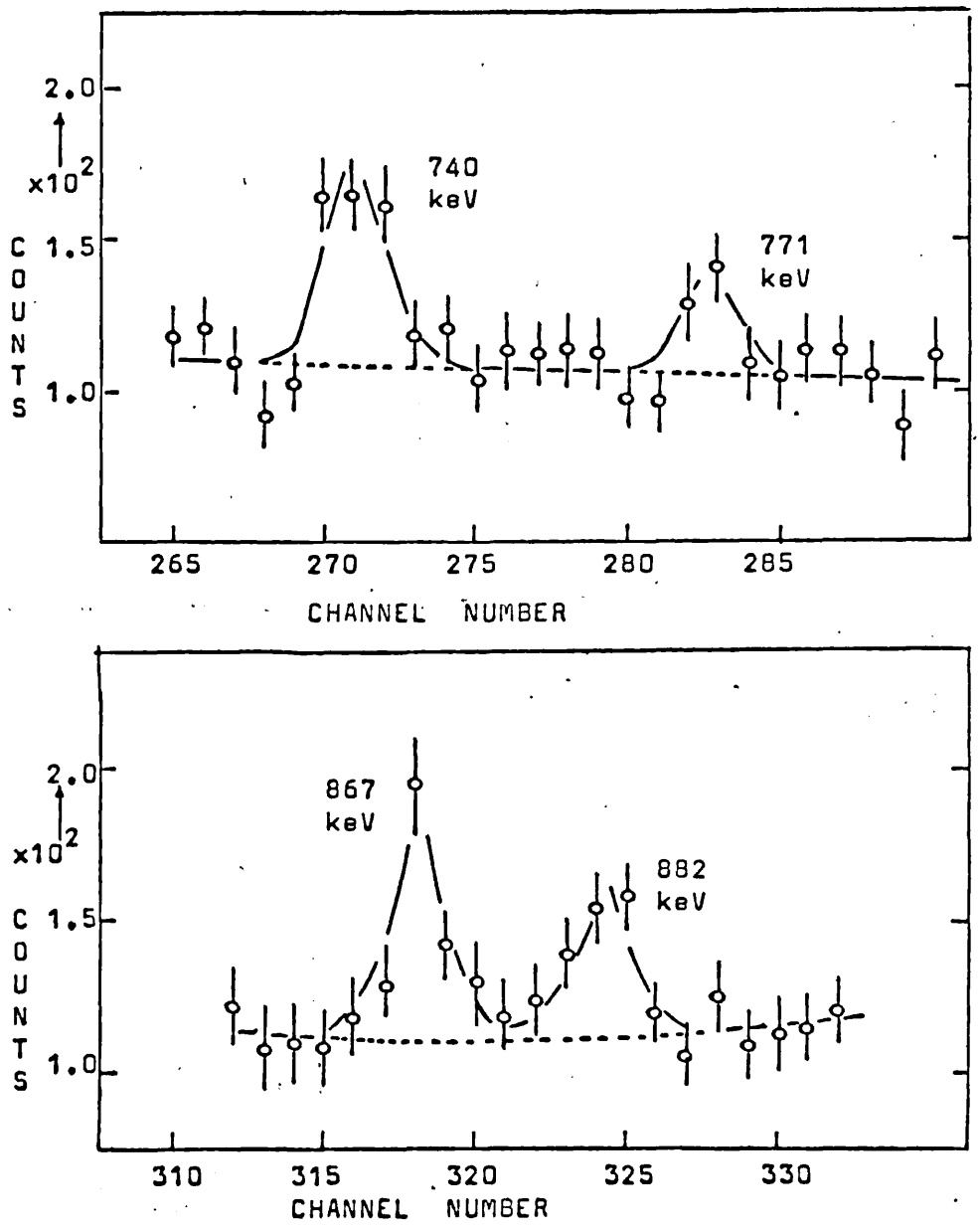

FIGURE 8.9 Portion of ^{76}As spectrum coincident with 657 keV region

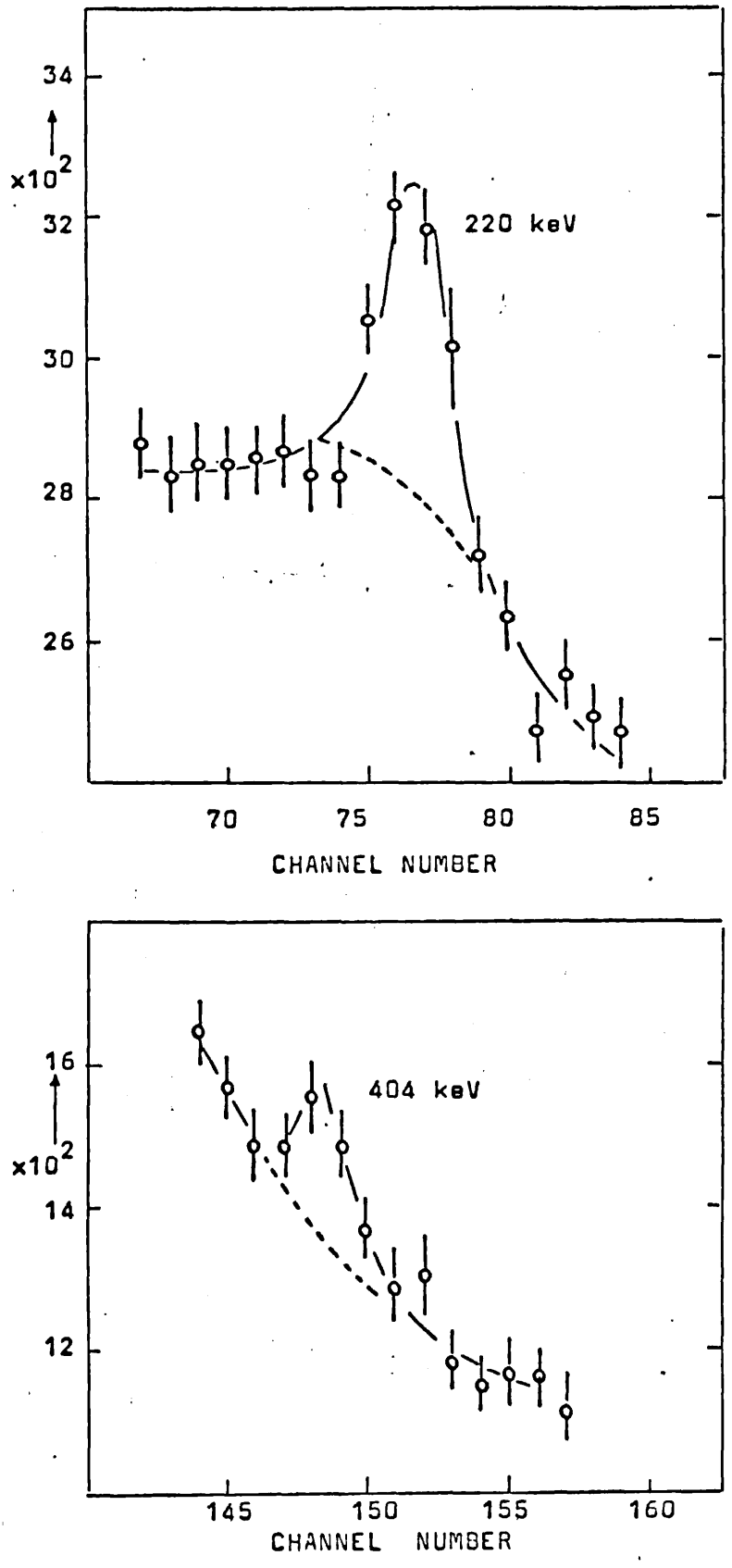

FIGURE 8.10 Portion of ^{76}As spectrum coincident with 772keV region

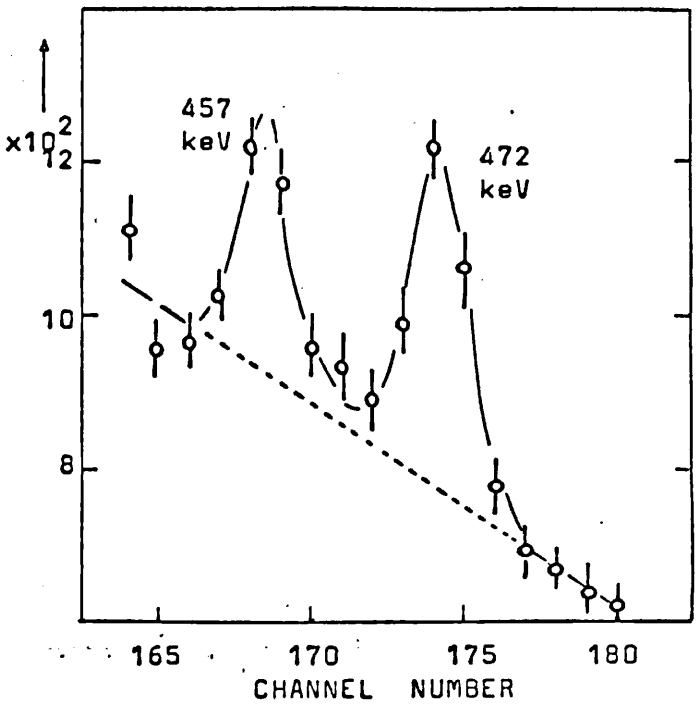

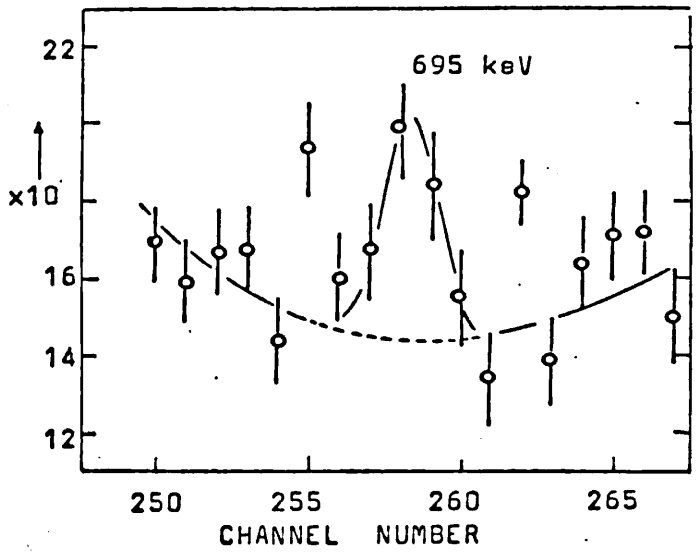

FIGURE 8.11 Portion of ^{76}As spectrum coincident with 772keV region

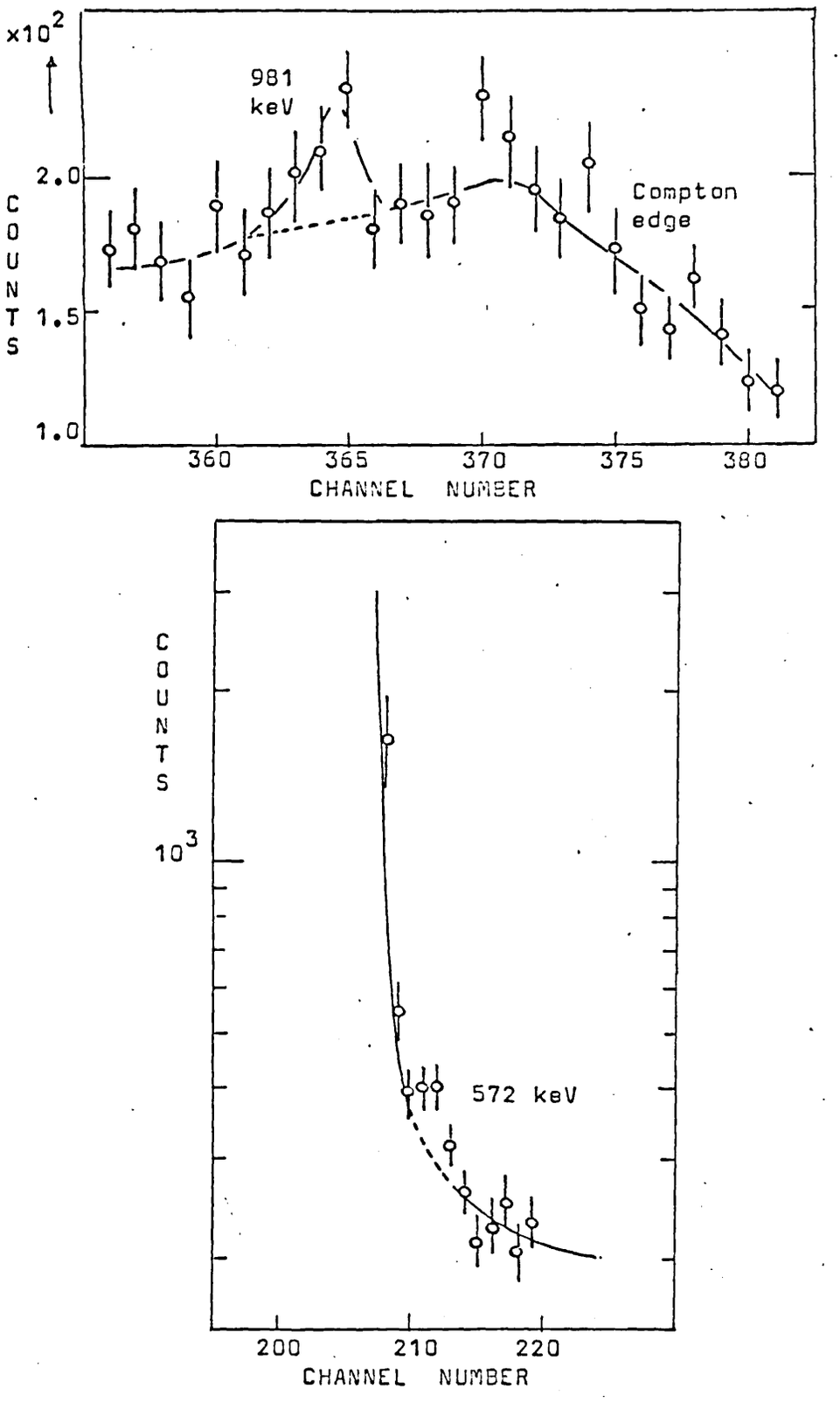

FIGURE 8.12 Portion of ^{76}As spectrum coincident with 772 keV region

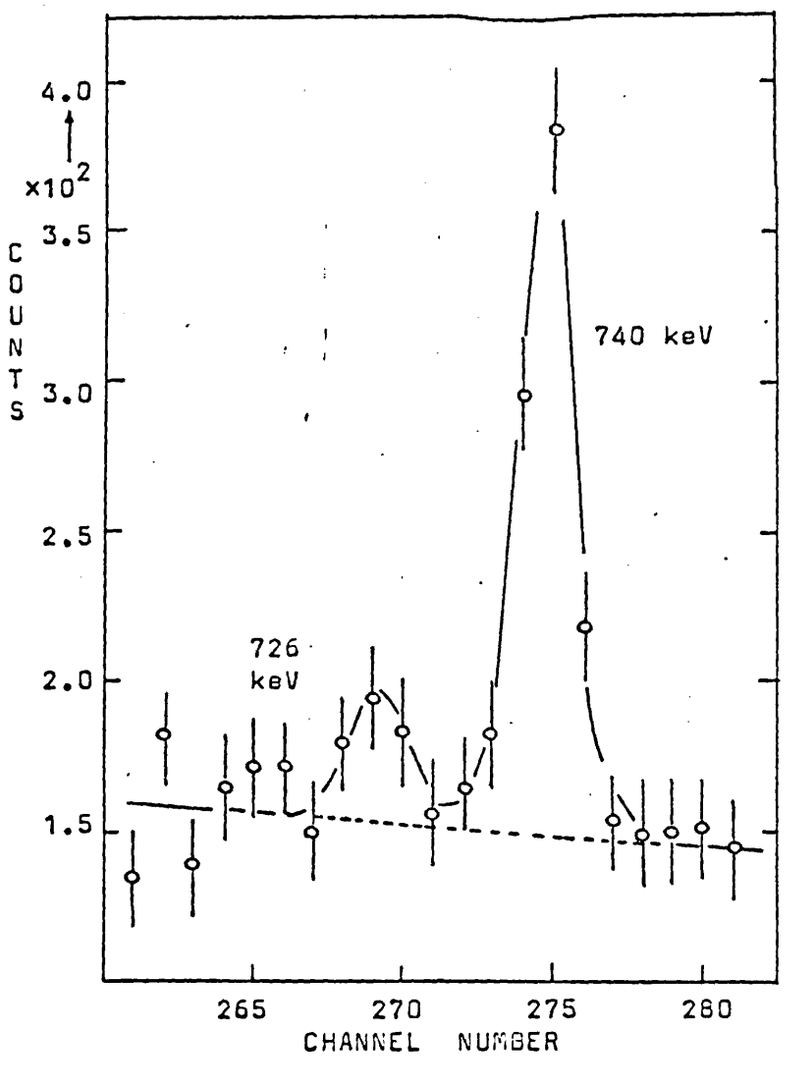

FIGURE 8.13 Portion of ^{76}As spectrum coincident with 772 keV region

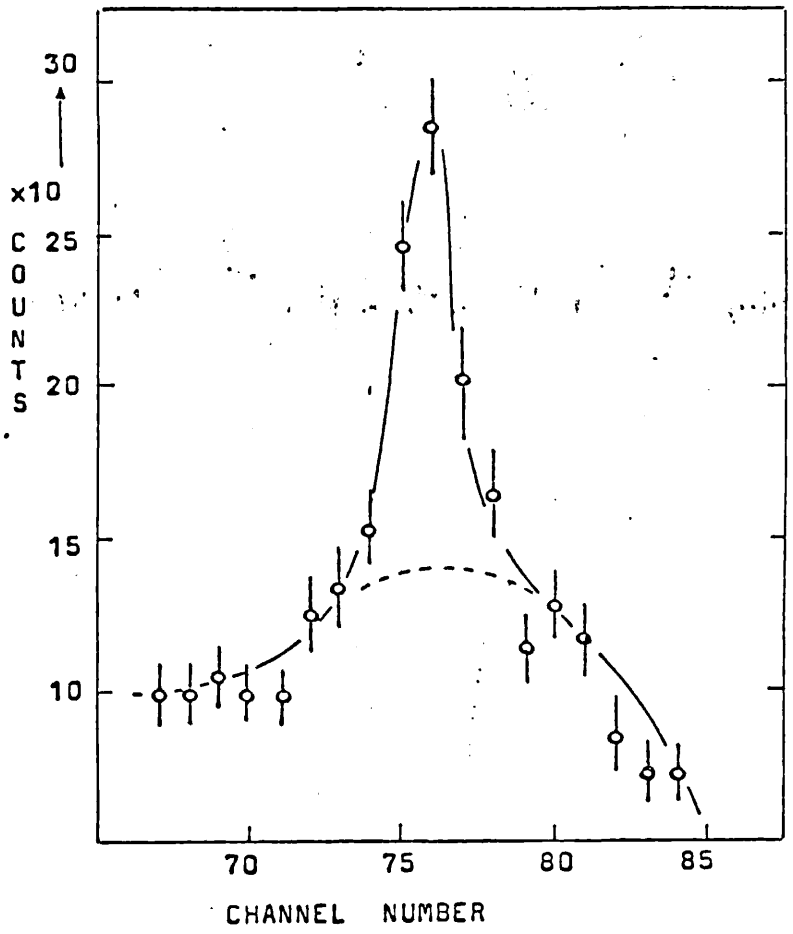

FIGURE 8.14 220 keV gamma-ray coincident with 1787keV region

the programme Sampo to obtain the relative intensities of the coincident gamma-rays.

8.6 Results from the coincidence spectra

The corrected spectra coincident with the 559 keV, 657 keV and 772 keV energy gates are shown in figures 8.2, 8.3 and 8.4 respectively. When analysed these spectra showed several peaks which were of small statistical significance. These peaks are identified in the figures and are shown in detail in figures 8.5, 8.6, 8.7, 8.8 (coincident with 559 keV), figure 8.9 (coincident with 657 keV) and figures 8.10, 8.11, 8.12 and 8.13 (coincident with 772 keV). Figure 8.14 shows the spectrum coincident with the gate at 1787 keV. Table 8.3 gives the results of the computer analysis.

For each coincident gamma transition an 'enhancement factor' was calculated from the relative intensity found in the coincidence spectrum and the relative intensity of the transition in a singles spectrum. Although the absolute value of this quantity was on an arbitrary scale and was thus of no significance, the values fell into groups according to the energy level which was fed by the coincident gamma-rays. There was, however, no guarantee that the values were unique for a given level and the large errors involved often made the resolution of the groups difficult.

The values obtained are shown in figures 8.15 and 8.16 and do give a guide in checking the decay scheme.

The conclusions from the coincidence runs are shown in figures 8.17, 8.18 and 8.19 for the 559 keV, 657 keV and 772 keV energy gates respectively. Most of the main transitions agree with the previous workers on this isotope. The main differences are that the 726.4 keV gamma-ray was definitely placed between the 2514 keV level and the 1787 keV level in agreement with Ardissan et al.[71], Funel et al.[73] and Iizawa[72]. This gamma-ray can not be positioned as suggested by Mcmillan et al.[70] as it should then show the same 'enhancement factor' as the 457 keV and 696 keV transitions in coincidence with the 772 keV gate. Also its partial inclusion in this same energy gate would result in a coincident 772 keV transition. No evidence was found for this. In addition, this energy gate at 772 keV produces a coincident gamma-ray of 1228 keV which further confirms the position of the 726 keV gamma-ray.

The 358 keV transition reported by Funel et al.[74] could not be identified in either a singles spectrum or in coincidence with the 772 keV gamma gate but the presence of the 740 keV and the 980 keV gamma-rays could imply a transition of this energy.

ENERGY keV	RELATIVE INTENSITY Coinc. 559 keV	Coinc. 657 keV	Coinc. 772 keV
220			0.85±0.17
303.4	0.33±0.07		
316.6	0.38±0.07		
403.8			0.75±0.30
457.1	0.73±0.30		1.58±0.30
471.8	0.69±0.30	0.81±0.16	2.34±0.30
559.1	77.5±12	100	100
562.7	30.8±5		
572.0		0.99±0.40	0.58±0.20
657.1	100	3.3±0.5	14.6±2.0
665.2	11.7±2		
693.8	0.29±0.09		0.54±0.20
726.4			0.42±0.10
739.6	2.1±0.3	0.67±0.13	2.1±0.3
771.4	2.3±0.3	0.30±0.10	
867.3	2.65±0.4	0.77±0.15	1.4±0.3
881.5	0.99±0.20	0.60±0.12	0.66±0.20
980.6	0.58±0.20		0.56±0.20

(continued overleaf)

TABLE 8.3 COINCIDENCE INTENSITIES FOR ^{76}As

ENERGY	RELATIVE INTENSITY		
keV	Coinc. 559 keV	Coinc. 657 keV	Coinc. 772 keV
1052.3	0.48±0.15		
1129.6	3.0±0.5		3.0±0.5
1212.5	16.6±3.0	12.5±2	14.5±2
1215.7	5±2		
1228.2	28±4		1.8±0.4
1438.7	3.2±0.5	2.3±0.3	1.3±0.3
1453.2	1.0±0.2	0.90±0.17	0.8±0.2
1532.4	0.73±0.14		
1567.4	0.26±0.08		
1610.7			
1787.1			
1869.4	1.0±0.2		
1955.1			
2095.9	6.1±0.9		
2110.4	6.0±0.9		
2429.0			
2655.6			

TABLE 8.3 (continued)

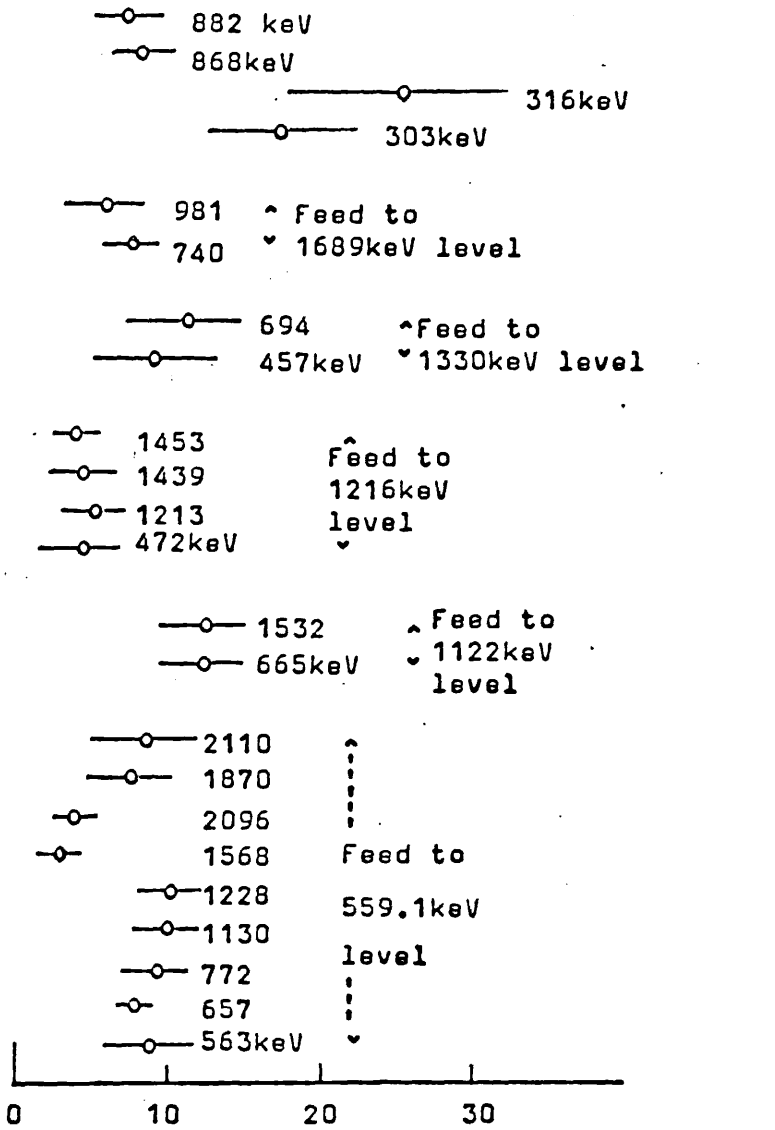

FIGURE 8.15 Intensities in ^{76}As coincidence spectrum relative to a singles spectrum

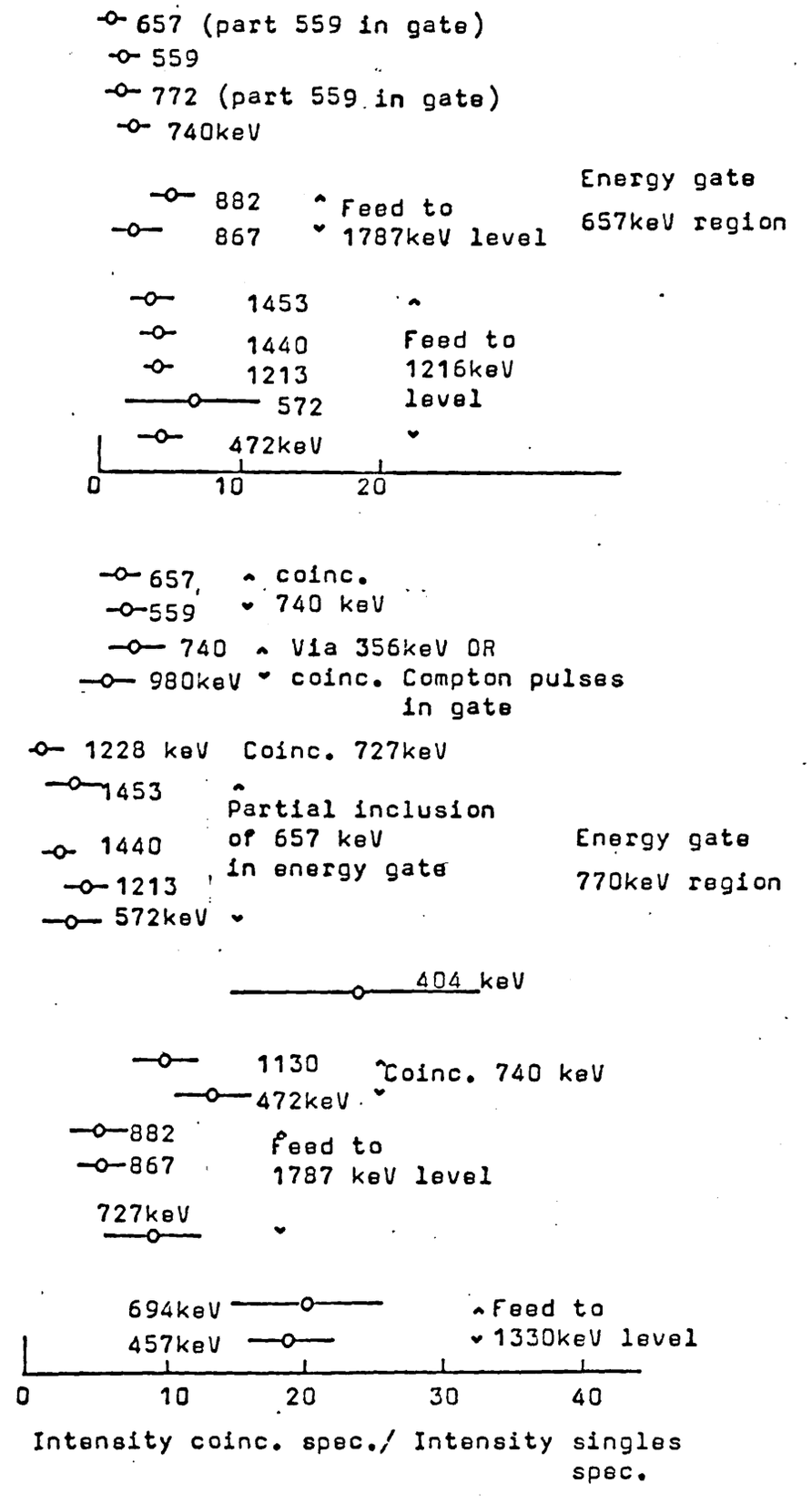

FIGURE 8.16 Intensities in ^{76}As coincidence spectra relative to a singles spectrum

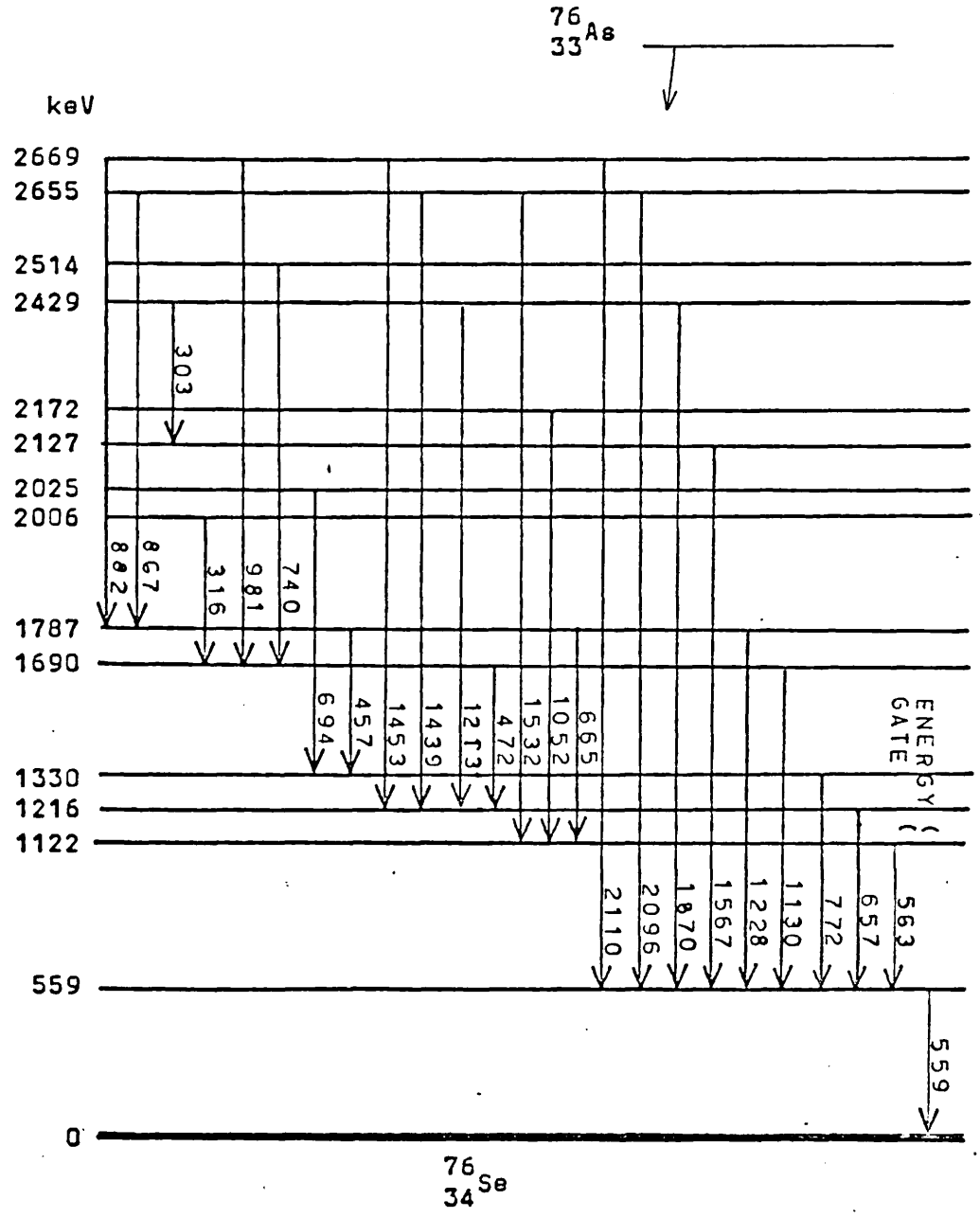

FIGURE 8.17 ^{76}As transitions observed in coincidence with 559 keV region

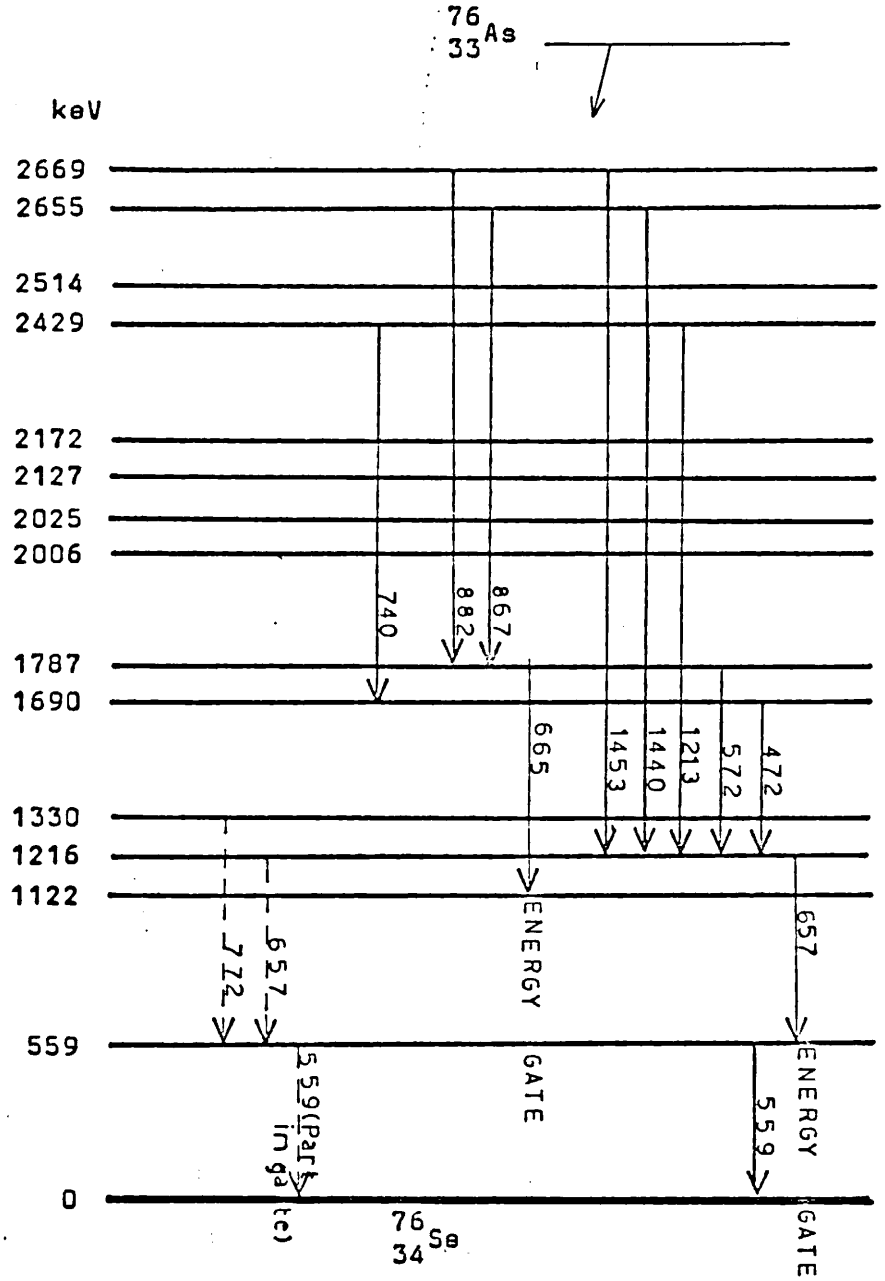

FIGURE 8.18 ^{76}As transitions observed in coincidence with 657 keV region

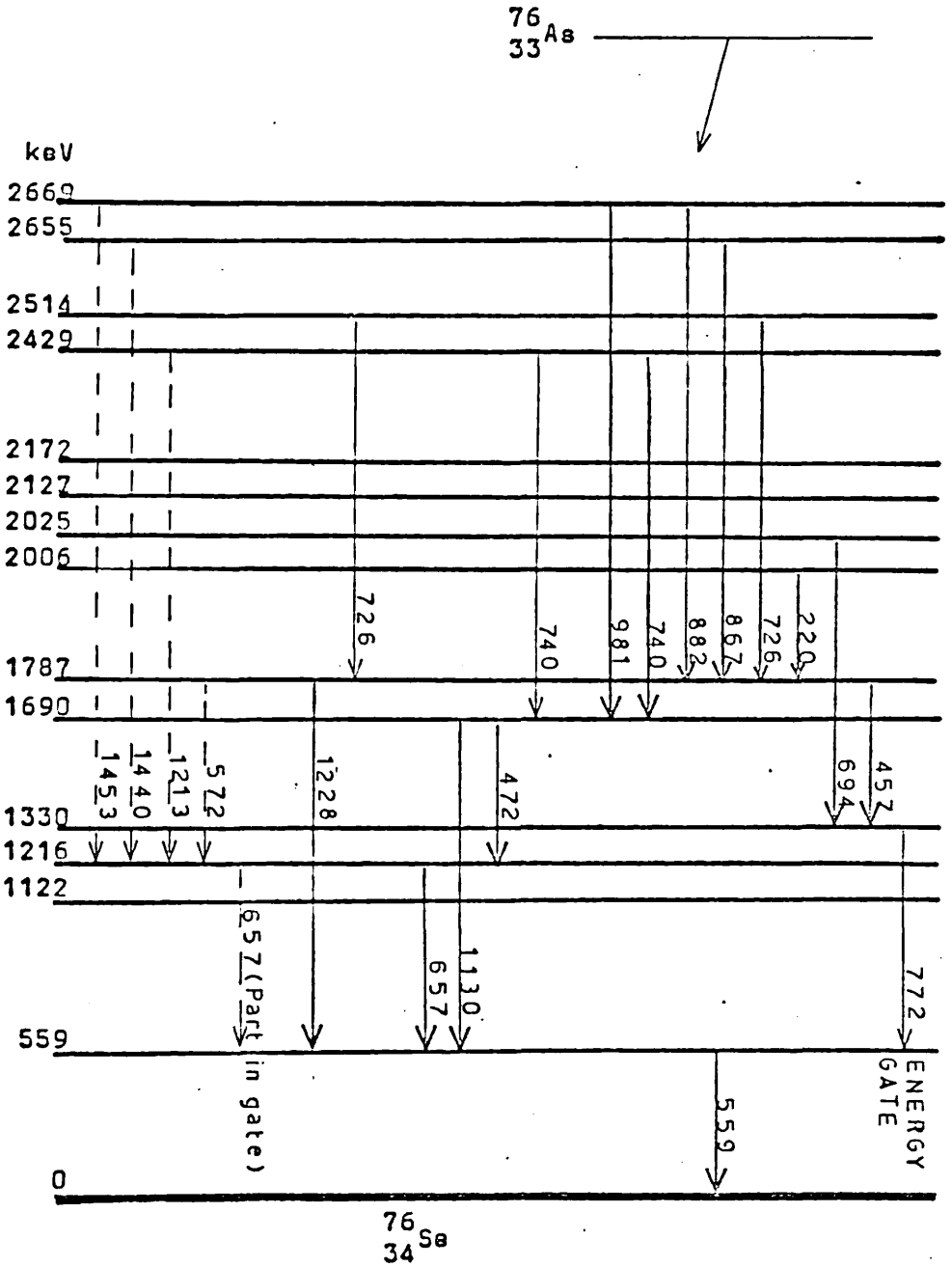

FIGURE 8.19 ^{76}As transitions observed in coincidence with 770 keV region

The 1051 keV gamma transition reported by Iizawa et al.[73] was not seen in a singles spectrum but some evidence for it was identified in coincidence with the 559 keV gate (figure 8.7).

The most significant result to emerge was the presence of two gamma-rays at 303.4 and 316.6 keV. These were identified both in a singles spectrum and in coincidence with the 559 keV gate. These might explain the two different positions suggested in the decay scheme by previous authors for a 303 keV transition. Also the spectrum in coincidence with an energy region around 772 keV showed a gamma-ray of energy 220 keV and a peak of the same energy was found in coincidence with the energy gate at 1787 keV. This, combined with the reported coincidence[72] between a '303' keV gamma-ray and a gate at 1220 keV suggests an energy level at 2006 keV which de-excites by a 220 keV transition to the 1787 keV level and by a 317 keV transition to the 1688.5 keV level.

8.7 Conclusions

The results obtained offer no support for energy levels at 2542, 2365, 2348 and 2088 keV as proposed by Iizawa et al.[72]. The level proposed by McMillan et al.[70] to account for the 727 keV gamma-ray is shown to be unnecessary

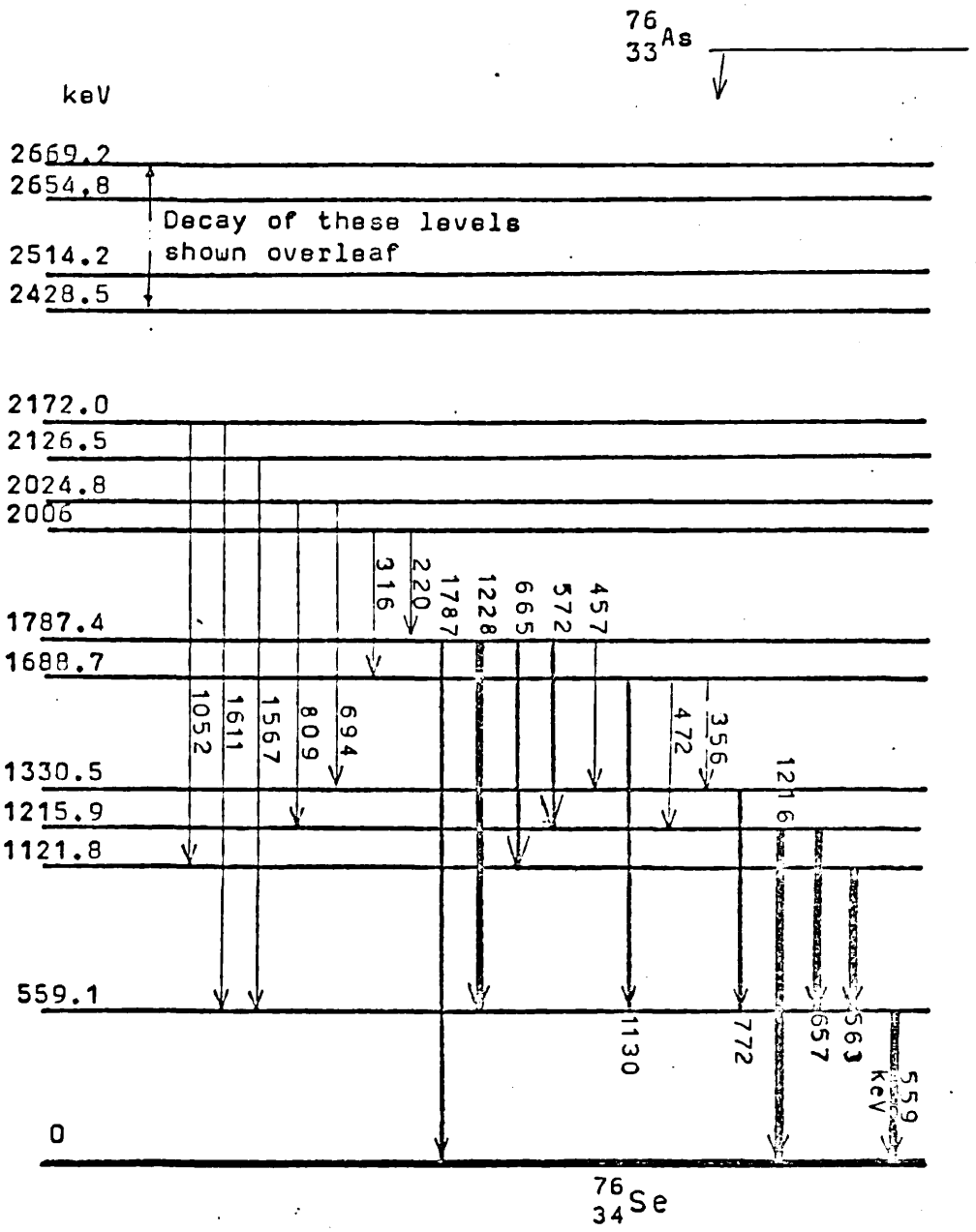

FIGURE 8.20 ^{76}As decay scheme from present work

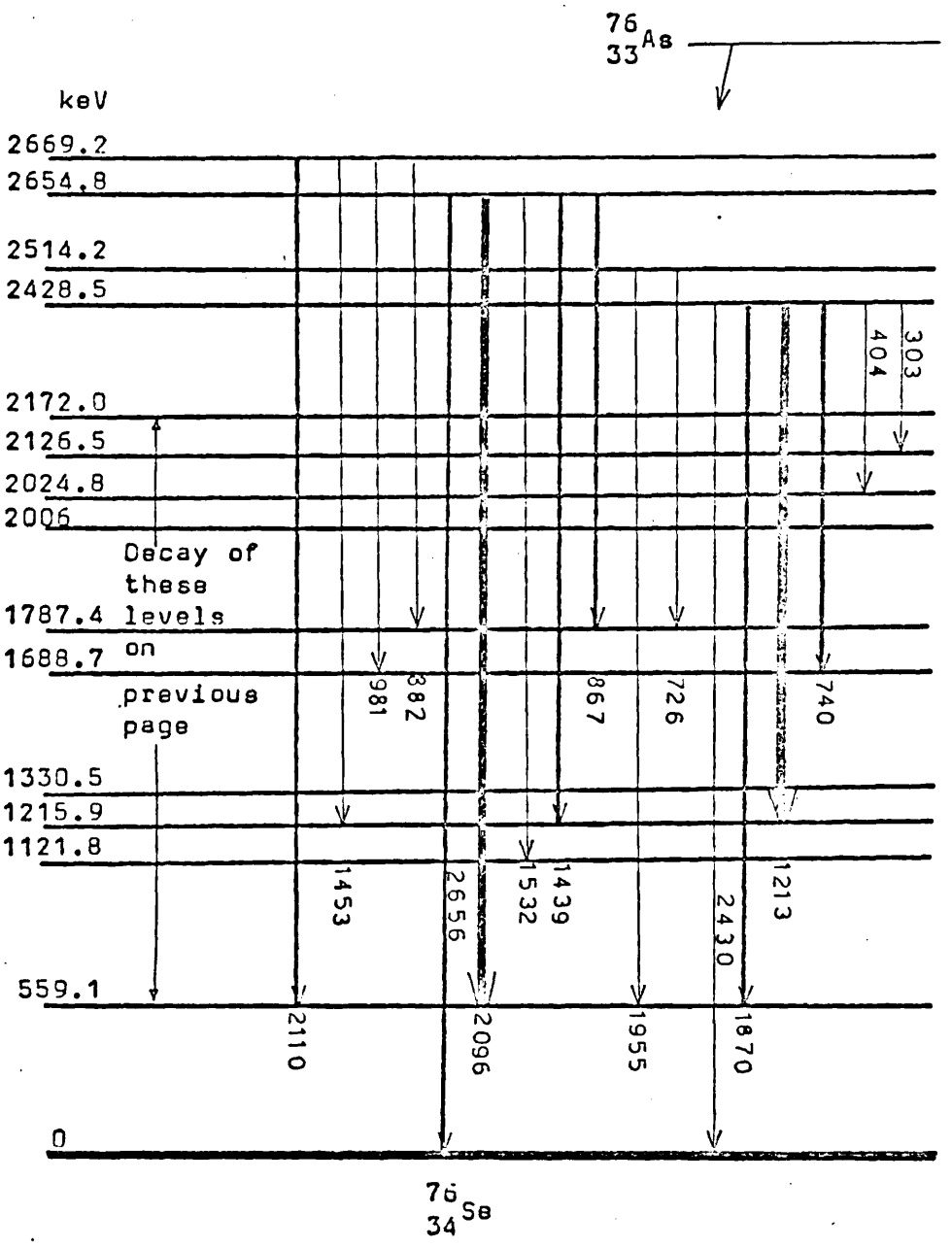

FIGURE 8.20 (continued)

by the coincidence results which place this gamma-ray between two established levels. Also the additional level placed at 2866 keV by McMillan and Pate[70] is not supported by this work. The level at 2024.8 keV proposed by several authors[71, 72, 73] is supported by these results.

The final decay scheme obtained from the coincidence results and the singles spectra is shown in figure 8.20. The previously unreported gamma transitions of energies 220 and 317 keV have been included and the level energies have been calculated from the measured gamma-ray energies.

The results suggest that the resolution of a NaI detector is not sufficient to allow a confident identification of many of the cascades involved. The use of another Ge(Li) detector would offer an advance in this direction only if a sufficiently high efficiency detector was available as the coincidence counting rates would decrease. At 1 MeV a scintillation counter with a $1\frac{1}{2}$" x $1\frac{1}{2}$" crystal and passing an energy gate of $\pm$10 keV still produces a coincidence efficiency with a Ge(Li) detector of about two or three times that obtained when the NaI counter is replaced by a Ge(Li) detector having an efficiency of 4% that of a 3" x3" NaI crystal. However, the improvement in gating energy resolution gained might well outweigh this disadvantage.

CHAPTER 9 GENERAL CONCLUSIONS

This work has shown that, although the Ge(Li) detector has far surpassed the NaI detector in its energy resolution, the efficiency of a Ge(Li) detector does severely limit the evaluation of weak intensity transitions both in singles spectra and in coincidence work. The use of Ge(Li) detectors in coincidence does require a good timing system so that a small resolving time can be employed without loss of coincidence efficiency; thus allowing a stronger source to be used with the consequent decrease in counting time. The facilities of dual parameter work, ideally linked to a small local computer, would also afford a more realistic collection rate for data on complex decay schemes such as ^{76}As.

The use of a special purpose X-ray Ge(Li) detector has proved useful in searching for low energy gamma-rays, particularly in the presence of intense higher energy photons.

The systems used in this work have enabled the author to evaluate some aspects of the decay schemes for each of the three isotopes studied although more work with two Ge(Li) detectors would obviously be of use in the study of ^{76}As.

The detailed conclusions for the isotopes have been presented in their respective chapters.

Acknowledgements

I would like to record my appreciation and thanks to Professor H.C.W. Richardson for his supervision of this work and for the provision of much of the apparatus used.

I am deeply grateful to my husband, Mr R.N. Thomas, for his support, patience and tolerance throughout the course of the work.

Thanks are also given to Mr F. Grimes and Mr A. King for workshop support and their dedication in maintaining the Ge(Li) detectors.

I would also like to thank Mr A. Betts, Mr A. LeMottee and Mr W.A. Baldock and other members of the technical staff for help throughout this work.

REFERENCES

1) R.E. Berg & E. Kashy Nucl.Instr.&Meths. 39 (1966) 169

2) A. Notea & E. Elias Nucl.Instr.&Meths. 86 (1970) 269

3) L. Riedinger et al. Phys.Rev. C (1970) 2358

4) J.J. Sapyta et al. Nucl.Phys. A139 (1969) 161

5) D.P. Donelly et al. Nucl.Instr.&Meths. 64 (1968) 26

6) J. Konijn & E.W.A. Lingeman Nucl.Instr.&Meths. 94 (1971) 389

7) Nuclear Data Tables 8 nos 5-6 (1971)

8) H.E. Jackson et al. Phys.Letters 17 (1965) 324

9) H.J. Levy & R.C. Ritter Nucl.Instr.&Meths. 49 (1967) 359

10) I.K. MacKenzie et al. Nucl.Instr.&Meths. 101 (1972) 149

11) B.S. Dzelepow et al. Nucl.Phys. 8 (1958) 250

12) G. Walford & C.E. Doust Nucl.Instr.&Meths. 62 (1968) 353

13) G.T. Ewan & A.J. Tavendale AECL no 2079

14) C.M. Davisson: α, β & γ-ray spectroscopy vol.1 p827
ed. K. Siegbahn

15) S. Wagner et al. IEEE Trans.Nucl.Sci. NS19 (1972) 380

16) T.S. Nagpal & R.E. Gaucher Nucl.Instr.&Meths. 89 (1970) 311

17) G. Bertolini et al. IEEE Trans.Nucl.Sci. NS19 (1972) 135

18) T.A.E.C. Pratt Nucl.Instr.&Meths. 99 (1972) 205

19) W. Michaelis Nucl.Instr.&Meths. 70 (1969) 253

20) R.G. Helmer et al. Nucl.Instr.&Meths. 47 (1967) 305

21) F.C.P. Huang et al. Nucl.Instr.&Meths. 68 (1969) 141

22) R.G. Helmer et al. Nucl.Instr.&Meths. 57 (1967) 46

23) J.W. Tepel Nucl.Instr.&Meths. 40 (1966) 100

24) J.T. Routti & S.G. Prussin Nucl.Instr.&Meths.72(1969)125

25) A.H. Wapstra: α, β & γ-ray spectroscopy vol.1 p541
edited by K. Siegbahn

26) J.B. Birks: The theory & practice of scintillation
counting ch5 p169

27) J.E. Draper & R.L. Hickok Rev.Sci.Instr. 29 (1958) 1047

28) J. Braunsfurth & H.J. Körner Nucl.Instr.&Meths. 34 (1965)202

29) H.L. Malm IEEE Trans.Nucl.Sci. NS13 (1966) 385

30) G.C. Giesler et al. Nucl.Instr.&Meths. 91 (1971) 313

31) C.M. Lederer et al. Table of Isotopes p210 Wiley

32) N. Imanishi et al. Nucl.Phys. A125 (1969) 626

33) W. Scholz & F.B. Malik Phys.Rev. 176 (1968) 355

34) Mathilde de Croës et al. Arkiv. für Pysik 16 (1960) 567

35) W.F. Edwards et al. Nucl.Phys. 26 (1961) 649

36) E.P. Grigoriev et al. Nucl.Phys. 14 (1960) 443

37) P. Jahn et al. Zeit.Phys. 210 (1968) 245

38) J. Varma & M.A. Eswaran Phys.Rev. 125 (1962) 656

39) P. Venugopala Rao et al. Nucl.Phys. 81 (1966) 296

40) W. Pratt Nucl.Phys. A147 (1970) 601

41) D.E. Raeside et al. Nucl.Phys. A130 (1969) 677

42) T. Paradellis et al. Nucl.Phys. A131 (1969) 378

43) R.L. Robinson et al. Nucl.Phys. A104 (1967) 401

44) W. Pratt Nucl.Phys. A170 (1971) 223

45) Report Issledovanie Spectrov ^{75}Se Joint Inst. for Nucl. Research DUBNA (USSR) lab.of Neutron Phys. 1966

46) D.E. Alburger et al. Phys.Rev. 99 (1955) 605

47) F.P. Brady et al. Nucl.Phys. 66 (1965) 365

48) Avivi I. Yavin et al. Phys.Rev. 100 (1955) 171

49) N.H. Lazar et al. Phys.Rev. 98 (1955) 710

50) J.R. Prescott Proc.Phys.Soc. 67A (1954) 540

51) G. Chilosi et al. Nucl.Phys. 53 (1963) 235

52) R.L. Robinson et al. Nucl.Phys. 64 (1964) 281

53) M.H.L. Pryce Proc.Phys.Soc. 65A (1952) 773

54) V. Klemt & J. Speth Nucl.Phys. A161 (1971) 273

55) K. Harada & S. Pittel Nucl.Phys. A159 (1970) 209

56) H.V. Klapdor et al. Nucl.Phys. A152 (1970) 263

57) O. Häusser & D. Ward Bull.Am.Phys.Soc. 15 (1970) 805

58) L.A. Sliv & I.M. Band: α, β & γ-ray spectroscopy Appendix 5 p.1639 ed. K. Siegbahn

59) J. Blomqvist et al. Ark.Fys. 16 (1960) 545

60) I.M. Govil & C.S. Khurana Nucl.Phys. 60 (1964) 666

61) D.H. White et al. Bull.Am.Phys.Soc. 10 (1965) 13

62) G. Bäckström et al. Ark.Fys. 17 (1960) 393

63) J.D. Kurbatov et al. Phys.Rev. 98 (1955) 674

64) V.D. Vitman et al. Bull.Acad.Sci. USSR 28 (1965) 139

65) T. Nagarajan et al. Nucl.Phys. A137 (1969) 467

66) R.K. Girgis et al. Nucl.Phys. 13 (1959) 461

67) N.N. Delyagin et al. JETP(Sov.Phys.) 11 (1960) 799

68) J. Aten et al. Compt.Rend.Serie C 265 (1967) 465

69) J. Murray et al. Can.J.Phys. 45 (1967) 1221

70) D.K. McMillan et al. Nucl.Phys. A174 (1971) 604

71) G. Ardisson et al. Nucl.Phys. A179 (1972) 545

72) K. Iizawa et al. J.Phys.Soc.Japan 30 (1971) 901

73) G. Funel & C. Ythier C.R.Acad.Sc. 272 (1971) 158

74) G. Funel C.R.Acad.Sc. 274 (1972) 662

75) R.N.Thomas & R.V. Thomas Nucl.Instr.&Meths. 104 (1972)137

NUCLEAR INSTRUMENTS AND METHODS 104 (1972) 137–139; © NORTH-HOLLAND PUBLISHING CO.

A DEVICE FOR MAINTAINING A CONSTANT DETECTOR COUNTING RATE FROM A DECAYING RADIOACTIVE SOURCE

R. N. THOMAS and R. V. THOMAS

Physics Department, Bedford College, University of London, England

Received 4 May 1972

A device is described with which the counting rate in a detector used to measure the gamma-ray spectrum of a decaying radioactive source may be kept constant, by controlled movement of the source towards the detector. A stabilization of counting rate to within ±1% of the desired magnitude is obtained over a period of several half-lives. An alternative application of the same circuit enables a replenishment of the source whenever the counting rate falls below a pre-set level.

1. Introduction

Gamma-ray spectroscopic studies of radioactive decay processes encounter second-order effects which degrade the energy resolution and calibration when detector counting rates are not constant, as is the case with measurements in which the half-life of the nuclide under investigation is less than or comparable with the counting time required for good statistical accuracy.

The dependence of measured pulse amplitude and resolution on counting rate is a well-known feature of nuclear counting systems and can be caused by a number of non-ideal aspects of the detector and linear amplifier system. Many of these effects can be minimized by the use of techniques such as baseline restoration, correctly trimmed pole-zero cancellation, spectrum stabilization, etc., but in most systems the maintenance of good energy resolution requires that counting rates should be kept to a level of a few thousand per second. It is with high-resolution semiconductor detectors that the effects of changing counting rate are potentially most serious but even with scintillation counters the effect can be apparent and a number of techniques have been described[1–4]) for stabilizing photomultiplier gains against the effects of changing counting rate. The limitation of counting rate to a few thousand c.p.s. is sometimes of little consequence but, if the source being studied is one with a short half-life, the outcome is a fall in counting rate to a low level of a few hundred per second within a few half-lives, with a consequent increase in the time needed to obtain a given statistical accuracy. Recent papers by Görner et al.[5,6]) have described a technique for exponentially changing the multichannel analyser livetime as the accumulation of a spectrum proceeds, thereby cancelling the exponential fall in counting rate as the source decays. However, this technique does nothing to overcome the adverse effects of changing counting rate in the preceding amplifiers and detector.

More direct solutions are to restore the strength of the source at periodic intervals or to move it closer to the detector as it decays. We have used both of these methods in a recent study of 28 h ^{76}As with a control circuit described in this article which can be used either to move the source towards the detector in such a manner that a constant counting rate results, or to replenish the source being counted whenever the rate falls below a pre-set threshold. The use of the device has resulted in a worthwhile saving in counting time and experimenters' time.

2. Circuit principles

The principle of operation of this device is that a ratemeter output (proportional to the detector counting rate) is compared with a pre-set reference voltage. When the ratemeter output falls below the reference level, a signal is sent to a small motorised trolley carrying the radioactive source which is then advanced towards the detector until the counting rate is restored. A conventional dc servomotor control would be unnecessarily elaborate for this application and the statistical fluctuations of the counting rate would produce a continuous 'hunting' effect. Simple dc control of the motor would require a significant off-balance signal before movement could be initiated, resulting in over-correction. Consequently, a pulsed technique was adopted in which a short pulse, of amplitude sufficient to apply a reliable starting torque to the motor and duration short enough to achieve only a small movement, was applied. It is important that the time between successive pulses should not be small compared with the integration time constant governing the response time of the ratemeter, otherwise over-correction of the counting rate would result. Provided that the rate of decay of the source is long

compared with this time, very satisfactory stabilization of counting rate results.

3. Circuit description

The circuit used is shown in fig. 1. An FET astable multivibrator (Q1, Q2) generates a square wave of 1 Hz, 0.1 Hz or 0.01 Hz (selected by SW1). This output triggers the SN74121 monostable, the output pulse duration of which is variable, by RV3, from 0.05 s to 0.1 s, producing a variable step-length for the motorized trolley.

The current output of the ratemeter which monitors the detector counting rate is applied across RV1, which is used to control the input sensitivity, and the potential difference across this variable resistor is amplified with a small gain by OPA1. This stage converts the floating output of the ratemeter used into one referred to ground. OPA2 is used as a voltage comparator, with which the input from OPA1 is compared with a reference voltage set by RV2. The gain of OPA2 is high and a sensitive trigger action results with very little hysteresis. For rate input levels greater than the reference level, the negative output of OPA2 is shorted to ground but for rate input levels less than the reference level, the output of OPA2 is driven to saturation and the emitter of Q4 rises to a little less than 5 V. The output state of OPA2 is displayed by the indicator lamps L1 (rate low) and L2 (rate high), driven by transistors Q5 and Q6.

The emitter voltage of Q4 is also applied to one input of the AND gate, the second input of which is the monostable output. Thus when the counting rate falls below the reference level, the monostable output pulses are transmitted to the miniature relay through the inverter buffer/driver and a 10 V pulse is supplied to the motor.

4. Operation and performance

When used to maintain a constant detector counting rate, an inexpensive and convenient mechanism for moving the radioactive source towards the detector is an electric model railway engine, running on a horizontal length of model railway track. This has advantages of simplicity, a well-defined path and a low moment-of-inertia motor. The circuit is set up by setting the source distance to give the counting rate desired and adjusting RV2 to equalize the inputs to OPA2. Under these conditions, the comparator oscillates (at a frequency too high to operate the relay) and both indicator lamps are illuminated at reduced intensity. The range of RV2 over which oscillation occurs is very small and a sensitive setting is possible. As the source decays, the counting rate falls until the comparator output goes to its 'high' dc level and a pulse is trans-

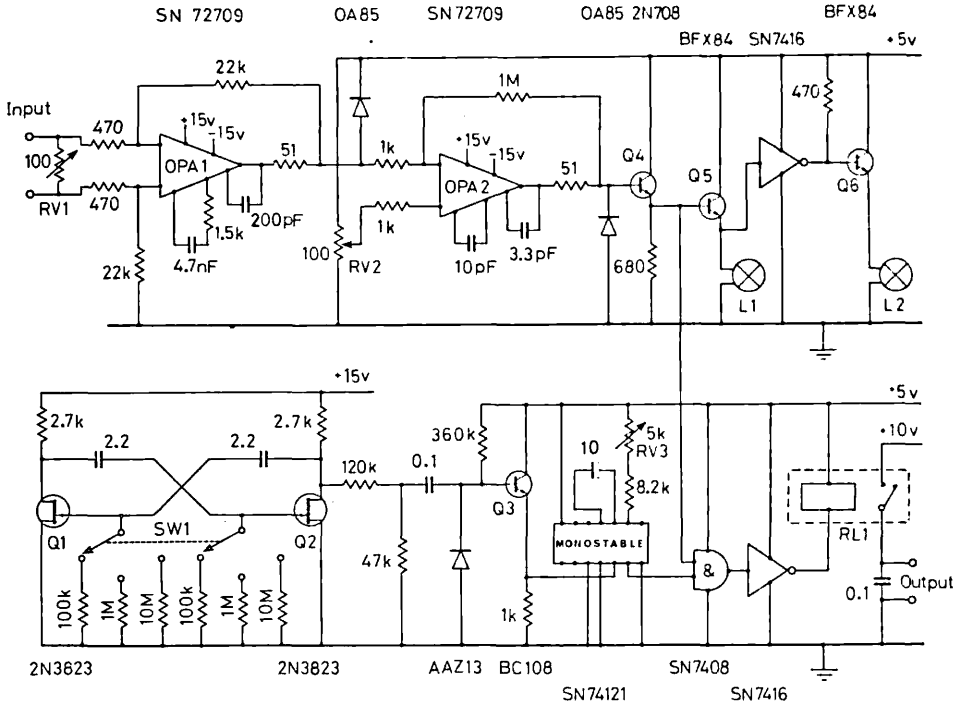

Fig. 1. Schematic diagram of the circuit.

ıted to drive the source towards the detector. The ıtance moved during this pulse can be varied by ∛3 from 2 mm to 5 mm. The long dwell time between ıses allows the ratemeter to respond to the changed ınting rate so that excessive over-correction is ıided.

We have found that this arrangement used in con-ıction with a study of 28 h ^{76}As has performed in a ıhly satisfactory manner and, over a period of three ys, has maintained the required counting rate to ıhin 1%. Fig. 2 shows the results of a simulated run the decay of a short-lived nuclide. For this purpose, ^{137}Cs source was used and the detector was moved ıay from the source at a constant rate of 3.8 mm/min. ıe source, mounted on the railway engine at a distance 80 mm from the detector, was allowed to follow the oving detector under the control of the circuit from e output of a ratemeter set to a time constant of 25 s. urve A shows that the counting rate was maintained ınstant to better than ±1%. Curve B shows the fall counting rate resulting from a movement of the ıtector at the same speed with the circuit not in use. In coincidence investigations using two detectors the rangement described above suffers from disadvantages. The source–detector geometry is difficult to optimise and a calculation shows that overall true-to-chance ratio is decreased by maintaining the counting rate by source movement in this manner. Consequently, the circuit has been used to control an alternative arrangement for replenishing the source as it decays. For this purpose, the sources have been made in the form of small tablets, formed prior to activation by compressing a mixture of the material to be irradiated (in this case As_2O_3) with a base of chromatographic cellulose and phenyl formaldehyde resin in a 3-ton press and curing at 120°C. The tablets contain exponentially increasing masses of the material to be activated and are stored, after activation, in a lead shielding cell mounted above and some distance from the detectors. A fall in counting rate initiates a pulse from the circuit described which operates two solenoids, one of which allows the tablet being counted to fall away from the counting position and the second releases a further tablet from the lead cell which falls under mechanical guidance to the counting position. This stronger source restores the counting rate to a more acceptable level. This method does not, of course, regulate the counting rate as closely as that obtained by linear movement of a single source but if sufficient tablets are used a reasonable constancy is maintained.

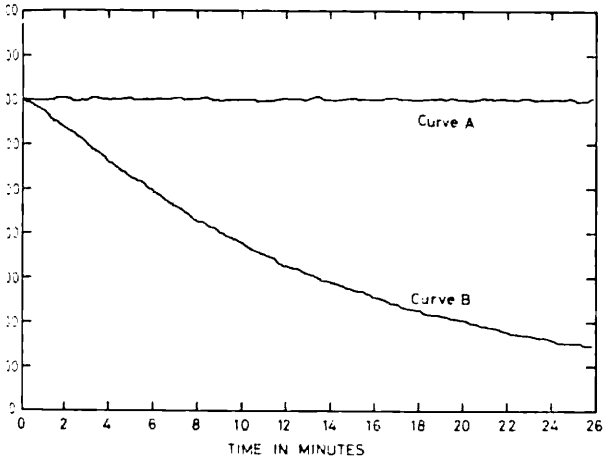

g. 2. Results of a simulated run showing the performance of : device. Curve A shows the degree of stabilization obtained en the source is made to follow a moving detector under the ıtrol of the circuit and curve B shows the fall in counting rate ısed by the increasing source–detector distance when the circuit is not used.

5. Conclusions

The automatic maintenance of a pre-set counting rate from a decaying source has resulted in a worthwhile reduction in resolution degradation and spectrum shift problems, with a considerable saving in counting time without frequent attention by the experimenter. The device described would be useful as a control for nuclides with half-lives down to a few minutes.

References

1) R. W. Hendrick, Rev. Sci. Instr. **27** (1956) 240.
2) A. Barna, Nucl. Instr. and Meth. **24** (1963) 247.
3) J. E. Brimhall and L. A. Page, Nucl. Instr. and Meth. **35** (1965) 328.
4) R. B. Galloway and D. G. Vass, Nucl. Instr. and Meth. **49** (1967) 55.
5) W. Görner, D. Peters and J. Zschau, Nucl. Instr. and Meth. **98** (1972) 371.
6) W. Görner and G. Höhnel, Nucl. Instr. and Meth. **88** (1970) 193.